Metabolic control of muscle and muscle stem cell function

THÈSE N^O 7169 (2016)

PRÉSENTÉE LE 1ER DÉCEMBRE 2016
À LA FACULTÉ DES SCIENCES DE LA VIE
CHAIRE NESTLÉ EN MÉTABOLISME ÉNERGÉTIQUE
PROGRAMME DOCTORAL EN BIOTECHNOLOGIE ET GÉNIE BIOLOGIQUE

ÉCOLE POLYTECHNIQUE FÉDÉRALE DE LAUSANNE

POUR L'OBTENTION DU GRADE DE DOCTEUR ÈS SCIENCES

PAR

Hongbo ZHANG

acceptée sur proposition du jury:

Prof. F. Radtke, président du jury
Prof. J. Auwerx, directeur de thèse
Prof. P. Muñoz-Cánoves, rapporteuse
Prof. B. Chazaud, rapporteuse
Prof. D. Suter, rapporteur

EPFL
ÉCOLE POLYTECHNIQUE
FÉDÉRALE DE LAUSANNE

Suisse
2016

Acknowledgements

This 5-year Ph.D. experience in Lausanne has become the most important and unforgettable part of my life. So now in the final stage of completing this thesis, I would like to take this opportunity to thank the people who have helped and supported me over the years.

First of all, I am tremendously grateful to my advisor, Prof. Johan Auwerx. I thank him for giving me the chance to perform my doctoral work in his world-renowned group. He provided me the courage and support to explore stem cell function as a novel research direction for his lab. Fortunately, this has proven to be an exciting and fruitful field when combined with energy metabolism. Importantly, Johan has taught me much more than how to perform research, as with many in the lab he has taught me passion and persistence to attain any goal in life. These lessons will undoubtedly help me for all my future pursuits. I would also like also to thank Prof. Kristina Schoonjans for her support and encouragement throughout my Ph.D. study, not only on my projects, but also instruction on how to be a good teacher.

Outside of my Ph.D., I spent 16 months at the University of Zurich before I moved to Lausanne. I would like to thank my supervisors Prof. Carsten Wagner and Dr. Andrease Serra in Zurich. They are well-rounded researchers with a true interest in helping young scientists like myself to pursue their dreams. As such, they supported my scientific interests when I decided to join the Dr. Johan Auwerx for new research direction.

I would like to emphasize that research in Johan's lab is about team work. Each of my thesis projects was performed together with Keir Menzies, Dongryeol Ryu, Karim Gariani and Peiling Luan. Being much more than colleagues, we became the building blocks for the Auwerx lab's NAD$^+$ team. Keir has given me sound scientific advice and was instrumental for helping me with my scientific writing skills. Without his dedication to my success I could not imagine finishing my publications, grant applications, as well as this Ph.D. thesis. As a very well-rounded scientist and friend, Dongryeol has spent many hours guiding me through basic experiments and was essential for my progress when solving the most difficult scientific puzzles. My discussions and work with Karim has helped me build a strong collaborative nature. And many thanks to Peiling, a very talented student, who did her master thesis with me and provided excellent assistance on my stem cell projects.

My deepest gratitude goes to all my past and present colleagues in Auwerx and Schoonjans labs. Dr. Eija Pirinen and Dr. Adriano Maida taught me experiment skills; Hao Li and Sorrentino Vincenzo helped with my writing and discussion; Thanks to Penelope Andreux,

Summary

Skeletal muscle composed of myofibers and a small amount of muscle stem cells (MuSCs). It plays important roles in energy metabolism. Some of the key metabolites, such as NAD^+ and acetyl-CoA, were recently found to regulate muscle and MuSCs function by modulating mitochondria function. In my PhD thesis projects, we aimed at exploring the link between NAD^+ levels, mitochondrial function, muscle structural homeostasis and MuSCs senescence. We also investigated the impact of acetyl-CoA on MuSCs activation and proliferation, through the control of protein acetylation. These projects mainly focus on three aspects:

Rejuvenation of adult stem cells by NAD^+ repletion. Aging is accompanied by SCs senescence. However, the initial signaling events mediating SCs senescence are not well defined. We demonstrate the importance of mitochondrial activity as a pivotal modulator of MuSCs senescence. MuSCs from aged mice have reduced NAD^+ levels, mitochondrial content and capacity for oxidative respiration. Importantly, the induction of the mitochondrial unfolded protein response (UPR^{mt}), subsequent to increasing cellular NAD^+ with the precursor nicotinamide riboside (NR), prevents MuSCs senescence and improves muscle function and regeneration in aged mice. NR also prevents MuSCs dysfunction in the *mdx* mouse, a known mouse model of accelerated MuSCs senescence. Extending these observations to other SC pools and on the organism as a whole, we demonstrate that NR delays neural and melanocyte SCs senescence, while also increasing mouse lifespan.

Control of MuSCs function by acetyltransferase KAT2A. MuSCs are essential for skeletal muscle homeostasis and repair. The mechanism controlling MuSCs maintenance and differentiation, however, remains elusive. We found that the acetyltransferase KAT2A expression is essential for myogenic differentiation of MuSCs. KAT2A loss-of-function in cells blocks MuSCs differentiation, and in mice impairs muscle regeneration after damage. The regulation of KAT2A in MuSCs function might rely on its ability to enzymatically acetylate other proteins, and in particular the MuSCs transcription factor PAX7.

NAD^+ repletion improves muscle function in muscular dystrophy. Duchenne muscular dystrophy (DMD) is caused by *dystrophin* gene mutations that lead to progressive muscle degeneration. Our bioinformatics analysis in mice and DMD patients suggests a role for NAD^+ in protecting the muscle from metabolic and structural degeneration. Validating these findings, we reveal that the *mdx* mouse is characterized by reductions in muscle NAD^+ levels, concurrent to increased PARP activity and reduced expression of nicotinamide phosphoribosyltransferase (NAMPT), the key enzymes for NAD^+ consumption and biosynthesis. Replenishing the NAD^+ pool by dietary NR supplementation benefits muscle

function in *mdx* and *mdx*/*Utr*$^{-/-}$ mice, an effect replicated in *C. elegans* models of DMD. The beneficial effects of NAD$^+$ repletion in muscular dystrophy rely on the improvement in mitochondrial function, structural protein expression and on reductions in general PARylation, inflammation and fibrosis.

In summary, our work demonstrates the critical role of NAD$^+$ and Acetyl-coA in maintaining muscle and MuSCs function. Repletion of NAD$^+$ levels, by NR administration, and/or boosting the function of acetyltransferase KAT2A might be attractive strategies to maintain muscle homeostasis and MuSCs function in aging and muscular dystrophy.

Key words: NAD$^+$, Muscle stem cell, KAT2A, Acetylation, Aging, Metabolism, Muscular dystrophy

Résumé

Le muscle squelettique est composé de myofibres ainsi que d'une petite quantité de cellules souches musculaires (CSM). Il joue un rôle important dans le métabolisme énérgétique. Il a été récemment mis en évidence que plusieurs métabolites majeurs tel que le nicotinamide adenine dinucleotide (NAD^+) et l'acétyl-CoA possèdent une activité régulatrice sur la fonction du muscle et des CSM en modulant la fonction mitochondriale. Les projets de ma thèse PhD ont eu pour but d'explorer le lien entre les niveaux de NAD^+, la fonction mitochondriale, l'homéostasie de la structure musculaire et la sénescence des CSM. Nous avons aussi investigué l'impact de l'acétyl-CoA sur l'activation et la prolifération des CSM au niveau du contrôle de l'acétylation des protéines. Ces projets se concentrent principalement sur trois aspects:

Rajeunissement des cellules souches adultes par réplétion de NAD^+. Le vieillissement est accompagné par une sénescence des CS. Cependant les événements initiaux de signalisation menant à la dégénérescence des CS ne sont pas clairement définis. Nous démontrons l'importance de l'activité mitochondriale comme pivots modulateurs de la sénescence des CSM. Les CSM de souris âgées présentaient une diminution du niveau de NAD^+, du contenu en mitochondrie et de la capacité de respiration oxydative. Notablement, l'induction de la réponse mitochondriale au stress protéotoxique en conséquence à l'augmentation du niveau cellulaire de NAD^+ à l'aide du précurseur de NAD^+ nommé nicotinamide riboside (NR) prévient la sénescence des CSM, améliore la fonction et la régénération musculaire chez les souris âgées.

Le NR prévient également la dysfonction des CSM chez les souris *mdx*, un modèle connu pour une sénescence accélérée des CSM. En élargissant ces observations à d'autres pools de CS et sur l'organisme entier, nous avons démontré que le NR retarde la sénescence des CS neurales et mélanocytaires tout en augmentant la durée de vie des souris.

Contrôle de la fonction des cellules souches musculaires par l'acétyltransferase KAT2A. Les CSM sont essentielles pour l'homéostasie et la réparation du muscle squelettique. Les mécanismes contrôlant la maintenance et la différentiation des CSM restent cependant non élucidés. Nous avons découvert que l'expression de l'acétyltransferase KAT2A est essentielle pour la différentiation myogénique des CSM. La perte de fonction de KAT2A bloque la différentiation des CSM et altère la régénération musculaire après un dommage chez la souris. La régulation de KAT2A sur la fonction des

CSM pourrait dépendre de sa capacité enzymatique à acétyler d'autres protéines et en particulier le facteur de transcription au niveau des CSM PAX7.

La réplétion de NAD$^+$ améliore la fonction musculaire dans la dystrophie musculaire. La dystrophie musculaire de Duchenne est causée par une mutation héritée au niveau du gène *dystrophin* qui mène à une dégénération progressive du muscle. Nos analyses bioinformatiques chez la souris et chez des patients atteints de maladie de Duchenne suggèrent un rôle protecteur du NAD$^+$ contre la dégénérescence musculaire métabolique et structurelle. Validant ces découvertes, nous avons observé que les souris *mdx* sont caractérisées par une diminution significative du niveau de NAD$^+$ musculaire et ce de manière concomitante à une augmentation de l'activité de PARP et à une réduction de expression de nicotinamidphosphoribosyltransferase (NAMPT) qui sont respectivement les enzymes clés pour la consommation et la synthèse de NAD$^+$. En reconstituant le pool de NAD$^+$ par une supplémentation alimentaire de NR, nous avons observé un bénéfice au niveau de la fonction musculaire chez les souris *mdx* et *mdx/Utr$^{-/-}$*. Cet effet bénéfique a également été reproduit sur un modèle de maladie de Duchenne chez le *C. elegans.* L'effet bénéfique de la réplétion en NAD$^+$ dans la dystrophie musculaire est pléiotropique et dépend de l'amélioration de la fonction mitochondriale, de l'expression de protéines structurelles et d'une réduction générale de la PARylation, de l'inflammation et de la fibrose.

En résumé, notre travail démontre le rôle critique du NAD$^+$ et de l'acétyl-coA dans le maintien de la fonction du muscle et des CSM. La réplétion des niveau de NAD$^+$ par l'administration de NR et/ou le stimulation de la fonction de l'acétyltransferase KAT2A pourrait représenté une stratégique attractive pour le maintien de l'homéostasies musculaire et la fonction des SCM dans le vieillissement et la dystrophie musculaire.

Mots clés: NAD$^+$, Cellules souches musculaires, KAT2A, Acétylation, Vieillissement, Métabolisme, Dystrophie musculaire

Table of contents

List of figures

List of tables

Chapter 1. Introduction

Partly adapted from:

Skeletal muscle, along with cardiac muscle and smooth muscle, constitutes our muscular system. It permits movement, maintains posture, supports breath and circulates blood throughout our body. Beside the locomotor function, skeletal muscle also plays essential roles in the energy metabolism(1-3). However, the functions of skeletal muscle can be compromised in diseases, such as muscular dystrophy, and in the process of aging(4-8). Moreover, muscle can be damaged even in the routine exercises, such as eccentric running(1). Replacing the damaged tissue by healthy muscle fibers, largely by muscle regeneration, therefore is very important in maintaining locomotor function, as well as metabolic homeostasis(9). In this section we discuss the basics of skeletal muscle structure, and introduce the maintenance of muscle homeostasis by muscle stem cell (MuSC)-reliant muscle regeneration. We highlight the pivotal role of energy metabolism, NAD$^+$ levels and mitochondrial function in supporting both muscle structural homeostasis and MuSCs function. Importantly, the metabolic control of muscle and muscle stem cell function largely depend on the post-translational modification (PTM): acetylation, through the lysine acetyltransferases (KATs) and lysine deacetylases (KDACs)(2).

1.1 Skeletal muscle and muscle structural homeostasis

1.1.1 Introduction to skeletal muscle

Skeletal muscle is a type of striated muscle and named after the fact that most of them are attached to the skeleton. Skeletal muscle is one of the three major muscle types and accounts for about 40% of adult human body weight. Through contraction and relaxation, skeletal muscles help to support movement, posture, blood circulation, breathing, swallowing, defecation, and urination. Additionally, skeletal muscles help with metabolic and temperature regulation.

Individual skeletal muscles are made up of large numbers of giant cells, known as muscle fibers (Figure 1.1). Each fiber is formed from the fusion of many precursor cells and is therefore multinucleated. In humans, muscle fibers are approximately 50 µm in diameter and 10 to 350 mm in length(10). They are arranged in bundles (called fascicle) and separated by sheets of connective tissue containing collagen called basal lamina. Each muscle fiber is surrounded by a cell membrane, which allows the contents of the fibers to be quite different from that of the body fluids outside them. Inside the fiber are the myofibrils, which constitute the contractile apparatus, and the sarcoplasmic reticulum, a system for controlling the myofibrils through changes in calcium concentration. Each myofibril runs the whole length of the muscle fiber with a variable number of segments, which called sarcomeres, the basic functional units of the muscle fiber and forms the basic machinery necessary for muscle contraction. The myofibril consists of myosin and actin proteins. The actual contraction takes

place by an interaction between the actin and myosin molecules (Figure 1.1). The net effect of many of these small movements and small forces is to shorten the myofibrils, and thus the whole muscle. Hence some part of the skeleton is moved, by means of the attachment of the muscle at each end to bone, directly or via tendons.
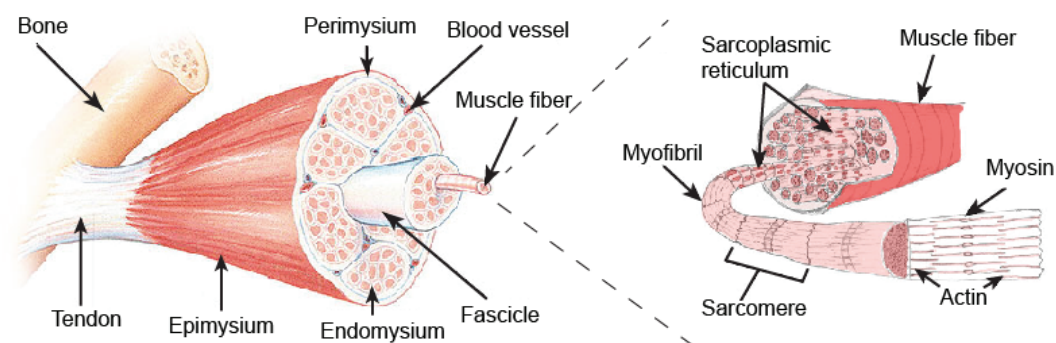
Figure 1. 1 Anatomy of skeletal muscle and muscle fibers

Skeletal muscles are normally attached to the bone by tendon and are covered in a layer of connective muscle tissue known as the epimysium. Muscle fibers are organized as bundles, known as fascicle, which are surrounded by blood vessels and another connective tissue, called perimysium. Muscle fibers are covered in a fibrous connective tissue, known as endomysium. Each muscle fiber itself contains cylindrical organelles known as myofibrils. Each muscle fiber contains hundreds to thousands of Myofibrils. These are bundles of actin and myosin proteins. Surrounding the myofibril there is a network of tubules and channels called the sarcoplasmic reticulum. Adapted from National Cancer Institute SEER training modules, NIH (training.seer.cancer.org).

1.1.2 The dystrophin associated protein complex (DAPC)

The peripheral myofibrils are connected to the sarcolemma along via interactions with subsarcolemmal protein complexes called costameres. Costameres consist mainly of proteins contained within protein complexes, named DAPC and the integrin-vinculin-talin complex (Figure 1.2)(11). These protein complexes transmit contraction forces from muscle fibers to the ECM and, eventually to neighboring myofibers(1). Beside the structural and mechanical function, there is evidence that the DAPC is involved in cell signaling via its interactions with calmodulin, Grb2 and nNOS(12).

The DAPC protein complex, in addition to dystrophin, encompasses intracellular (syntrophin, α-dystrobrevin, and nNOS), transmembrane (β-dystroglycan, sarcoglycans, and sarcospan), and extracellular proteins (α-dystroglycan and muscle-specific laminin) (Figure 1.2)(13, 14). Disruption of the DAPC, as a result of structural or posttranslational defects in one of the components building this protein complex, weakens the sarcolemma and causes different types of muscular dystrophy depending on the altered protein(11). Such as, mutations in genes encoding the subunits of the sarcoglycans cause sarcoglycanopathies, a subtype of recessively inherited limb-girdle muscular dystrophies; the four recessive limb girdle

muscular dystrophies 2D, 2E, 2C and 2F are caused by absence of the α, β, γ or δ sarcoglycans, respectively(*15*); and the deficiency or truncation of dystrophin causes Duchenne muscular dystrophy (DMD) and Becker muscular dystrophy (BMD), respectively, both of them are common types of muscular dystrophy in humans (*1*).
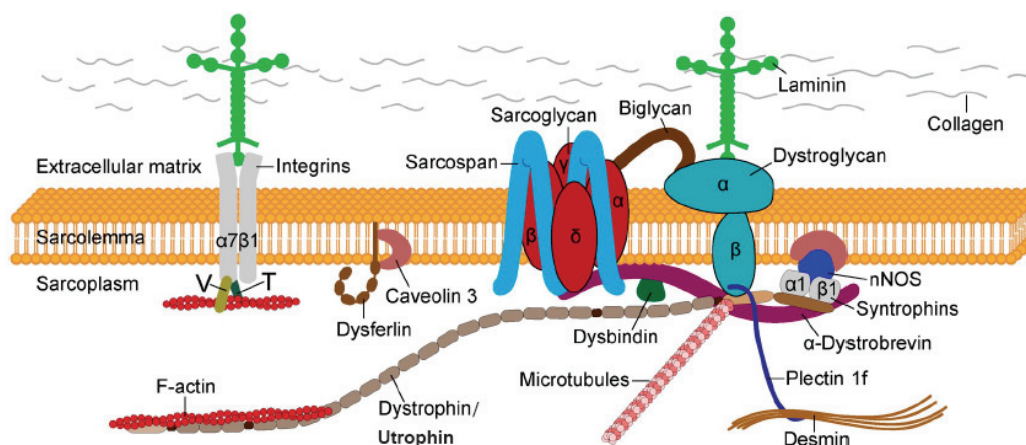
Figure 1. 2 The dystrophin associated protein complex (DAPC)

DAPC is a protein complex that connects the intracellular cytoskeleton to the extracellular matrix (ECM), which is composed of laminin, collagen, etc. The muscle-specific laminin directly interacts with α-dystroglycan, which in turn interacts with other DAPC components, which includes: β-dystroglycan. Dystrophin/utrophin α-dystrobrevin, syntrophin, plectin sarcoglycan and sarcospan complex, biglycan and caveolin-3. The α7β1 integrin dimer binds laminin extracellularly and actin intracellularly via the vinculin (V) and talin (T) proteins. Image from Rahimov et al, *J Cell Biol*, 2013 (*11*)

1.2.3 Muscular dystrophy

The muscular dystrophies are a group of heterogeneous muscular diseases characterized by progressive degeneration and weakness of skeletal muscle. The most common and severely debilitating neuromuscular disorder, DMD, affects 1 in 3,500 males(*16*). It is manifested by rapidly progressive proximal muscle wasting starting around 3 years of age, culminating with respiratory insufficiency and cardiac failure that leads to premature death by the mid-20s. The allelic disorder Becker muscular dystrophy (BMD) is less common and milder, with late disease onset and relatively advanced survival age. Both diseases are caused by mutations; in the DMD gene, the largest gene in the human genome, located on the X chromosome, which encodes the 427-kD protein dystrophin(*17-20*). As dystrophin is the important structural protein of DAPC complex and the integrity of DAPC is crucial for the contracting myofiber to withstand the mechanical stress generated by sarcomeres and to prevent its fragile sarcolemma from contraction-induced injuries(*21*). Deficiency of dystrophin therefore disrupts the DAPC, weakens the sarcolemma and causes muscular dystrophy.

Healthy muscle myofibers are roughly equal in diameter with multiple nuclei located to the periphery of the myofiber. However, dystrophic muscle displays variable size and centrally nuclei myofibers, which are caused by active muscle degeneration and regeneration. The muscle degeneration/damage activates MuSC to promote muscle regeneration. Although these cells are replenished by self-renewal, recurrent degeneration and regeneration of skeletal muscle in a diseased state depletes the MuSC pool and fails to further regenerate the muscle. Ultimately, this contributes to muscle wasting (discussed further in the next section)(1, 22), also known as muscle atrophy, a term that describes the loss of lean muscle mass. Furthermore, at the late stage of disease, atrophied muscle is gradually substituted by fibrous and fatty tissues, which is one of the hallmarks of muscular dystrophy. Disruption of sarcolemma causes leakage of muscle proteins such as creatine kinase (CK) into the serum. Thus, high level of CK concentration in circulating blood is used as another biomarker for DMD disease(1, 22).

Even though the understanding of various muscular dystrophies has advanced considerably during past decades, no treatment is currently available to stop or reverse any form of muscular dystrophy(23). Animal models are valuable tools for studying the pathogenesis of diseases and provide a test-bed for pre-clinical trials. To study DMD, two of the most widely used animal models are *mdx* and *mdx*/*Utr$^{-/-}$(Dko)* mice. The *mdx* mice do not express dystrophin but have a mild phenotype compared to humans. In contrast, the *Dko* mice, which are deficient for both dystrophin and another compensating muscle protein, utrophin, more closely resemble the human phenotype. Among the potential DMD treatments, boosting MuSCs function has been receiving more and more attention considering the appearance of MuSC depletion at the end of the disease(6, 24).

1.2 Muscle stem cells

1.2.1 Introduction to MuSCs

MuSCs (also known as satellite cells), residing between the basal lamina and the sarcolemma of the muscle fiber, are adult stem cells that can self-renew and are capable of generating skeletal muscle cells (differentiation). Since Alexander Mauro identified MuSCs at the periphery of adult skeletal muscle myofibers half a century ago(25), accumulating evidence confirmed the role of MuSCs as primary contributors to the postnatal growth, maintenance and repair of skeletal muscles(9). [^{3}H]thymidine tracing experiments indicated that MuSCs are mitotically quiescent in adult skeletal muscle, while upon muscle damage and/or exercise they rapidly enter the cell cycle(26). Activated MuSCs can then give rise to proliferating myoblasts, which fuse into multinucleated myotubes at the final stage of muscle regeneration(27). In addition to myogenic differentiation, activated MuSCs have to self-renew

to preserve the stem cell reservoir. The key mechanisms controlling and preserving the balance between self-renewal and differentiation of MuSCs throughout the lifespan of an individual have only been partially understood. In fact, complex genetic regulatory networks are involved in the control of MuSC maintenance and differentiation during myogenesis(*28*). Amongst all transcription factors, paired-box 7 (PAX7) and paired-box 3 (PAX3) are essential regulators of these transcriptional networks(*28*).

1.2.2 Roles of PAX3 and PAX7 in the formation of skeletal muscle

Pax genes, which encode transcription factors characterized by a Paired Domain (PD), play key roles in the formation of tissues and organs during embryonic development. Some of the PAX proteins also have an Octapeptide motif (OP) and a Homeobox DNA-binding domain (HD)(*29*). Based on the presence of these structural features and on the sequence homology between Paired Domains, the *Pax* gene family can be divided into four subgroups (Table 1.1). PAX factors belonging to the same class show partial overlap in terms of tissue specificity and spatiotemporal expression(*30*).

Table 1.1 The PAX family of regulatory factors in mammals

Pax genes	Structural characteristics	Expression in developing tissues/organs	Examples of human diseases associated with *Pax* mutations
Pax3	PD OP HD1/HD2/3	CNS, craniofacial tissue, trunk neural crest, somites/skeletal muscle	Waardenburg syndrome, rhabdomyosarcoma
Pax7		CNS, craniofacial tissue, somites/skeletal muscle	Melanoma, neuroblastoma, rhabdomyosarcoma
Pax4		Pancreas, gut	Diabetes
Pax6		CNS, pancreas, gut, nose, eye	Aniridia, cataracts, G1 tumors
Pax2		CNS, kidney, ear	Kidney disease, e.g., Colomba syndrome, renal carcinomas
Pax8		CNS, kidney, thyroid	Congenital hypothyroidism, thyroid follicular carcinomas
Pax5		CNS, B-lymphocytes	Lymphomas
Pax1		Skeleton, thymus, parathyroid	Vertebral malformations, e.g., Klippell-Feil syndrome
Pax9		Skeleton, thymus, craniofacial tissue, teeth	Oligodentia

Modified from: Buckingham *et al, Annu. Rev. Cell Dev. Biol*. (2007)(*31*)

PAX7 and PAX3 belong to the same PAX class of transcription factors and are paralogs with conserved amino acid sequences(*32*). PAX7 is usually highly expressed in quiescent MuSCs and in proliferating myoblasts(*33*). Knock-out of the *Pax7* gene in mice resulted in complete absence of MuSCs, which further caused muscle atrophy and ultimately led to death within the first 3 weeks of life (*34*). Though PAX7 together with its paralog PAX3 are key regulators of myogenesis, they have overlapping functions only in myogenic differentiation.

PAX3 is initially transcribed in the pre-somitic mesoderm adjacent to the first somite prior to confined expression in dermomyotome and myogenic progenitor cells that delaminate and migrate from the somites to more distant sites of myogenesis. Activated myogenic cells delaminate from the edge of the dermomyotome, a process which is associated with downregulation of PAX3, and rapidly differentiate(*35*). PAX3 is expressed throughout the dermomyotome, whereas PAX7 expression is originally induced in the central domain of dermomyotome in the mouse embryo, where PAX3/PAX7 positive cells reside. These double positive cells provide myogenic progenitors for muscle growth. In this situation, both PAX3 and PAX7 are essential for the survival of these myogenic progenitors and contribute to the growing skeletal muscle mass(*36*).

Distinct phenotypes of *Pax3*- or *Pax7*-knockout mice (Table 1.2) indicated that PAX3 is uniquely involved in embryonic development(*37*), while PAX7 plays an essential role in the specification of MuSCs(*31*). Despite the fact that PAX3 is expressed at an earlier embryonic stage than PAX7, PAX7 is upregulated in PAX3-deficient mice, potentially to compensate for the loss of PAX3(*38*). Of note, in *Pax7*-null mice, PAX3 cannot compensate for the deficiency of PAX7 in the establishment of satellite cell lineage(*39*). Although PAX7 can rescue almost all phenotypes caused by PAX3-deficiency, it is unable to fully recover the lack of delamination and long-range migration of muscle progenitors to the limb bud, which suggests that PAX3 is solely responsible for this developmental activity(*40*). Taken together, these results indicate that PAX3 and PAX7 have partially overlapping but not redundant roles in myogenesis.

Table 1.2 *Pax3* and *Pax7* mutant phenotypes and functions of these factors during prenatal myogenesis

Age	Pax3		Pax7		Pax3 and Pax7	
	Mutant phenotype	Function	Mutant phenotype	Function	Mutant phenotype	Function
E9.2-E12.5	-Reduced epaxial and hypaxial dermomyotome -Disorganised myotome	-Survival of hypaxial dermomyotome -Upstream regulation of myogenic hierarchies	Normal	Masked by PAX3	-Primary myotome reduced and disorganized -No limb and other muscles of migratory orgin	Survival and specification of embryonic myogenic
	-No migratory myogenesis	-Activation of c-met				
E12.5-E14.5	-Abnormal trunk myogenesis	-Consequences of early myogenic defects	Normal	Masked by PAX3	-Major trunk muscle deficit	Survival and specification of embryonic myogenic progenitor cells
	-No myogenic cells of migratory orgin (limb, diaphragm, prt of tongue, *etc*.)	-Consequences of early myogenic defects			-No limb and other muscles of migratory orgin	
E15-E18.5	-Embryonic lethality	-Consequences of early myogenic defects in few surviving foetuses	Normal	Masked by PAX3	-Complete mutants do not survive. Conditional not reported	N/A

Modified from Buckingham *et al, Seminars in Cell & Developmental Biology* 44 (2015)(*35*)

PAX3 and PAX7 not only control critical aspects of the behavior of muscle progenitor cells, including cell survival, cell proliferation and migration but also regulate the entry of these cells into the myogenic program(*31*).

As PAX3 has a robust expression exclusively in the embryo that is downregulated after birth, it was concluded that PAX3 plays an important role in orchestrating myogenesis in the embryo, yet is not required in most postnatal MuSCs. In contrast, PAX7 expression is maintained in all satellite cells and proliferating myoblasts but is sharply downregulated immediately before differentiation(*41*), implying a function of PAX7 in maintaining the undifferentiated state of MuSCs. Therefore, in response to muscle damage, activated MuSCs have to downregulate PAX7 and progressively initiate the synthesis of early myogenic regulatory factors (MRFs), such as Myogenic Factor 5 (MYF5) and Myoblast Determination Protein (MYOD), when withdrawing from the cell cycle and preparing for the myogenic differentiation(*42*) (Figure 1.1).

1.2.3 MRFs in myogenesis

Quiescent MuSCs are characterized by the expression of PAX7 but not MYOD or MYOG(*43*). Consequent to muscle damage, activation of MuSCs into myoblasts is typified by the upregulation of basic helix-loop-helix MRF transcription factors (MYF5, MYOD, MYOG, MRF4)(*44*). PAX3 and PAX7 lie upstream of the MRFs and the nature of the hierarchy depends on the spatiotemporal context(*45*). In embryonic myogenesis, PAX3 and PAX7 act upstream of both MYF5 and MYOD(*46*). In satellite cells of the postnatal skeletal muscle, MYOD expression depends on PAX3/7 while MYF5 is possibly independent of PAX regulation[13].

Gene targeting and expression analysis have displayed a functional classification of MRFs: MYF5 and MYOD belong to the group of determination factors, while MYOG and MRF4 constitute the differentiation factors(*47*). Entry into the myogenic program depends on the determination factors conferring the skeletal muscle identity, followed by activation of myogenic differentiation factors and consequent formation of skeletal muscles.

MYF5 and MYOD are expressed in proliferating myoblasts and subject to different cycle regulation(*48*). Previous work has demonstrated that MYF5 is expressed before MYOD at the onset of myogenesis(*49*). MYOD is shortly upregulated after the beginning of differentiation. The expression of MYOD as well as high levels of MYF5 led to the activation of MYOG that was reported to negatively regulate PAX7 at the protein level(*50*), and new muscle fiber formation (Figure 1.1). After this point, MYF5 and MYOD expression levels gradually decrease. The level of MYOG increases through differentiation, and then decreases prior to upregulation of MRF4(*51*). In addition to MRFs, the Myocyte Enhancer Factor 2 (MEF2) class of transcription factors also has an important regulatory role in the control of myogenesis(*52*).
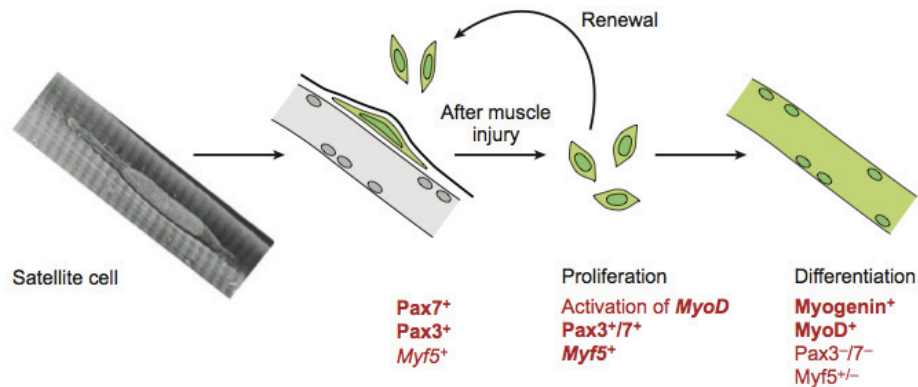
Figure 1. 3 MuSCs and regulation of muscle regeneration

MuSCs are located beneath the basal lamina of muscle fibers. In quiescence, these MuSCs are marked by PAX7 expression. After muscle injury, activated satellite cells start to express MYF5 and MYOD, downregulating PAX7 and differentiate into muscle fibers. Self-renewal of MuSCs is assured by the high level of PAX7. Modified from: Buckingham *et al., Annu. Rev. Cell Dev. Biol.* 2007(*31*).

1.2.4 MuSCs self-renewal

A hallmark of MuSCs is their ability to self-renew. This property is clearly demonstrated by their remarkable ability to sustain the capacity of muscles to regenerate. The most classic experiment proving the MuSCs self-renewal is transplantation of myofibers into the hind limb of the immunodeficient *mdx* (*scid-mdx*) mouse model(*53*). It was found that grafted MuSCs could undergo a 10-fold expansion via self-renewal. Additionally, one grafted fiber could give rise to more than 100 myofibers, which contain around 25000-30000 differentiated myonuclei(*54*). However, it remains intriguing to understand how MuSCs renew themselves. It is known that PAX7 plays important roles in controlling the cell decision of self-renewal or differentiation upon the activation of MuSCs.

After the accomplishment of muscle regeneration, activated MuSCs return to quiescence. The muscle regeneration process revealed that most MYOD[+] / PAX7^{+} proliferating MuSCs differentiate into MYOG^{+} cells, and only a small proportion of MYOD[+] / PAX7^{+} cells have been detected to repress MYOD expression and maintain PAX7 expression, eventually returning to quiescence(*9*) (Figure 1.3). The capacity of activated MuSCs to generate reserve cells may be an important mechanism to maintain the size of MuSCs reservoir. Recently, energy metabolism, especially the mitochondrial function has been linked the MuSCs activation/proliferation (*55*).

1.3 Skeletal muscle and energy metabolism

1.3.1 Energy metabolism in muscle

Skeletal muscles are not only indispensible for the locomotor function of the muscle but also serve as important metabolic organs in humans(*56-58*). Skeletal muscle is one of the main energy-consuming organs, burning glucose, triglycerides and ketone bodies for muscle contraction. It accounts for almost 80% of glucose utilization after insulin stimulation. Meanwhile, skeletal muscle can be used to generate heat (when shivering) and also function as storage of protein if we should face malnutrition. By modulating key metabolic signaling pathways, such as mTOR and sirtuins, energy metabolites directly affect both muscle and MuSCs function(*59*).

To deal with these divergent activities, skeletal muscles are composed of myofibers with large differences in metabolic profile and contractile speed(*60, 61*). The presently dominating classification system for mammalian skeletal muscle is based on myosin heavy chain (MHC) isoforms. The major fiber types are type I, IIa, IIx and IIb (Table 1.3)(*62*). Rodent muscles express all four types of MHC, whereas IIb MHC is not expressed in human muscle. Among different skeletal muscle fiber types, type I fibers can be categorized as red, slow-twitch, or oxidative muscle. High in mitochondria, these fibers primarily undergo oxidative metabolism using triglycerides as energy resource, and are resistant to fatigue. By contrast, type II skeletal muscle fibers can be categorized as white, fast-twitch, or glycolytic muscle. These fibers are relatively low in mitochondria, primarily undergo glycolytic metabolism using fast energy resources, such as glucose and creatine phosphate. Fast-twitch muscles are susceptible to fatigue (Table 1.3)(*63*). The muscle fiber type transformation for slow-twitch muscle to fast-twitch muscle was found in metabolic diseases as well as aging, which accomplice with worse metabolic status. Inversely, exercise helps the opposite muscle fiber transformation and better energy metabolism(*64*). It is interesting that different muscle types differ in the density of MuSCs. Within the same muscle, the number of MuSCs found on slow muscle fibers is generally higher than those on fast myofibers(*65*). Whether the higher content of MuSCs in slow-twitch muscle fibers has biological significance in metabolism or muscle regeneration is unknown.

Alterations of skeletal muscle energy metabolism are always accompanied with systemic metabolic disorder. For instance, in obesity and type II diabetic patients, lipid accumulation is found in the skeletal muscle(*66*).

Table 1.3 Skeletal muscle fiber types

	Type I fiber	Type IIa fiber	Type IIx fiber	Type IIb fiber
Contraction time	Slow	Moderately fast	Fast	Very fast
Maximum duration of use	Hours	<30min	<5min	<1min
Resistance to fatigue	High	Fairly high	Intermediate	Low
Power produced	Low	Medium	High	Very hight
Activity used for	Aerobic	Long-term anaerobic	Short-term anaerobic	Short-term anaerobic
Mitochondrial density	High	High	Medium	Low
Capillary density	High	Intermediate	Low	Low
Oxidative capacity	High	High	Intermediate	Low
Glycolytic capacity	Low	High	High	High
Major storage fuel	Triglycerides	CrP, glycogen	CrP, glycogen	CrP, glycogen
Muscle fiber size	Small	Medium	Medium	Large
Color	Dark red	Red	White red	White

CrP, creatine phosphate. Table modified from Pette *et al.*, *Microsc Res Tech*, 2010(*63*)

1.3.2 Energy metabolism regulation by the skeletal muscle

Not only skeletal muscle energy metabolism, through controlling cellular key metabolites, such as NAD^+ and Acetyl-CoA levels, regulates muscle and muscle stem cell function, on the other hands, skeletal muscle also modulates energy metabolism. Skeletal muscle regulates systemic energy metabolism mainly at two levels: 1, Skeletal muscle itself is one of the main tissue that syntheses and consumes energetic metabolites. And 2, Skeletal muscle synthesizes and secretes multiple factors, known as myokines, to regulate systemic energy metabolism. Some of these myokines are primarily expressed in muscle while others are expressed also in other tissues. Among all myokines, myostatin and interleukin -6 (IL-6) are examples of well studied in their roles of metabolic regulation (Figure 1.5)(*67*).

Myostatin acts as Transforming growth factor β (TGFβ) ligand. It is expressed almost exclusively in skeletal and cardiac muscle. Myostatin-deficient animals have a doubling of muscle mass, and myostatin inhibition has been proposed to delay age-related sarcopenia by preserving muscle mass and possible strength (*67*). In addition to the regulation of muscle mass, myostatin knock-out animals have improved insulin sensitivity and reduced fat mass(*68*). Exercise increases systemic insulin sensitivity, which might be mediated by the production of the myokines insulin-like growth factor-1 (IGF-1), IL-6 etc. Although muscle-derived IGF-1 is not detected in the circulation, it induces muscle hypertrophy in an autocrine/paracrine fashion following exercise. Furthermore, several IGF-binding proteins (IGFBP-3, -4, -5, and -6) are expressed in muscles. They differ in their capacity to enhance or block the anabolic effects of IGF-1 by sequestering it, extending its half-life, or inhibiting its interaction with IGF-1 receptors located on the muscle and MuSCs(*67*). IL-6 has been

proposed to act on the insulin-producing pancreatic β islets, therefore regulates systemic energy metabolism(*69*).

Moreover, the metabolism in skeletal muscle also changes the level of several metabolites, such as NAD^+ and acetyl-coA. These metabolites affect multiple aspects of systemic energy metabolism and MuSC function, often by participating in post-translational modification events (PTMs) (*2*).
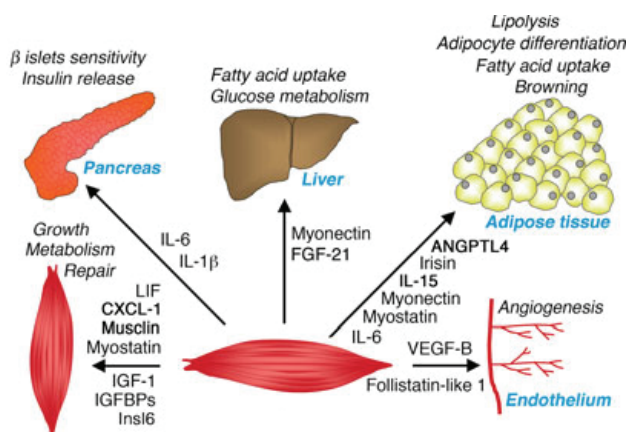
Figure 1. 4 Systemic regulation of metabolism by myokines

Myokines modulate several metabolic processes in the pancreas, liver, adipose tissue, endothelium, the muscle itself, and other tissues, and may influence mammalian lifespan. Adapted from Demontis et al., *Aging Cell*, 2013(*67*)

1.4 Modulation of energy metabolism by protein acetylation

1.4.1 KATs and KDACs

Reversible acetylation, as a type of PTMs of proteins, was initially described as an epigenetic regulatory mechanism governing DNA accessibility. Since then, this process emerged to control not only histone but also non-histone acetylation for integrating key physiological processes such as, metabolism, circadian rhythm and cell cycle along with gene regulation in various organisms. The reversibility of acetylation makes it especially favorable for protein regulation in adaptation to metabolic changes. These acetylation reactions are catalyzed by KATs (previously known as histone acetyltransferases, HATs), which transfer an acetyl group from acetyl-CoA to a lysine residue on histone or non-histone proteins. In opposition, KDACs can remove these acetyl groups from lysines using either zinc as a cofactor or NAD^+ as a co-substrate.

Both KATs (Table 1.4) and KDACs (Table 1.5) are protein superfamilies comprised of several subfamilies. In higher eukaryotes, KATs can be classified as the nuclear localized A-

type group or the cytoplasmic localized B-type group (*70*). Briefly, the three main subfamilies of A-type KATs include: the Gcn5-related N-acetyltransferases (GNATs), p300/CREB-binding protein (p300/CBP, including p300 and CBP proteins) and the MOZ, YBF2, SAS2 and TIP60 (MYST) families (Table 1.4)(*70*). Aside from these general canonical KAT families, there are several other nuclear enzymes that posses acetyltransferase activity, including nuclear receptor coactivators (NCOAs)(*70*), TATA box binding protein (TBP)-associated factor 1 (TAF1)(*70*) and circadian locomotor output cycles kaput (CLOCK)(*71*). A-type KATs catalyze most of the transcription-related acetylation events(*70*). Conversely, B-type KATs likely catalyze the acetylation of newly synthesized histones in the cytoplasm and regulate their cytosolic-nuclear transport(*72*). Reversing the effects of KATs, KDACs are grouped into four classes, depending on sequence homology and domain organization. Specifically, classes I, II and IV identify different groups of zinc-dependent KDACs, whereas class III KDACs consists of NAD^+-reliant sirtuins, ranging from SIRT1 to SIRT7 (Table 1.5)(*73*).

Table 1.4 The cellular location, activity, targets and null phenotype of lysine acetyltransferases

Sub-family	Enzyme	Location	Enzyme activity	Targets	Null phenotype
GNAT	KAT2A	N	A	H3, H4, PGC-1α , α-tubulin	Embryonic lethal
	KAT2B	N	A	H3, H4, ERRα, ACL, MYOD1	Developmentally normal
	HAT1	C, N	A	Newly synthesized cytoplasmic histones	Neonatal lethality
	ATF2	N, M	A	H2B, H4	Neonatal lethality
p300/CBP	p300	N, C	A	H2A, H2B, H3, H4, FXR, PPAR-γ, PEPCK-C, PLAG1, SIRT2, p53, HDAC1, BCL6, MYOD1	Embryonic lethal
	CBP	N, C	A	H2A, H2B, H3, H4, PPAR-γ, MYOD1	Embryonic lethal
MYST	KAT5	N, C	A	H2A, H4, (H3)	Embryonic lethal
	KAT6A	N	A	H3, H4, p53	Embryonic or neonatal lethal
	KAT6B	N	A	H3, H4	Partial postnatal lethality
	KAT7	N	A	H3, H4	Embryonic lethal
SRCs	NCoA-1	N, C	A	H3, H4	Obesity, abnormal metabolism and reproductive system
	NCoA-2	N, C	A	H3, H4	Smaller size, abnormal reproductive system
	NCoA-3	C, N	A	H3, H4	Reduced bodyweight, abnormal metabolism
Others	TAFII250	N	A, P, U-A	H3, H4, (H2A), p53	Unknown
	GTF3C-α	N	A	H2A, H3, H4	Embryonic lethal
	CLOCK	N, C	A	H3, H4, GR, ARNTL1	Abnormal circadian phase

A, acetylation; C, cytosol; M, mitochondria; N, nuclear; P, phosphorylation; U-A, ubiquitin-activating/conjugating. H, histone.

Both KATs and KDACs are highly conserved. For instance, both the mammalian GNAT and sirtuin family homologue genes also exist in yeast and plants(*74-76*). Here we will predominantly focus on the GNAT enzymes, KAT2A/B, and pertinent classes of KDACs, such as the sirtuins, as the main regulators of energy metabolism in organisms ranging from yeast to mammals.

1.4.2 SIRT1, a typical KDAC in energy metabolism

The importance of KDACs in energy metabolism was exemplified by the identification of the yeast ortholog of the mammalian sirtuin, Sir2p, as a regulator of lifespan extension during caloric restriction (CR)(*77, 78*). Now described to be involved in a large spectrum of key signaling pathways, researchers have chronicled the many ways in which sirtuins and other KDACs influence energy metabolism(*75, 79*).

Table 1.5 The cellular location, activity, targets and null phenotype of lysine deactelyases

Sub-family	Enzyme	Location	Enzyme activity	Targets	Null phenotype
I	HDAC1	N,C	DA	H2A, H2B, H3, H4, AR, SHP, p53, MYOD1, E2F1, STAT3	Embryonic lethal
	HDAC2	N	DA	H2A, H2B, H3, H4, GR, YY1, BCL-6, STAT3	Neonatal lethality, smaller size
	HDAC3	N	DA	H2A, H2B, H3, H4, SHP, YY1, Eryf1, p65, STAT3, MEF2D	Embryonic lethal
	HDAC8	N, C	DA	H2A, H2B, H3, H4, SMC-3, ERRα	Partial neonatal lethality
IIA	HDAC4	N, C	DA	H2A, H2B, H3, H4, GCM1, Eryf1, HP1-β	Postnatal lethality, smaller size
	HDAC5	N, C, GA	DA	H2A, H2B, H3, H4, GCM1, SMAD7, HP1-β	Cardiac hypertrophy
	HDAC7	N, C, M	DA	H2A, H2B, H3, H4, PLAG1	Embryonic lethal
	HDAC9	N, C	DA	H2A, H2B, H3, H4	Cardiac hypertrophy
IIB	HDAC6	C, N	DA	H2A, H2B, H3, H4, α-tubulin , HSP90, SHP, SMAD7	Higher body weight, abnormal immune and skeletal system
	HDAC10	C	DA	H2A, H2B, H3, H4	Unknown
III	SIRT1	N, C	DA, DC	H2A, H3, H4, PGC-1-α, PPAR-γ, FOXO1, FOXO3, CRTC2, AceCS, p53, NOTCH1, p65, HIF-1α, LXRβ, FXR	Developmental defects
	SIRT2	C	DA, DC	H3, H4, ACL, α-tubulin, PEPCK-C, FOXO1, p65	Developmentally normal
	SIRT3	M	DA, DC	LCAD, HMGCS2, GDH1, SOD, IDH-2, OXPHOS, AceCS2	Developmentally normal
	SIRT4	M	ADPR, L, B	GDH1, MCD, PDC	Developmentally normal
	SIRT5	M, C, N	DA, DM, DS, DG	CPS1	Developmentally normal
	SIRT6	N	DA, ADPR, D	H3, IGF-1, HIF-1α, KAT2A, p65	Premature aging
	SIRT7	N	DA	H3, GABPB-1, p53, SMAD6	Smaller size, short lifespan, heart defects
IV	HDAC11	N, C, PM	DA	H2A, H2B, H3, H4	Developmentally normal

ADPR, ADP-ribosylation; B, biotinylation; C, cytosol; D, deacylation; DA, deacetylation;DC, decrotonylation; DM, demalonylation; DS, desuccinylation; DG, deglutaryation; GA, Golgi apparatus; L, lipoylation; M, mitochondria; N, nuclear; PM, plasma membrane.

The seven mammalian sirtuins have distinct subcellular localizations, enzymatic activities and targets (Table 1.5)(*75*). SIRT1, SIRT6 and SIRT7 are predominantly localized to the nucleus and deacetylate histones, transcription factors/cofactors, and metabolic enzymes. For example, SIRT1 deacetylates a wide range of metabolic regulators, including the peroxisome proliferator-activated receptor γ coactivator 1α (PGC-1α)(*80, 81*), Forkhead box protein O 1 (FOXO1)(*82, 83*), liver X receptors (LXR)(*84, 85*), cAMP response element-binding protein (CREB) regulated transcription coactivator 2 (CRTC2)(*86*), peroxisome proliferator-activated receptor-γ (PPARγ)(*87*), and acetyl-CoA synthetase 1 (ACSS2)(*88*), amongst many other targets. The general effect of SIRT1 activation is to boost mitochondrial function and promote catabolism(*81, 89-91*).

1.4.3 KATs in energy metabolism

Consistent with the crucial role of KDACs on energy metabolism, KATs are also pivotal regulators of metabolism. Among them, KAT2A, also known as the general control of amino

acid synthesis 5 (GCN5), KAT2B, alternatively named p300/CBP associated factor (P/CAF), were demonstrated to play important roles in metabolism.

KAT2A is the only nuclear acetyltransferase reported to acetylate PGC-1α *in vivo* and *in vitro*, leading to the attenuation of the activity of PGC-1α, one of the main mitochondrial biogenesis and function regulators(*92*). The ability of KAT2A to inhibit PGC-1α, can be enhanced by either SIRT6 (*93*) or insulin-induced cyclin D1 (CCND1)/ cyclin-dependent kinase 4 (CDK4) activity(*94*), by deacetylating or phosphorylating KAT2A in the liver, respectively. This KAT2A-mediated inhibition of PGC-1α in the liver reduces gluconeogenesis. In contrast, KAT2A-mediated repression of PGC-1α is reversed either with the repression of SIRT6, following glucagon-cAMP-protein kinase A (PKA) signaling(*93*), or with the induction of CBP/p300-interacting transactivator 2 (CITED2), found to bind KAT2A and block its interaction with PGC-1α(*95*). On a whole body level, KAT2A can inhibit PGC-1α-mediated energy expenditure, which is further fine-tuned by NCOA3(*96*). Specifically, NCOA3 binds to and activates the *Kat2a* promoter thereby increasing KAT2A expression, leading to PGC-1α acetylation and reduced mitochondrial energy expenditure in muscle and brown adipose tissue(*96*). Aside from KAT2A, KAT2B was also reported to regulate gluconeogenesis in the liver, however, the observed effects are controversial as both inhibitory(*97*) and stimulatory(*98*) outcomes have been demonstrated. One study suggested that KAT2B is recruited, along with WD repeat-containing protein 5 (WDR5), to gluconeogenic genes to induce histone H3 acetylation, resulting in gluconeogenesis(*98*). In contrast, another study found that KAT2B could acetylate and induce PGC-1α proteasomal degradation, prohibiting the gluconeogenic effect of PGC-1α(*97*). The discrepancy between these findings will require further investigation.

Considering the embryonic lethality of a germline *Kat2a*-deficiency(*99*), creating *Kat2a* and *Kat2b* tissue-specific deficient mouse lines would help to tease out the different and redundant roles of these KATs on a tissue-by-tissue basis. A more extensive examination of the tissue-specific expression levels of these GNATs under various physiological conditions, and if they potentially regulate each other, would also help to further elucidate the differences between KAT2A and KAT2B.

1.4.4 Importance of NAD⁺ for acetylation/deacetylation processes

It was first hypothesized that NAD^+ may act as the principal metabolite regulating protein deacetylation following the discovery that it is essential for the activity of sirtuins(*77*). This dynamic role of NAD^+ in the regulation of sirtuin activity has now been well-established(*100-103*), implying that the availability of NAD^+ for sirtuin-directed deacetylation has a robust

effect on the acetylation status of the proteome and consequently cellular metabolic homeostasis.

NAD^+ exists in different pools in cells. Experimental evidence concerning the exchange of NAD^+ between the nucleus and cytosol is lacking, nonetheless these two pools have been classically considered to be relatively homogenous(104, 105). However, since neither NAD^+ nor NADH can diffuse through membranes(106, 107), the subcellular translocation and localized synthesis of NAD^+ using precursors, such as NAM or NAM mononucleotide (NMN), likely govern subcellular NAD^+ pool dynamics (Figure 1.5)(108, 109). This is supported by the finding that mice deficient in the nuclear NMNAT1 enzyme, important for nuclear NAD^+ synthesis from NAM or NMN, are embryonic lethal, indicating that cytosolic or mitochondrial NAD^+ synthesis by NMNAT2 or NMNAT3 cannot compensate for the loss of nuclear NAD^+ synthesis during embryogenesis(110). Interestingly, the mitochondrial NAD^+ pool is also separated from the rest of the cell(109, 111) and can be maintained even if cytosolic NAD^+ levels are perturbed(109, 112, 113). In fact, evidence is accumulating that mitochondria possess their own machinery for NAD^+ production(107, 109, 111) and can therefore be, at least acutely, self-sufficient. Furthermore, the NAD^+ ratio between the nucleo-cytosolic and mitochondrial pools appears to be tissue-specific. For instance, mitochondrial NAD^+ constitutes 70% of the total cellular NAD^+ in cardiac myocytes(112), 50% in neurons(114) and 30-40% in hepatocytes and astrocytes(114, 115). Interestingly, changes in exogenous NAD^+ were shown to influence mitochondrial NAD^+ levels more than the cytoplasmic NAD^+ pool(116). Yet despite this surprising observation, the mitochondrial and cytoplasmic pools are still inherently interconnected through the exchange of NADH and NAD^+ between the cytosol and the mitochondria via the malate-aspartate and glycerol-3-phosphate shuttles.
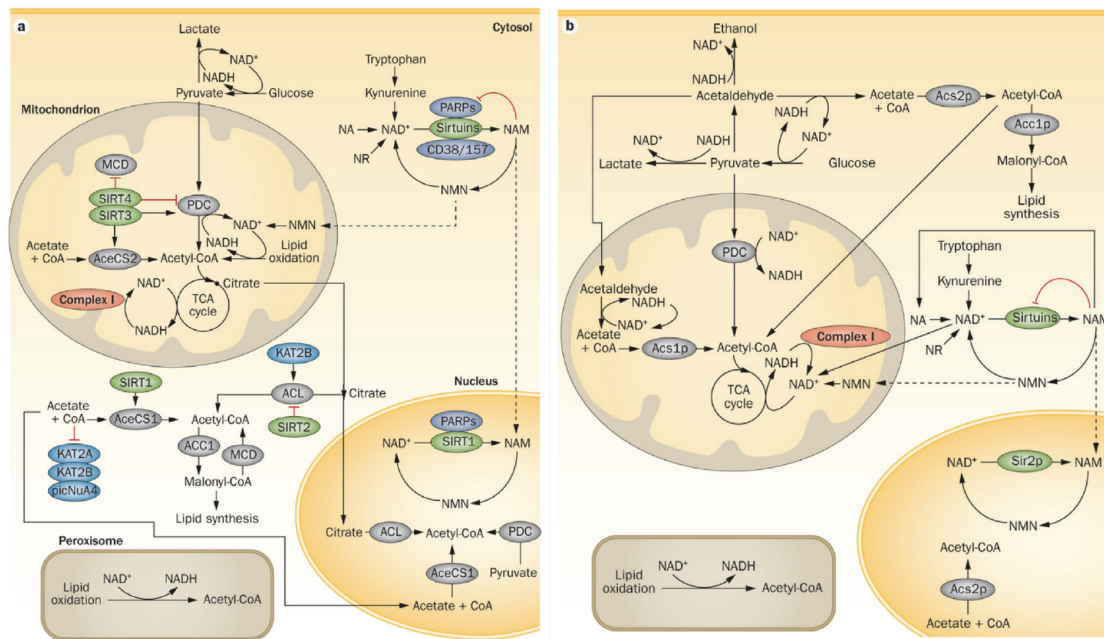
Figure 1. 5 NAD⁺ and acetyl-CoA subcellular distributions in mammals and yeast

A, In mammals, *de novo* NAD⁺ synthesis occurs in the cytosol, whereas NAD⁺ salvage from NAM or NMN can take place in cytosol, nucleus and mitochondria. PARPs and CD38/157 compete with surtuins for NAD⁺, the availability of which also depends on the cytosolic or mitochondrial conversion of NAD⁺ to NADH. Acetyl-CoA generated from glycolysis and lipids in the cytosol can contribute to the mitochondrial acetyl-CoA pool. In the cytosol, acetyl-CoA can be produced from acetate by AceCS1 or from citrate by ACL. Cytosolic acetyl-CoA can be transformed into malonyl-CoA by ACC1, during lipid synthesis. Malonyl-CoA can be reconverted to acetyl-CoA by MCD. Citrate and acetate from cytosol can diffuse into the nucleus, where they are converted to acetyl-CoA by ACL and AceCS1, respectively. Nuclear PDC also contributes to the nuclear acetyl-CoA pool. **B**, In yeast, pyruvate can be converted to acetyl-CoA via the PDC or it can be converted to acetaldehyde, then acetate and finally to acetyl-CoA in mitochondria or the cytosol. Acetate to acetyl-CoA conversion is catalysed by Acs1p in the mitochondrion or Acs2p in the cytosol. In mitochondria, acetyl-CoA enters the TCA cycle whereas in the cytosol acetyl-CoA is used by Acc1p in the first step of lipid synthesis. Unlike mammals, in yeast, lipid oxidation is restricted to the peroxisome. Yeast lacks ACL and MCD orthologues so they cannot produce acetyl-CoA from citrate or malonyl-CoA. Pathways that need further validation are indicated by dashed lines. Sirtuins are shown in green, KATs in blue, enzymes affecting acetyl-CoA levels in grey and non-sirtuin NAD⁺-consuming enzymes in black. ACL, ATP-citrate lyase; ACSS1 and ACSS2 or Acs1p and 2p, acetyl-CoA synthetases 1 and 2; ACC1 or Acc1p, acetyl-CoA carboxylase; ETC, electron transport chain; KAT, lysine acetyltransferase; MCD, malonyl-CoA decarboxylase; NA, nicotinic acid; NAD⁺, nicotinamide adenine dinucleotide; NAM, nicotinamide; NMN, NAM mononucleotide; NR, nicotinamide riboside; PARP, poly ADP-ribose (PAR) polymerase; PDC, pyruvate dehydrogenase complex; SIRT, sirtuin; Sir2p, sirtuin 2; TCA cycle, tricarboxylic acid cycle.

Overall, the dynamic cellular ratio of oxidized to reduced forms of NAD⁺ molecules is governed by multiple reactions involving the interconversion of NAD⁺ and NADH (Figure 1.5). Within the cytosol, glycolysis of glucose into two pyruvate molecules generates two NADH molecules, which can be reoxidized by lactate dehydrogenase in the cytosol or by the electron transport chain (ETC) in the mitochondria. Within the mitochondria, the pyruvate

dehydrogenase complex (PDC) converts a single pyruvate molecule into acetyl-CoA, producing one molecule of NADH. This acetyl-CoA molecule then enters the tricarboxylic acid (TCA) cycle to generate three more molecules of NADH and one molecule of $FADH_2$, which pass on their electrons to the ETC to produce ATP.

Both the *de novo* biosynthesis and salvage pathways contribute to intracellular NAD^+ formation (Figure 1.6)(*104, 117-119*). The *de novo* synthesis pathway, starting from the essential amino acid tryptophan, produces NAD^+ in the cytosol, the location for all enzymes catalyzing this process(*104, 120*). NAD^+ can also be synthesized from precursor molecules, such as, NAM or nicotinamide riboside (NR), through common components of the NAM salvage pathway(*118*) or from nicotinic acid (NA), which is converted to NAD^+ through the Preiss-Handler pathway (Figure 1.6).
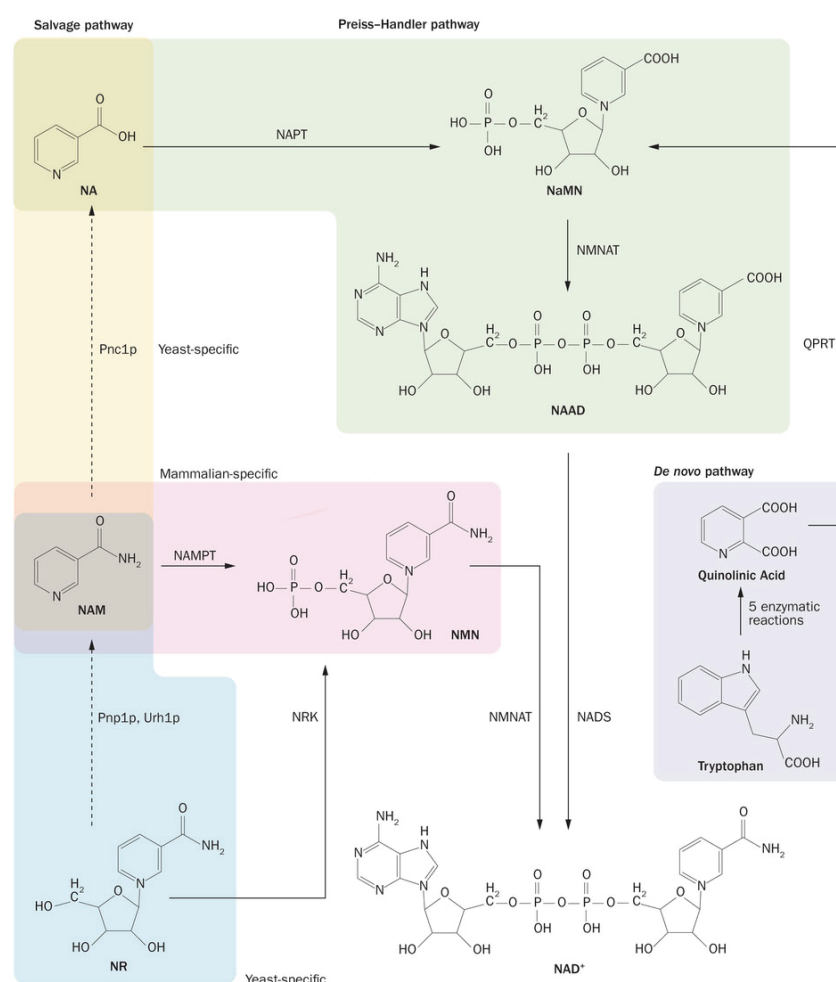
Figure 1. 6 Pathways leading to the NAD^+ production

De novo synthesis of NAD^+ begins with tryptophan (purple) and includes five enzymes (not represented on the figure): tryptophan 2,3-dioxygenase (hepatic) or indoleamine 2,3-dioxygenase 1 (nonhepatic), arylformamidase, kynurenine 3-mono oxygenase, kynureninase and 3-hydroxyanthranilic acid dioxygenase. NA leads to NAD^+

synthesis through the Preiss–Handler pathway (green), and shares the same intermediate, NaMN, as de novo synthesis. In yeast, NAM is converted into NA by the nicotinamidase Pnc1p (yellow), while in mammals NAM leads to the production of NMN, catalysed by the enzyme NAMPT (pink). NR is converted to NMN in both mammals and yeast; however, yeast can also convert NR to NAM via the enzymes Urh1p and Pnp1p (blue). Reactions not catalysed/present in mammals indicated by dashed lines. Abbreviations: NA, nicotinic acid; NAD^+, nicotinamide adenine dinucleotide; NADS, NAD^+ synthase; NAM, nicotinamide; NAMPT, nicontinamide phosphoribosyltransferase; NAPT, nicotinic acid phosphoribosyltransferase; NMN, NAM mononucleotide; NMNAT, nicotinamide mononucleotide adenylyl transferase; NR, nicotinamide riboside; NRK, nicotinamide riboside kinase; Pnc1p, pyrazinamidase/nicotinamidase 1; Pnp1p, purine nucleoside phosphorylase; QPRT, quinolinate phosphoribosyltransferase; Urh1p, uridine hydrolase.

Irrespective of the precursor used for NAD^+ biosynthesis, NAD^+ salvage is the most important process for maintaining NAD^+ levels, making the rate-limiting enzyme for this pathway, nicotinamide phosphoribosyltransferase (NAMPT)(103), crucial for cellular metabolism. Specifically, NAMPT metabolizes NAM into NMN(121). NMN can then be converted into NAD^+ by NMN adenylyltransferase 1 (NMNAT1) in the nucleus,(122, 123) NMNAT2 in the cytosol and Golgi(108, 123) or NMNAT3 in the cytosol and mitochondria (Figure 1.7)(108, 109, 124). The expression levels and the requirement for NAMPT varies considerably between different tissues in mice, with the highest levels detected in brown adipose tissue (BAT), liver and kidney(125). Accordingly, NAMPT overexpression increases NAD^+ levels followed by SIRT1 activation(109, 126-128). In contrast, Nampt-deficiency reduces NAD^+ levels in mice(125).
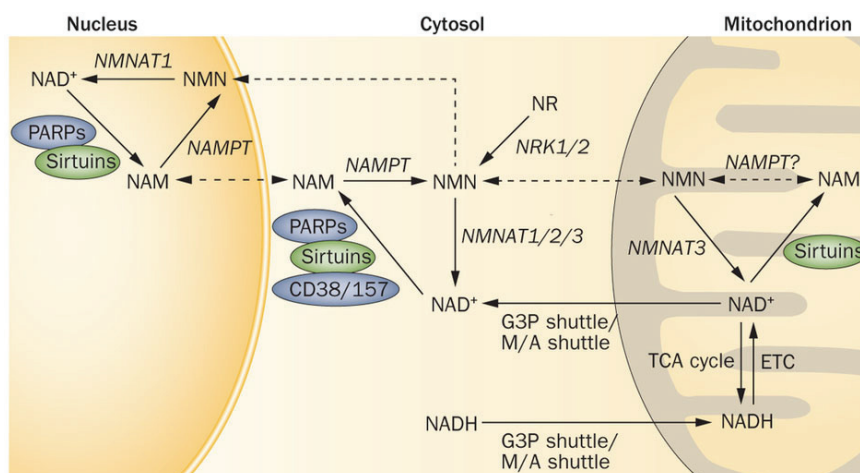
Figure 1. 7 Cross-compartmental junctions in cellular NAD^+ metabolism

In the nucleus, NAM and NMN are likely to be transported into the mitochondrial and nuclear compartments from the cytosol. Specific NMNAT isoforms and NAMPT are required in each compartment for the salvage of NAD^+; however, the presence of NAMPT in the mitochondria is unconfirmed. In addition to the import of reducing equivalents of NADH by the malate–aspartate and glyceraldehyde 3-phosphate shuttles, the TCA cycle also contributes to the overall level of mitochondrial NADH. The reducing power of NADH is then used to make ATP by the electron transport chain, producing NAD^+ and ATP. Pathways that need further validation indicated by dashed

lines. Abbreviations: ETC, electron transport chain; G3P, glucose-3-phosphatase; M/A, malate–aspartate; NAD^+, nicotinamide adenine dinucleotide; NAM, nicotinamide; NAMPT, nicontinamide phosphoribosyltransferase; NMN, NAM mononucleotide; NMNAT, nicotinamide mononucleotide adenylyl transferase; NR, nicotinamide riboside; NRK, nicotinamide riboside kinase; PARP, poly ADP-ribose (PAR) polymerase; TCA, tricarboxylic acid.

Interestingly, of all the NAD^+ precursors, NR appears to be the only metabolite transported directly into the cell, in both yeast and mammalian cells. This was hypothesized following observations that NMN must first be converted to NR, in the periplasmic space by Pho5p in yeast(*129*) and through an unknown mechanism in mammals(*130*), before it is transported to the cytosol. NR can then be converted back to NMN, through several pathways for NAD^+ biosynthesis in yeast(*131*), while in mammalian cells it is converted to NMN through phosphorylation by the NR kinases 1 and 2 (NRK1 & 2)(*132*). Since the mitochondrial compartment lacks NRK activity(*130*), it is likely that NR is converted into NMN in the cytosol, which is then supplied to other compartments, such as the mitochondria (Figure 1.7)(*108, 109*).

The beneficial effects of promoting NAD^+ biosynthesis, either by enhancing the activity of enzymes involved in NAD^+ production or via administration of NAD^+ precursors, on sirtuin activity and metabolic homeostasis have been established in numerous studies(*101, 103, 131, 133-136*).

1.5 Control of MuSCs function through protein acetylation

1.5.1 Linking histone acetylation and MuSCs function

Despite the fact that transcriptional regulation is important in MuSCs function, epigenetic control also plays a crucial role during myogenesis. Chip-seq approaches provided direct evidence that with ageing, epigenetic changes accumulate and may lead to functional decline in quiescent MuSCs(*137*). Recently, the role of the deacetylase SIRT1 in skeletal MuSCs has been brought to light(*55*). It was reported that transition of MuSCs from quiescence to proliferation requires metabolic reprogramming, decreasing the activity of the histone deacetylase SIRT1. This led to the elevated H4K16 acetylation levels and activation of muscle genes transcription. As the acetylation event is reversible, there are possibly KATs that could reverse the deacetylation catalyzed by SIRT1 and enhance MuSCs differentiation. In fact, it was shown that upon muscle differentiation, p300 is enriched at distinct *Myod* regulatory elements, resulting in an increase of histone acetylation correlating with *Myod* expression(*138*). In spite of many reports on the impacts of histone acetylation during MuSCs differentiation or self-renewal, only a limited number of studies investigated the role of the acetylation of transcription factors in MuSCs function.

1.5.2 KAT2B and p300/CBP in muscle differentiation

Histone acetyltransferases (HATs) are considered to play a crucial role in the transcriptional activation of DNA that is tightly packed in the chromatin. Biochemical experiments provided evidence that hyperacetylated histones accumulate within transcriptionally active chromatin, whereas hypoacetylated histones accumulate within transcriptionally silenced chromatin. P300/CBP and KAT2B coactivators have acetyltransferase activities and regulate transcription, cell cycle progression and differentiation. KAT2B can associate with P300/CBP and MYOD to form a multimeric protein complex, which has been proven to be critical for MYOD-directed transcription and myogenic differentiation(*139*). In muscle specific differentiation, KAT2B and P300/CBP both function as coactivators, but contribute differentially to the MYOD-directed transcriptional stimulation, with KAT2B providing the acetyltransferase function and P300/CBP bringing all components of the complex together(*139*). Furthermore, KAT2B-mediated acetylation of MYOD is proven to be functionally relevant as a non-acetylatable MYOD mutant loses transcriptional and myogenic potency(*140*).

1.5.3 Role of KAT2A in stem cells

Similar to KAT2B, KAT2A also physically interacts with p300/CBP(*141*), but mice lacking p300/CBP showed phenotypes different from those lacking KAT2A, which suggest that function of KAT2A is unique and not supplementary to p300/CBP(*142*). The conclusion from these phenomena is that different histone acetyltransferases are required as cofactors for specific development processes. In recent years, the role of KAT2A in other tissues has been gradually deciphered. Mice with a conditional *Kat2a* allele were created as well as mice with a knock-in of a mutant *Kat2a* lacking catalytic activity, both exhibiting a neuronal phenotype with absence of apoptosis(*143*). KAT2A was also identified as being essential for normal embryonic stem cell pluripotency(*144*). More recently, the loss of KAT2A has been reported to accelerate cerebellar degeneration in a mouse neurodegeneration model(*145*). Apart from the interaction between KAT2A and p300/CBP, the importance of the interaction of KAT2A with other cofactors in development processes is still not very clear. KAT2A was shown to be an important transcriptional cofactor for *Myc in vivo* with an impact on neural stem cell differentiation(*146*), reflected by an upregulation of neuronal differentiation genes and a downregulation of a cluster of genes that inhibit differentiation in both *N-myc*- and *Kat2a*-KO mice. Despite this evidence of KAT2A regulating stem cell function, the role of KAT2A as an acetyltransferase in MuSCs is still unknown.

Chapter 2. Rejuvenation of adult stem cell by NAD$^+$ repletion

Adapted from:

Zhang, H., Ryu, D., Wu, Y., Gariani, K., Wang, X., Luan, P., D'Amico, D., Ropelle, E. R., Lutolf, M. P., Aebersold, R., Schoonjans, K., Menzies, K. J.[#] & Auwerx, J.[#] NAD$^+$ repletion improves mitochondrial and stem cell function and enhances life span in mice. *Science*, 352 (6292): 1436-1443 (2016).

2.1 Abstract

Adult stem cells (SCs) are essential for tissue maintenance and regeneration yet are susceptible to senescence during aging. We demonstrate the importance of the amount of the oxidized form of cellular nicotinamide adenine dinucleotide (NAD^+) and its impact on mitochondrial activity as a pivotal switch to modulate muscle SC (MuSC) senescence. Treatment with the NAD^+ precursor nicotinamide riboside (NR) induced the mitochondrial unfolded protein response (UPR^{mt}) and synthesis of prohibitin proteins, and this rejuvenated MuSCs in aged mice. NR also prevented MuSC senescence in the *mdx* mouse model of muscular dystrophy. We furthermore demonstrate that NR delays senescence of neural SCs (NSCs) and melanocyte SCs (McSCs), and increased mouse lifespan. Strategies that conserve cellular NAD^+ may reprogram dysfunctional SCs and improve lifespan in mammals.

2.2 One sentence summary

NR rejuvenates stem cells and improves mouse lifespan

2.3 Introduction

In adults, tissue homeostasis is highly dependent on stem cell (SC) function. These adult SCs are not only essential in continuously-proliferating tissues, like the hematopoietic, intestinal and skin systems, but also in normally quiescent tissues, such as skeletal muscle and brain that require regeneration after damage or exposure to disease (*147*). Aging is accompanied by a decline in adult SC function, termed SC senescence, which leads to loss of tissue homeostasis and regenerative capacity (*148, 149*).

Homeostasis and regeneration of skeletal muscle depends on normally quiescent muscle stem cells (MuSCs), which are activated upon muscle damage to expand and give rise to differentiated myogenic cells that regenerate damaged muscle fibers (*1, 65*). These responses are blunted in aged muscle, probably because of reduced number and function of MuSCs (*150-152*). In aging, MuSC dysfunction may be caused by extrinsic signals (*4, 153*) or intrinsic cellular senescence signaling pathways (*154*) or both. One general regulator of cellular senescence, cyclin-dependent kinase inhibitor 2A (CDKN2A, p16^{INK4A}), shows increased expression in geriatric MuSCs, which causes permanent cell cycle withdrawal and senescence of MuSCs in very old mice (28-32 months of age) (*154*). However, reductions in MuSC number and function can already be observed before this stage (*150, 154*), indicating that MuSC senescence may be initiated at an earlier time point. Pre-geriatric mice, approximately two years old, can exhibit features of MuSC senescence (*5, 7, 152, 155, 156*). However, the early mechanisms that instigate MuSC senescence are still largely unknown.

One of the hallmarks of organismal aging is the appearance of mitochondrial dysfunction (*148, 149*). Mitochondrial dysfunction, induced by calorie-dense diets or aging, can result from depletion of NAD$^+$ (the oxidized form of nicotinamide adenine dinucleotide), whereas NAD$^+$ repletion, with precursors such as nicotinamide riboside (NR), can reverse this process (*101, 157-160*). Stem cells are thought to rely predominantly on glycolysis for energy, a process that would reduce cellular concentrations of NAD$^+$ (*161*). Mitochondrial function is linked to SC maintenance and activation (*55, 162-164*), yet its role in senescence is unknown.

2.4 Results

2.4.1 Mitochondrial dysfunction is a biomarker of MuSC senescence

To identify the role of mitochondrial function in SCs we compared MuSCs from young and aged mice to investigate SC senescence. To identify the principal mechanisms initiating MuSC senescence, we examined publically available MuSC gene expression datasets from young (~3 months) and aged (~24 months) mice using gene set enrichment analysis (GSEA; GEO dataset IDs: GSE47177(*7*), GSE47104(*155*) and GSE47401(*152*)). Enrichment scores of young *versus* aged datasets revealed upregulation of senescence pathways and downregulation of cell cycle pathways with age (Figure 2. 1A, and figure 2. S1, A and B). This is consistent with the idea that irreversible cell cycle arrest is a primary marker of cellular senescence (*148, 149*). In all three datasets, tricarboxylic acid (TCA) cycle and oxidative phosphorylation (OXPHOS) pathways were among the most downregulated pathways in aged MuSCs (Figure 2. 1A, and figure 2. S1, A and B). Analysis of gene ontology (GO) terms that were significantly (Gene Set Enrichment Analysis; FWER $p<0.05$) downregulated in aged MuSCs, further demonstrated links to mitochondrial function (figure 2. S1C). Common downregulated genes during aging showed a substantial overlap (113 genes; 11.59%) with mitochondrial genes (*165*) (Figure 2. 1B), in contrast to the minimal (11 genes; 1.92%) overlap amongst common upregulated genes (figure 2. S1D). Among the 113 downregulated mitochondrial genes in aged MuSCs, 41.6% were related to the TCA cycle and OXPHOS (figure 2. S1E), which is higher than their percent composition of the whole mitochondrial proteome (~14%)(*166, 167*). This indicates a dominant decline in expression of mitochondrial respiratory genes in aged MuSCs. The reduction in mitochondrial OXPHOS and TCA cycle genes was consistent for all independent datasets (figure 2. S1, F and G). We isolated primary aged and young MuSCs and confirmed reduced abundance of OXPHOS and TCA cycle transcripts (Figure 2. 1C), and reduced oxidative respiration rates in both freshly isolated (Figure 2. 1D) and cultured MuSCs (figure 2. S1H). MuSC mitochondrial dysfunction in aged mice was further confirmed by the loss of mitochondrial membrane potential (Figure 2. 1E) and a reduction in cellular ATP concentrations (Figure 2.

1F). Several important markers and regulators of the UPR^{mt}, a stress response pathway that mediates adaptations in mitochondrial content and function, were downregulated in aged MuSCs (figure 2. S1F and Figure 2. 1G). Despite the absence of consistent changes in cyclin-dependent kinase inhibitor 2A (CDKN2A) (figure 2. S1I) or mitogen-activated protein kinase 14 (MAPK14; p38) pathways, previously reported to regulate MuSC senescence, expression of cell cycle genes was decreased and expression of genes encoding the senescent proinflammatory secretome was increased (figure 2. S1, I-K). The reduction in cell cycle signaling was accompanied by increased expression of genes in the cyclin-dependent kinase inhibitor 1 (CDKN1A; p21^{CIP1})-mediated pathway (figure 2. S1K), suggesting that early senescence in MuSCs may involve CDKN1A.
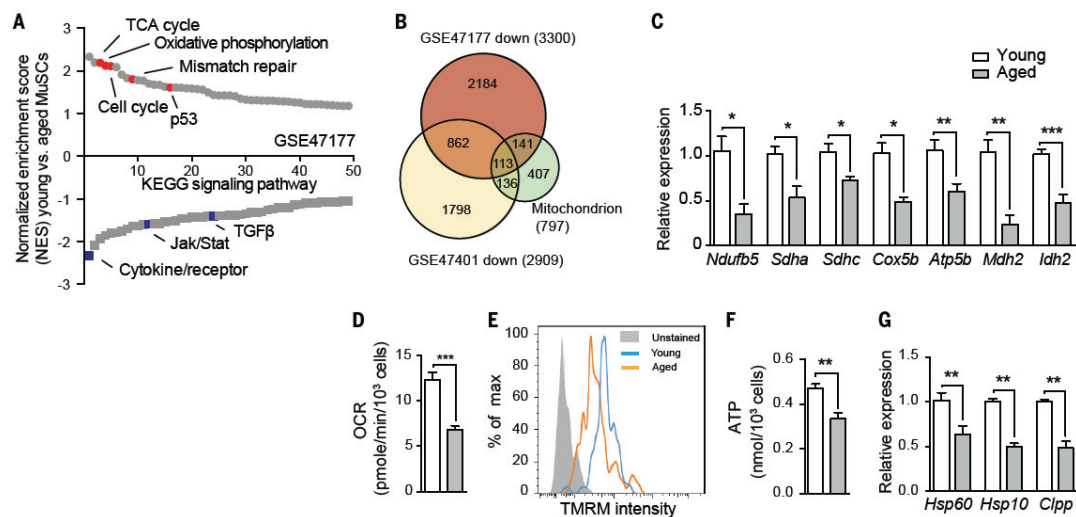
Figure 2. 1 Mitochondrial dysfunction in muscle stem cells (MuSCs) during aging

A, Gene-set enrichment analysis (GSEA) demonstrates up- and downregulated signaling pathways in MuSCs from two-year-old mice, compared to four-month-old mice. Analysis of microarray data from the publicly available GEO data set (accession number GSE47177) using Kyoto encyclopedia of genes and genomes (KEGG) enrichment. Signaling pathways were ranked on the basis of normalized enrichment scores (NESs); positive and negative NESs indicate down- or upregulation in aged MuSCs, respectively. Specific pathways related to MuSC function are highlighted in red and blue. **B**, Area-proportional Venn diagram representing 113 common genes between the significantly downregulated genes (P < 0.05) in MuSC transcriptomes originating from aged mice (GSE47177 and GSE47401 (*155*)), and genes from the human mitochondrial transcriptome (*165*). **C-G**, Young (1 month old) and aged (22-24 months old) C57BL/6J mice received a dietary supplement with NR for 6 weeks. **C**, qRT-PCR validation of transcriptional changes in mitochondrial genes of freshly sorted MuSCs. **D**, Oxygen consumption rate (OCR) in freshly isolated MuSCs, following 16h of recovery at 37°C. **E-F**, Mitochondrial membrane potential, measured by tetramethylrhodamine, methyl ester (TMRM) assay (H) and cellular ATP levels (I) in freshly isolated MuSCs. **G**, Relative gene expression for UPR^{mt} genes and cell senescence markers in freshly sorted MuSCs. Data are normalized to *36b4* mRNA transcript levels. All statistical significance was calculated by *Student*'s *t* test. All data are shown as mean ± s.e.m. *P < 0.05, **P < 0.01, ***P < 0.001. **C-D** and **F-G**, n=6; **E**, n=3 mice per group.

2.4.2 NAD⁺ repletion improves MuSC function in aged mice

Given the importance of NAD^+ concentrations in the control of mitochondrial function (*101, 104*), we examined the potential of NAD^+ repletion to improve MuSC numbers and muscle function in aged mice. Amounts of NAD^+ in freshly isolated MuSCs were lower in those isolated from aged mice and 6 weeks of NR treatment increased NAD^+ concentration in MuSCs from young and old mice (Figure 2. 2A). Amounts of NADH were relatively stable (figure 2. S2A). Muscle from aged mice contained fewer MuSCs (Figure 2. 2, B and C and figure 2. S2, B and C). However, NR treatment increased MuSC numbers in young and old mice (Figure 2. 2, B and C and figure 2. S2, B and C). The increase in MuSC numbers was confirmed with paired box protein Pax-7 (PAX7) staining, a known MuSC marker (*65*) (Figure 2. 2D and figure 2. S2, D and E). The effect of NR in young or aged mice appeared not to result from changes in muscle or body mass, as these measures remained comparable among all groups over the short treatment period (figure 2. S2, F to I). NR treatment also enhances muscle function in aged animals through an independent mechanism acting directly on the muscle fibers (*101*), as was apparent from improvements in maximal running times and distances, along with limb grip strength in aged mice (Figure 2. 2, E to G). Young animals showed no such changes (figure 2. S2, J to L).
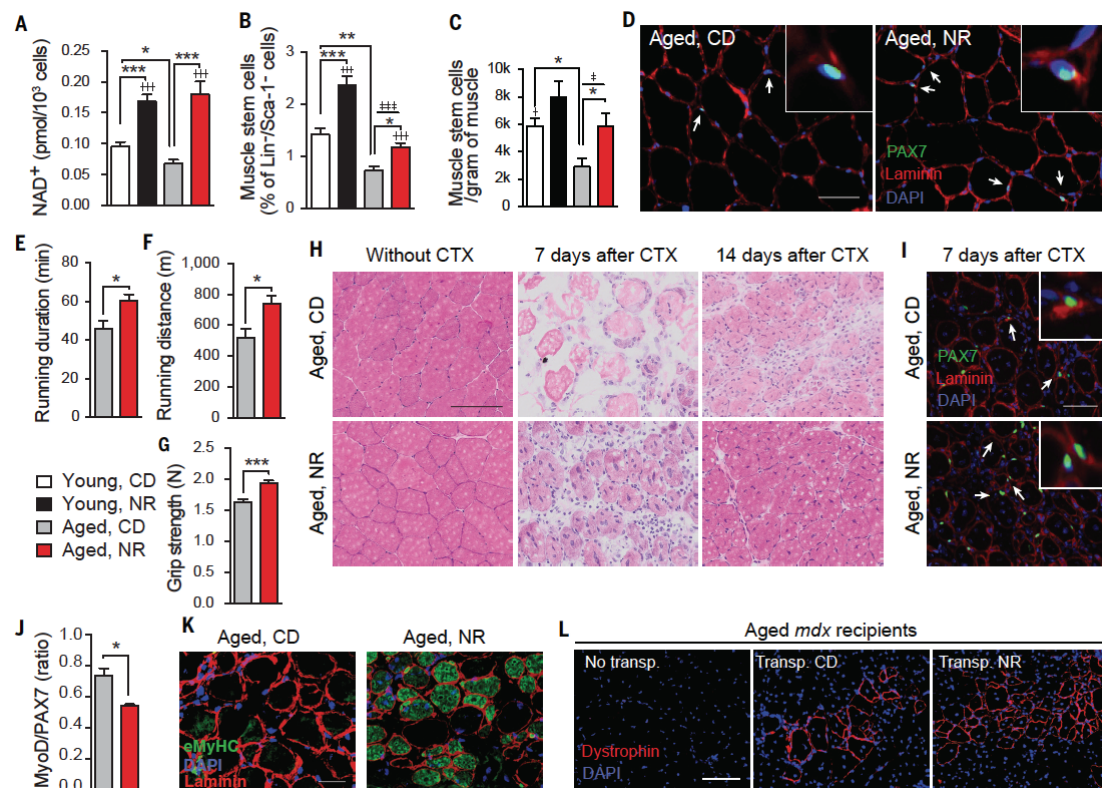
Figure 2. 2 Improved muscle stem cell numbers and muscle function in NR-treated aged mice

Young (3 months old) and aged (22-24 months old) C57BL/6J mice received chow diet (CD) or CD supplement with NR for 6 weeks. All results are compared to age-matched mice given a control diet. **A**, NAD$^+$ concentrations in freshly isolated MuSCs. **B-C**, Percentage of FACS quantified CD34$^+$/integrin α7$^+$/Lin$^-$/Sca-1$^-$ MuSCs relative to the total Lin$^-$/Sca-1$^-$ cell population (B) or to muscle weight (C). **D**, Representative images of PAX7 and laminin immunostained tibialis anterior (TA) muscle. Arrows point to PAX7-positive SCs. 20 x 20µm insets show a single MuSC. Scale bar = 50µm. **E-G**, Comparison of maximal running duration (E), running distance (F) and grip strength (G) in NR-treated aged mice. **H**, H&E stained TA tissue-sections from NR-treated aged mice 7 and 14 days after cardiotoxin (CTX)-induced muscle damage. Scale bar = 100µm. **I**, Images of PAX7 and laminin immunostained TA muscle cross-sections taken from NR-treated aged mice 7 days after CTX-induced muscle damage. Arrows point to PAX7-positive MuSCs. 20 x 20µm insets show a single MuSC. Scale bar = 50µm. **J**, Quantification of the signal intensity ratio between MYOD1 and PAX7 in PAX7-positive MuSCs, performed on sections isolated 7 days after muscle damage in aged mice. Images not shown. **K**, Newly regenerated muscle fibers, stained by embryonic myosin heavy chain (eMyHC) 7 days after muscle damage in aged mice. Scale bar = 50µm. **L**, Dystrophin immunostaining of TA muscle sections in aged (16 months old) *mdx* mice 4-weeks after receiving transplantations of MuSCs isolated from control or NR-treated aged C56BL/6J donors. Scale bar = 100µm. All statistical significance was calculated by *Student*'s *t* test or two-way ANOVA. All data are shown as mean ± s.e.m. *P < 0.05, **P < 0.01, ***P < 0.001. Main effects for treatment or age are denoted as † or ‡, respectively, with interactions denoted as ε. **A**, n = 6 mice; **B-D** and **H-K**, n = 3-6 mice per group; **E-G**, n = 10 control diet; n = 7 NR-treated mice; **L**, n = 12 donor mice, n = 3 recipient mice for each treatment. Corresponding young control data for Fig 2, E to I are found in S2, J to O, respectively.

Impairments in muscle regeneration efficiency have been linked to the decline in MuSC function in aged mice (*150*). We therefore examined the benefits of NR on muscle regeneration with cardiotoxin (CTX)-induced muscle damage (*65*). NR treatment accelerated muscle regeneration in aged and young mice (Figure 2. 2H and figure 2. S2M). NR-induced improvements in regeneration were paralleled by increases in PAX7-stained MuSCs in aged mice (Figure 2. 2I and figure 2. S2N), but not in young mice (figure 2. S2, O and P). NAD$^+$ repletion also improved the stemness of the aged MuSCs, as demonstrated by a reduction in myoblast determination protein 1 (MYOD1)-stained PAX7 immunostained cells (Figure 2. 2J and figure 2. S2Q), as MYOD1 is a transcriptional factor that activates MuSC differentiation. 7 days after CTX-induced damage, NR-treated aged mice exhibited improvements in embryonic myosin heavy chain staining, a protein expressed in fetal and newly regenerating adult muscle fibers (*168*) (Figure 2. 2K). When MuSCs were transplanted from NR-treated or control aged mice into *mdx* mice (figure 2. S2R) (a mouse model of Duchenne muscular dystrophy that gradually loses MuSC function in aging due to the strain of continual muscle regeneration). MuSCs isolated from NR-treated donors more effectively replenished the MuSC compartment and stimulated myogenesis of dystrophin-positive myofibers when transplanted into either young or aged *mdx* recipients (figure 2. S2S and Figure 2. 2L, respectively). Thus, NR treatment can both improve muscle regeneration and MuSC transplantation efficiency.

The inappropriate accumulation of non-myogenic fibro-adipogenic progenitors (FAPs) and inflammatory cells have been reported to impair MuSC function and muscle regeneration, especially in aged muscle or with chronic damage, as found in *mdx* mice (*169*). NR treatment largely attenuated increases in FAP numbers 7 days after CTX induced damage in aged mice, but had no effect on FAPs under basal conditions (figure 2. S2, T to V). This effect is consistent with benefits to FAP clearance in later periods of muscle regeneration (*169*). NR also alleviated macrophage infiltration 7 days after CTX induced regeneration in aged mice (figure 2. S2, W and X).

2.4.3 NR prevents MuSCs senescence by improving mitochondrial function

To explain the improvements in MuSCs from aged animals after NAD^+ repletion, we examined effects on MuSC senescence. Freshly isolated MuSCs from NR-treated young and aged mice were immunostained for phosphorylation of histone 2A.X at Ser139 (γH2AX), a marker of DNA damage (*148*). γH2AX-stained nuclei were more abundant in MuSCs from aged animals, and staining was reduced with NR treatment (Figure 2. 3, A and B, young controls found in figure 2. S3, A and B). The reduction of the nuclear damage response in MuSCs was confirmed by a single-cell gel electrophoresis (comet) assay, a sensitive measure of DNA strand breaks as an indicator of senescence (Figure 2. 3C), as well as by staining for β-galactosidase, another classical senescence marker (*148*) (figure 2. S3C). A 6-hour NR treatment of late passage C2C12 myoblasts also reduced the expression of cell senescence and apoptosis markers (*170*) (Figure 2. 3D). MuSCs isolated from NR-treated aged mice showed enhanced potential to form myogenic colonies (Figure 2. 3E and figure 2. S3D). Thus, NR exerts a protective effect against intrinsic MuSC senescence.
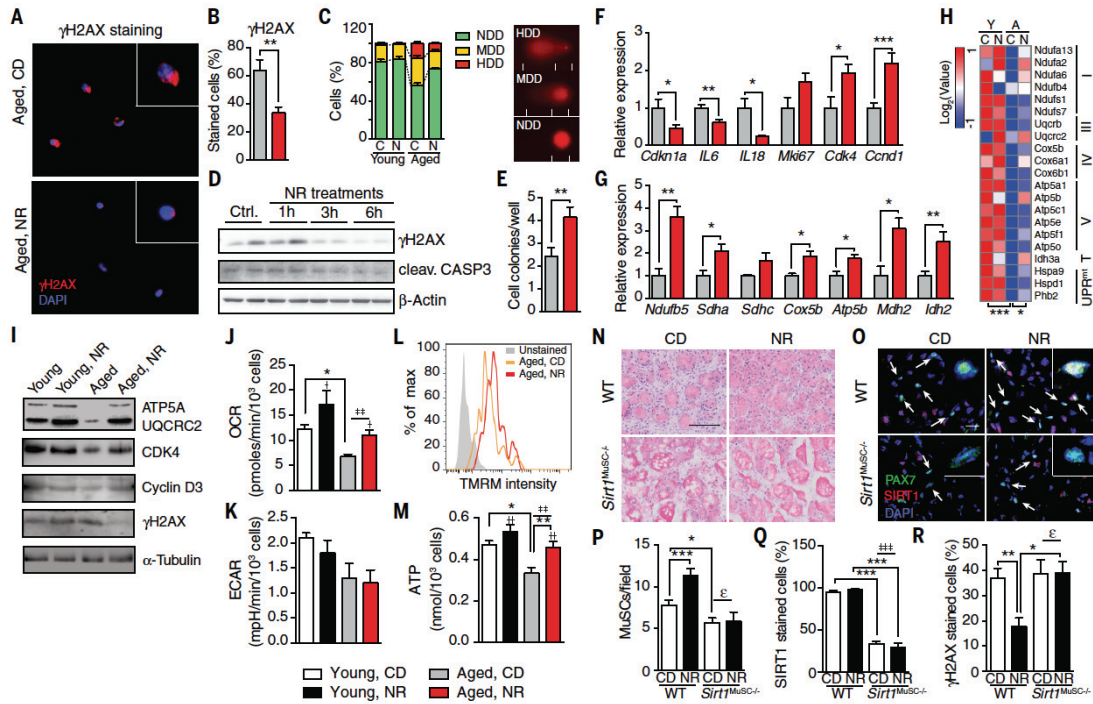
Figure 2. 3 NR treatment prevents MuSC senescence and improves mitochondrial function

Aged (22-24 months old) C57BL/6J mice or 8 months old SIRT1^MuSC-/- mice received a dietary supplement with NR for 6 weeks. All isolated MuSCs were freshly FACS sorted for assay. Most comparative data from young mice (1 month old) are presented in Figure 2. S3. **A**-**B**, Immunostaining (A) and quantification (B) of γH2AX staining in freshly sorted MuSCs from aged mice. 20 x 20μm insets show single MuSCs. **C**, Single-cell gel electrophoresis (comet) assay of MuSCs from aged mice. C, chow diet; N, NR treated. NDD, non-damaged DNA; MDD, moderately-damaged DNA; HDD, heavily-damaged DNA. **D**, Proteins levels in C2C12 myoblasts with NR treatment for 1, 3 or 6 hrs. **E**, Colony formation ability assay in isolated MuSCs. **F-G**, Quantification of transcript expression for cell cycle and inflammatory secretome genes (F) or OXPHOS and TCA cycle genes (G) in MuSCs. **H**, Abundance of proteins from MuSCs of young (Y) and aged (A) mice fed with a chow (C) or NR diet (N). Protein abundance was calculated using peptide intensity detected in the SWATH-MS map. Roman numerals indicate corresponding OXPHOS complexes. T, TCA cycle. **I**, Protein levels in MuSCs. **J-K**, OCR (J) and ECAR (K), in MuSCs following 16h of recovery at 37°C. **L**, Mitochondrial membrane potential, measured by a TMRM assay in MuSCs. **M**, Cellular ATP concentration in MuSCs. **N**, H&E stained TA muscle from wild type or SIRT1^MuSC-/- mice 7 days after cardiotoxin (CTX)-induced muscle damage. Scale bar = 100μm. **O-Q**, Representative images (O) and quantification of PAX7-positive MuSCs in random fields of view (160x160μm) (P) and the percentage of SIRT1-positive MuSCs (Q) in immunostained TA 7 days after CTX-induced muscle damage. Arrows point to PAX7-positive MuSCs. 20 x 20μm insets show a single MuSC. Scale bar = 50μm. **R**, Quantification of γH2AX-positive MuSCs in immunostained TA 7 days after CTX-induced muscle damage. All statistical significance was calculated by *Student*'s *t* test or two-way ANOVA. All data are represented as mean ± s.e.m. *$P < 0.05$, **$P < 0.01$, ***$P < 0.001$. Main effects for treatment or age are denoted as † or ‡, respectively, with interactions denoted as ε. **A**-**C**, and **N-R** n = 3-6 mice per group; **E**, n = 24 in each group; **F-G and J-M**, n = 6 mice per group; **H**, protein extracted and pooled from 6 mice in each group. Corresponding young control data found in Figs. 3, A, B, E, F, G and L are found in Figs. S3 A, B, D, E, F and G, respectively.

29

NR treatment of MuSCs from aged mice reduced abundance of mRNAs encoding CDKN1A and related proinflammatory proteins and increased the expression of cell cycle genes (Figure 2. 3F). These effects were not seen in non-senescent MuSCs from young animals (figure 2. S3E). NR treatment of MuSCs from aged animals increased expression of genes whose products function in the TCA cycle and OXPHOS (Figure 2. 3G), an effect that was not evident in young animals (figure 2. S3F). To quantify protein expression level at different conditions, we applied a new mass spectrometry-based proteomics technique, the sequential windowed acquisition of all theoretical fragment ion mass spectra (SWATH-MS)(*171*), which allows accurate and reproducible protein quantification across sample cohorts. Using this technique, we have quantified the expression changes of more than 1100 proteins in MuSCs across the various conditions. The SWATH-MS results show that a significant amount of proteins that function in OXPHOS and in the UPR^{mt} were decreased in MuSCs from aged animals (Figure 2. 3H). The overall amount of these same proteins was increased after NR supplementation (two-way AVOVA test, $P < 0.05$, Figure 2. 3H). Protein immuno-blotting of freshly isolated MuSCs from aged animals confirmed increased expression of proteins related to cell cycle and senescence that could not be detected by SWATH-MS (Figure 2. 3I).

MuSCs from NR treated aged mice exhibited increases in oxidative respiration (Figure 2. 3, J and K). NR-treated MuSCs from aged animals also showed increased mitochondrial membrane potential (Figure 2. 3L and figure 2. S3G) and increased abundance of ATP (Figure 2. 3M). To test whether this protective effect of NR on MuSC senescence relies on mitochondrial function we created a tamoxifen-inducible sirtuin-1 (SIRT1) MuSC-specific knockout mouse (SIRT1$^{MuSC-/-}$), by crossing SIRT1$^{flox/flox}$ mice with the Pax7^{creER} strain. SIRT1 is an NAD$^+$-dependent deacetylase that increases mitochondrial biogenesis (*101*). The beneficial effect of NR on muscle regeneration after CTX injection appeared attenuated in SIRT1$^{MuSC-/-}$ mice (Figure 2. 3N). Supporting this qualitative observation, SIRT1-knockout in MuSCs blocked the beneficial effects of NR on MuSC activation (Figure 2. 3, O to Q) and senescence (Figure 2. 3R and figure 2. S3H) 7 days after regeneration. These data indicate that NR inhibits MuSCs senescence by improving mitochondrial function in a SIRT1-dependent manner. This finding is consistent with a report linking FOXO3 activation, a SIRT1 target, to improved mitochondrial metabolism in hematopoietic stem cells (*172*).

2.4.4 Rejuvenating MuSCs by activating the UPR^{mt} and prohibitin pathways

We further explored how UPR^{mt} might regulate senescence by examining the role of prohibitins, a family of stress response proteins. Prohibitins sense mitochondrial stress and modulate senescence in fibroblasts in mammals (*173*), maintain replicative lifespan in yeast (*174*), and promote longevity in worms (*175*), animals that lack adult SCs. Expression of prohibitins, *Phb* and *Phb2,* was reduced in the bioinformatics analysis (figure 2. S1F), and in

freshly isolated aged MuSCs (figure 2. S4A). NR increased the expression of prohibitin proteins in C2C12 myoblasts (Figure 2. 4A) and transcripts in MuSCs of young and aged mice (Figure 2. 4B and figure 2. S4B). NR treatment was also shown to increase the expression of prohibitins concurrent to markers of UPR^{mt} and cell cycle (figure 2. S4C). Moreover, the overexpression of prohibitins, in the absence of NR, likewise increased UPR^{mt} and cell cycle protein expression (Figure 2. 4C). Demonstrating the dependency of the NR effect on prohibitins, improvements in UPR^{mt} and cell cycle protein expression were not observed with NR treatment following the knockdown of prohibitins (Fig 4D and figure 2. S4D). To confirm the regulation of prohibitins on cell cycle proteins and to explore the effect of prohibitins on MuSC function, *Phb* was depleted *in vivo* through an intramuscular injection of *shPhb* lentivirus (PHB and PHB2 are functional only as a heterozygous protein complex) (*176*). Impairment of muscle regeneration and a reduction in MuSC numbers was observed in sh*Phb* lentivirus injected mice, 7 days after CTX-induced muscle regeneration (Figure 2. 4, E and F). Quantifying these results, *Phb* knockdown is shown to block the NR induced increase of MuSCs number upon regeneration (Figure 2. 4, G and H). Importantly, *Phb* knockdown does not induce more MuSCs senescence in aged mice, yet prevents the beneficial effect of NR on MuSCs senescence (Figure 2. 4I and figure 2. S4E). Initiation of the UPR^{mt} by thiamphenicol also induced expression of prohibitins and cell cycle genes in C2C12 cells (figure 2. S4F). These results indicate that NR activates the UPR^{mt} and the prohibitin signaling pathway, as it inhibits MuSC senescence.
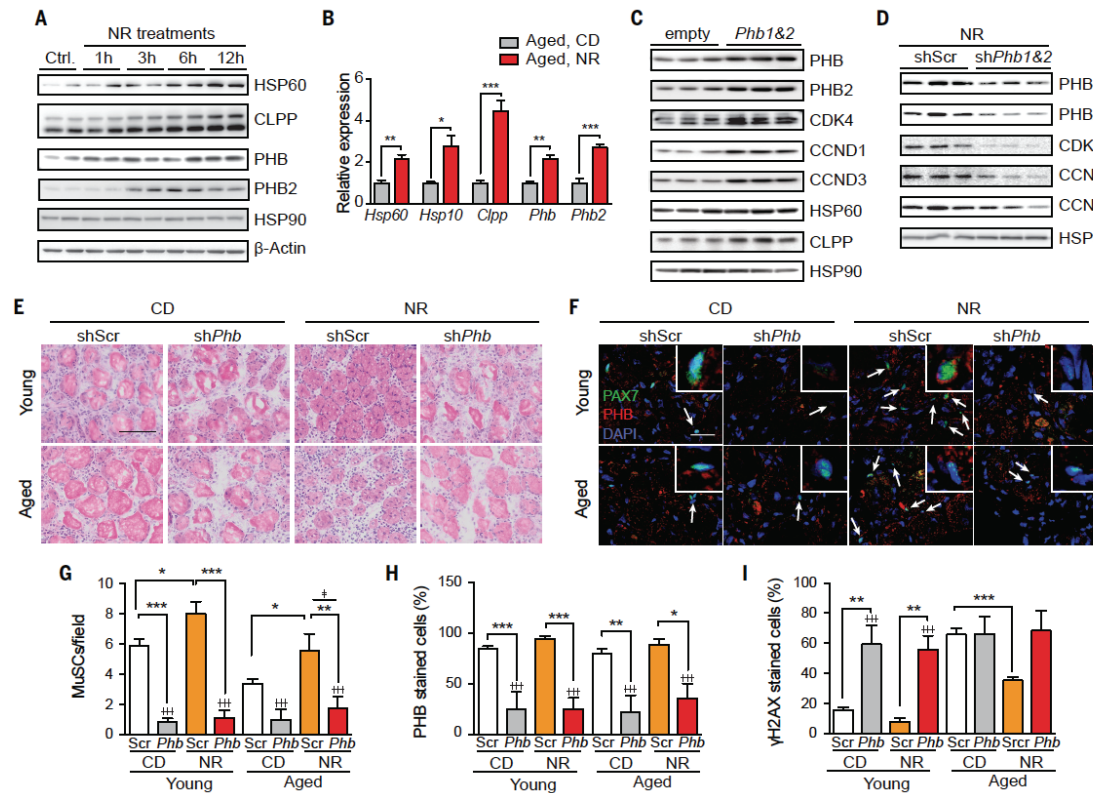
Figure 2. 4 Effects of NR on prohibitins, UPR^mt and MuSC senescence

A, Expression of HSP60, CLPP and prohibitins in C2C12 myoblasts upon NR treatment at the indicated time points. **B**, Quantification of transcript expression for UPR^{mt} and prohibitin genes in MuSCs from aged (22-24 months old) C57BL/6J mice following 6 weeks of chow or NR diets. **C**, Expression of prohibitins and cell cycle proteins in C2C12 myoblasts with the combined overexpression of *Phb* and *Phb2*. **D**, Expression of prohibitins and cell cycle genes with a 6-hour NR treatment in C2C12 myoblasts after a combined *Phb* and *Phb2* shRNA knockdown. **E**, H&E staining of TA muscle in NR-treated or intramuscular sh*Phb* lentivirus-injected C57BL/6J mice 7 days of after cardiotoxin (CTX)-induced muscle damage. Scale bar = 100μm. **F-H**, Representative images (F) and quantification of PAX7-positive MuSCs in randomly chosen field of views (160x160μm) (G) and the percentage of PHB-positive MuSCs (H) in immunostained TA muscle 7 days after CTX-induced muscle damage. Arrows point to PAX7-positive MuSCs. 20 x 20μm insets show single MuSC. Scale bar = 50μm. **I**, Quantification of γH2AX-positive MuSCs in immunostained TA muscle cross-sections taken from control and NR-treated mice 7 days after CTX-induced muscle damage. All statistical significance was calculated by *Student*'s *t* test or two-way ANOVA. All data are represented as mean ± s.e.m. *$P < 0.05$, **$P < 0.01$, ***$P < 0.001$. Main effects for treatment or age are denoted as † or ‡, respectively, with interactions denoted as ε. **B**, n = 6 mice; **E-I**, n=3 mice per group. Corresponding young control data found in Figure 2. 4B are found in figure 2. S4B.

2.4.5 NR reprograms senescence prone MuSCs in *mdx* mice

With continuous muscle regeneration, MuSCs in *mdx* mice are abnormally active at a young age, leading to MuSC depletion and dysfunction later in life. As a result, primary MuSCs isolated from 14-week-old *mdx* mice were more intensively and frequently stained with β-galactosidase and had a larger cell size than those of control mice (Figure 2. 5A and figure 2.

S5, A and B). Similar to the effect in aged animals, NR treatment of *mdx* mice increased MuSC numbers by ~1.8 fold *in vivo* (Figure 2. 5, B to D and figure 2. S5, C and D), as also confirmed by PAX7 immunostaining (figure 2. S5E). Along with the increase in MuSCs, there was an increase in regenerated muscle fibers following NR treatment (Figure 2. 5E and figure 2. S5F). We extended this analysis by examining the self-renewal capacity of *mdx* mouse MuSCs. The cellular redox ratio decreases as MuSCs differentiate (*177*), which can be detected by an increase in 450nm autofluorescence (*178*). In line with NR increasing the number of MuSCs in *mdx* mice, we found reduced autofluorescence from MuSCs isolated from these animals (Figure 2. 5, F to H). We performed β-galactosidase staining on primary MuSCs that had been isolated from *mdx* mice treated or without NR treatment *in vivo*, and were then further cultured with or without NR *in vitro*. MuSCs isolated from NR-treated mice were less prone to senescence (Figure 2. 5I and figure 2. S5G). When MuSCs isolated from control *mdx* mice were treated with NR *in vitro* there was also a reduction in senescence (Figure 2. 5I and figure 2. S5G). The inhibition of MuSCs senescence in NR-treated *mdx* mice was confirmed by the attenuation of. γH2AX and cleaved caspase-3 immunostaining (Figure 2. 5J). To evaluate MuSC function, CTX-induced muscle regeneration was examined in NR-treated *mdx* mice. Consistent with the prevention of MuSC senescence, muscle regeneration was improved with NR in both aged (Figure 2. 5K and figure 2. S5H) and young *mdx* mice (figure 2. S5I). We also examined the effect of NR on the FAP population and muscle regeneration in *mdx* mice. NR treatment increased MuSCs and reduced FAP numbers in basal conditions and 7 days after CTX-induced damage (figure 2. S5, J to L). Abnormal activation of FAPs in *mdx* mice contributes to fibrosis (*169*). *mdx* mice treated with CTX and then exposed to NR showed lower levels of macrophage infiltration 7 days after damage (figure 2. S5, M and N). Our results hence indicate a beneficial effect of NR on MuSC function and regeneration in *mdx* mice.
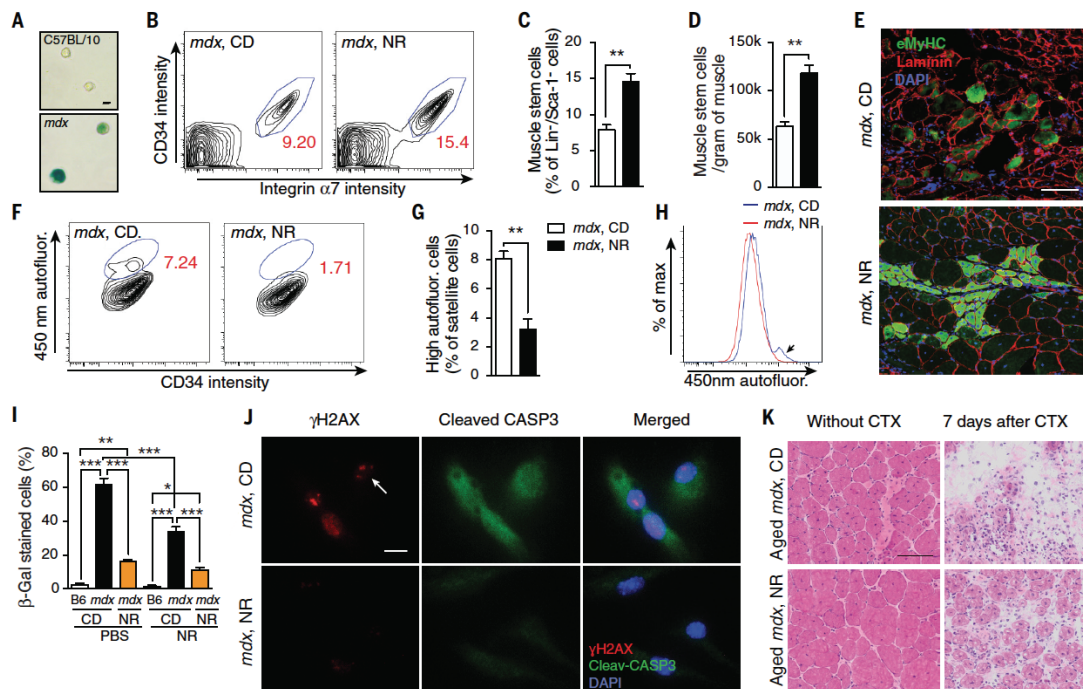
Figure 2. 5 Increased stem cell number and function in NR-treated *mdx* mice

mdx mice received a dietary supplement with NR for 10 weeks. All results were compared to *mdx* mice given a control diet. **A**, β-galactosidase staining of MuSCs isolated from C57BL/10SnJ or *mdx* mice and cultured *in vitro* for three generations. Scale bar = 10μm. **B-D**, FACS contour plots of Sca-1$^-$/Lin$^-$ cells isolated from muscle. Percentage of the CD34$^+$/integrin α7$^+$/Lin$^-$/Sca-1$^-$ MuSC populations are noted in red in contour plots (B), and quantified relative to the total Lin$^-$/Sca-1$^-$ cell population (C) or to muscle weight (D). **E**, Immunostaining of and eMyHC$^+$ fibers in tissue-sections of NR-treated *mdx* mice 7 days after CTX-induced muscle damage. **F-H**, FACS contour plots (F), quantification (G) and distribution (H) of MuSC autofluorescence as a measure of the relative NAD(P)H concentration upon UV light excitation. Autofluorescence emission was detected using 405/450 nm. Arrow in (H) points to the highly autofluorescent stem cell population. **I**, Quantification of β-galactosidase staining of FACS-sorted MuSCs from C57BL/6J (B6), untreated (*mdx*) or NR-treated *mdx* (*mdx* with NR) mice challenged with PBS or NR for 6 hours *in vitro*. **J,** Immunostaining showing γH2AX and cleaved caspase-3 in MuSCs cultured *in vitro* for three generations. Arrow points to a γH2AX-positive nucleus. Scale bar = 10μm. **K,** H&E staining of tissue-sections from NR-treated aged *mdx* mice (16 months old) with 7 days of recovery following CTX induced muscle damage. Scale bar = 100μm. All statistical significance was calculated by *Student*'s *t* test or one-way ANOVA. All data are represented as mean ± s.e.m. *$P < 0.05$, **$P < 0.01$, ***$P < 0.001$. **A-H** and **J-K**, n = 3-5 per treated group; I, n = 3 mice and n = 6 *in vitro* treatments. More than 500 cells were quantified in each condition.

2.4.6 NR attenuates senescence of neural stem cells and melanocyte stem cells and increases mouse lifespan

Aging is accompanied by a decline in the number and function of neural stem cells (NSCs) (*163*) and melanocyte stem cells (McSCs) (*179*). Therefore, to examine the generalized importance of NAD$^+$ homeostasis in somatic SCs, we assessed the effect of NR in NSCs from aged mice. NR increased proliferation as shown by 5-ethynyl-2-deoxyuridine **(**EdU) and antigen Ki-67 (Ki67) staining, and induced neurogenesis indicated by doublecortin (DCX)

staining, in both the subventricular zone (SVZ) (Figure 2. 6, A to D) and the dentate gyrus (DG) of the hippocampus (figure 2. S6, A to D) in aged mice. Nicotinamide mononucleotide (NMN), another NAD^+ precursor, also has beneficial effects in aged neural stem cells (*163*). Similarly, NR rescued the decline of McSCs in hair follicles of aged mice, as reflected by increases in mast/stem cell growth factor receptor Kit (c-KIT) and short transient receptor potential channel 2 (TRP2), known McSCs markers, in NR-treated aged mice (Figure 2. 6, E and F). NR treatment of C57BL/6J mice slightly increased lifespan (chow diet, mean 829±12.0; NR, mean 868±12.4 days, *p* = 0.034) (Figure 2. 6G). The beneficial effect of NR on survival was further confirmed by Cox proportional hazards analysis (Figure 2. 6H). Although the lifespan benefit is small, it was obtained with the NR treatment commencing late in life at 24 months. This argues that aging, in part, may stem from the dysregulation of general SC NAD^+ homeostasis.
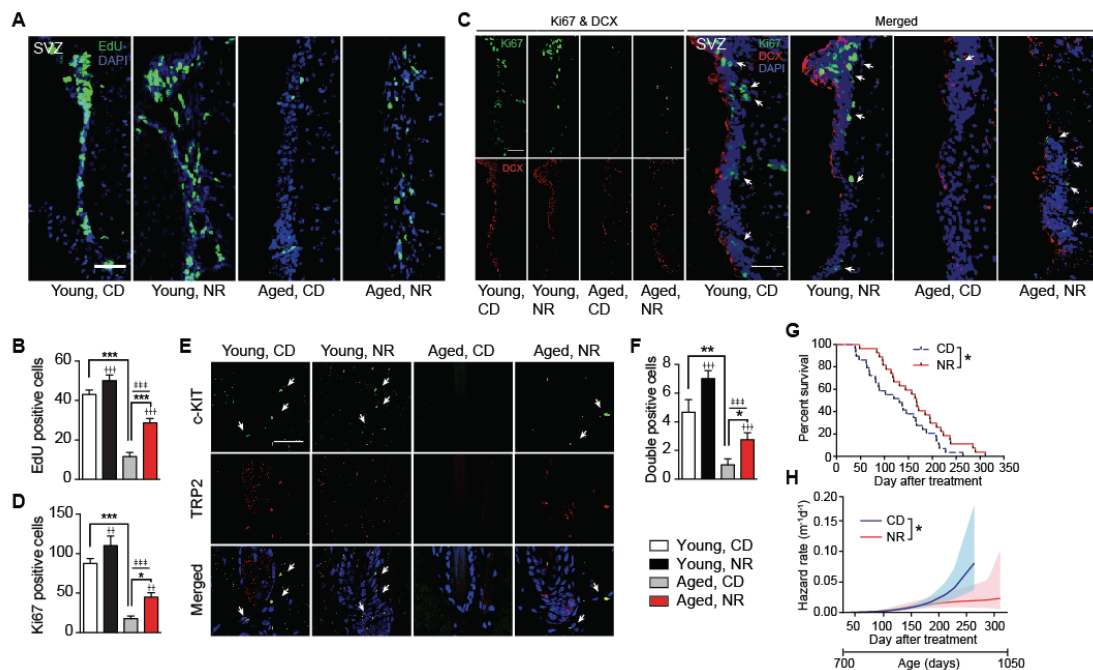
Figure 2. 6 NR improves neural and melanocyte stem cell (NSC and McSC) function and increases the lifespan of aged C57BL/6J mice

Aged (22-24 months old) C57BL/6J mice received a dietary supplement with NR for 6 weeks. **A-B**, Representative images (A) and quantification (B) of EdU-positive NSCs in the subventricular zone (SVZ) from young and aged mice following NR treatment. Scale bar = 50μm. **C-D**, Representative images (C) and quantification of Ki67- and doublecortin (DCX)-positive NSCs in the subventricular zone (SVZ) harvested from young and aged mice treated with or without NR (D). Arrows point to Ki67-positive NSCs. Scale bar = 50μm. **E-F**, Representative images (E) and quantification (F) of c-KIT and TRP2 double positive McSCs in the bulge of hair follicles from dorsal skin harvested from young and aged mice treated with or without NR. Arrows point to double positive McSCs. Scale bar = 50μm. **G**, Kaplan-Meier survival curves of control- and NR-treated aged mice, with the NR treatment beginning at 2 years (700 days) of age. **H**, Hazard rate decreased under NR treatment.

Individual lifespans were collected and used to estimate the hazard function of each population using numerical differentiation of the Kaplan–Meier survival estimator (solid lines). The shaded areas represent the 95% confidence bands of the true hazard. The p value was calculated with the use of a Cox proportional hazards model. All statistical significance was calculated by *Student*'s t test or two-way ANOVA, except in (G and H). All data are represented as mean ± s.e.m. *$P < 0.05$, **$P < 0.01$, ***$P < 0.001$. Main effects for treatment or age are denoted as † or ‡, respectively, with interactions denoted as ε. **A-F**, n = 6, **H**, n=30 per treated group.

2.5 Conclusions

Oxidative stress, potentially introduced by mitochondrial respiration, is thought to be circumvented in stem cells by their reliance on glycolysis as a primary energy resource (*180*). However, our study demonstrates that mitochondrial oxidative respiration is important for the functional maintenance of multiple types of adult SCs during aging. In fact, the reduction in cellular NAD^+ pools blunts the adaptive UPR^{mt} pathway (*158*), ultimately leading to a loss of mitochondrial homeostasis with a concurrent reduction in the number and the self-renewal capacity of MuSCs. Accordingly, by boosting MuSC concentration of NAD^+, proteotoxic stress resistance may be restored due to the activation of the UPR^{mt} pathway, stimulating the prohibitin family of mitochondrial stress sensors and effectors. This will in turn improve mitochondrial homeostasis, protecting MuSCs from senescence and safeguarding muscle function in aged mice (figure 2. S6E). Most importantly, using a MuSC-specific loss-of-function model for *Sirt1*, an essential regulator governing mitochondrial homeostasis (*181*), the importance and essential nature of the relationship between the NAD^+-SIRT1 pathway, mitochondrial activity and MuSCs function was unequivocally established *in vivo*. Maintaining healthy mitochondria, by replenishing NAD^+ stores, seems furthermore to have beneficial effects beyond MuSCs, and also protect NSC and McSC populations from aging

In combination, our results demonstrate that the depression of prohibitin signaling, leading to mitochondrial dysfunction, can be reversed in aging using a nutritional intervention to boost NAD^+ concentrations in SCs, and suggest that NAD^+ repletion may be revealed as an attractive strategy for improving mammalian lifespan.

2.6 Supplementary materials

2.6.1 Experimental methods

Animals. Young (1 month old) and aged (20-24 months old) C57BL/6JRj mice were purchased from Janvier Labs. Five weeks old male C57BL/10SnJ and C57BL/10ScSn-Dmd^{mdx}/J mice, were purchased from The Jackson Laboratory. SIRT1$^{MuSC-/-}$ mice were created at the EPFL SPF animal core facility by crossing SIRT1$^{flox/flox}$ mice (*157*) with the Pax7^{creER} strain (B6.Cg-Pax7$^{tm1(cre/ERT2)Gaka}$/J, purchased from Jackson laboratory). Mice were fed with pellets containing vehicle or NR (400 mg/kg/day) for 6-8 weeks. The pellets were

prepared by mixing powdered chow diet (2016S, Harlan Laboratories) with water or with NR dissolved in water. Pellets were dried under a laminar flow hood for 48 hours. Animal phenotyping experiments were carried out according to standard operational procedures (SOPs) established and validated within the Eumorphia program (*182*). To induce SIRT1 knockout in MuSCs, a 20mg/ml of Tamoxifen/corn oil solution was given to SIRT1$^{flox/flox}$:Pax7^{creER} mice via intraperitoneal injection for 5 consecutive days at 1mg/10g of mouse body weight. SIRT1$^{flox/flox}$ mice were injected at the same dosage of tamoxifen and served as controls. All mice were housed in micro-isolator cages in a room illuminated from 7:00am-7:00pm with *ad libitum* access to diet and water. Animal experiments were authorized by the local animal experimentation committee of the Canton de Vaud under licenses 2665 and 2890.

Endurance running test. Mice were fasted 2 hours before running on a treadmill. The exercise regimen commenced at a speed of 9cm/s with an inclination of 5 degrees. The speed was gradually increased 3cm/s every 12 minutes. Mice were considered to be exhausted, and removed from the treadmill, following the accumulation of 5 or more shocks (0.1 mA) per minute for two consecutive minutes. The distance traveled and time before exhaustion were registered as maximal running distance and period(*101, 157*).

Grip strength test. Muscle strength was assessed by a grip strength behavior task. The grasp strength of each mouse for all four limbs was measured on a pull-grid assembly connected to a grip strength meter (Columbus Instruments). The mouse was drawn along a straight line parallel to the grid until the grip was broken, providing the peak force in grams. This was repeated 4 times with 5 min intervals between measurements.

Survival test. Sixty 24-months-old C57BL/6JRj mice were randomly divided into two groups. Mice were housed with no more than 4 mice per cage. Cohorts of 30 mice were fed with a control chow diet with or without NR (400 mg/kg/day) supplementation. Mice were observed daily to record their survival – i.e. when they were found dead or were determined to be moribund by an experienced veterinary physician. Survival analyses were performed using the Kaplan-Meier method and the significance of differences between survival curves calculated using the log rank test (*133*). The time-dependent hazard rate was estimated through numerical differentiation of the Kaplan–Meier cumulative hazard estimate. To generate confidence bands for the true hazard rate under the assumption that it is locally smooth, death times were fitted with a piecewise-polynomial B-spline hazard model using the R package bshazard (*183*). The *p* value was calculated with the use of a Cox proportional hazards model (*184*).

FACS based muscle stem cell isolation. Gastrocnemius, soleus, quadriceps, and tibialis anterior muscles from both limbs were excised and transferred into PBS on ice. All muscles were trimmed, minced and digested with 0.1mg/ml of type II collagenase (Sigma) in PBS for 15 min at 37°C. Samples were then centrifuged at 750g for 5min and further digested in 1 mg/ml of collagenase/dispase (Roche) for 30 min at 37°C. Muscle slurries were sequentially filtered through 100, 70 and 40 μm cell strainers. The isolated cells were then washed in washing buffer (PBS + 2.5% FBS) then resuspended in 200μl of washing buffer and immediately stained with antibodies, including the MuSC markers CD31 (1:800, eBioscience, eFluor450 conjugated); CD34 (1:200, eBioscience, eFluor660 conjugated); CD45 (1:200, eBioscience, eFluor450 conjugated); CD11b (1:400, eBioscience, eFluor450 conjugated); Sca-1 (1:1000, eBioscience, PE-Cy7 conjugated); and α7 integrin (1:300, MBL) for 30 min at 4°C. Secondary staining was performed with a mixture of goat anti-mouse antibody (1:800, Life technologies, Alexa Fluor 488 conjugated) and propidium Iodide (PI, Sigma) for 15 min at 4°C in the dark. Stained cells were analyzed and sorted using the FACSAria II instrument (BD Biosciences). Debris and dead cells were excluded by forward scatter, side scatter and PI gating. Cells were sorted either directly on slides for immunostaining or into lysis buffer for NAD$^+$ measurements and into TriPure (Roche) reagent for RNA extraction.

Cell culture and treatments. FACS sorted MuSCs were grown on a 10% Matrigel (Corning)-coated dish and flasks with Fams F-10 media (Gibco), supplemented with 20% fetal bovine serum (FBS, Gibco), 2.5ng/ml basic fibroblast growth factor (bFGF, Sigma) and penicillin/streptomycin (1x, Gibco). Dishes were coated with 10% growth factor-free Matrigel solution on ice for 7 min then transferred to a 37°C cell culture incubator overnight before use. Cells were grown for three generations *in vitro* before experiments with cells plated and passaged at 10^3 cells/ml and 50% confluence, respectively. C2C12 mouse myoblasts were grown in DMEM (4.5g/L glucose, Gibco) supplemented with 10% FBS and penicillin/streptomycin (1x, Gibco). Cell transformations with *Phb* (Santa Cruz) and *Phb2* shRNA (Santa Cruz) were performed using jetPEI DNA transfection kit (Polyplus), according to manufacturer's instructions. Cells were treated with 1mM NR or PBS for 6 hours before cell harvesting or fixation.

Single-cell gel electrophoresis (comet) assay. The alkaline comet assay was performed according to the manufacturer's instructions (Trevigen, 4250-050-K). Briefly, FACS sorted MuSCs were resuspended in PBS and combined with molten LMAgarose (37°C) at the final concentration of $1x10^4$ cells/ml. 50 μl of this LMAgarose dilution was immediately pipetted onto sample areas of CometSlides and allowed to stay 10min at 4°C in dark. After 60 minutes cell lysis, CometSlides were immersed in Alkaline unwinding solution for 60min at 4°C. Alkaline electrophoresis was then performed at 21 volts for 30min at room temperature.

Slides were then washed in distilled water, followed by 70% ethanol and dried for 15min at 37°C. After staining with Propidium Iodide (PI), all CometSlides were then completely dried and observed under a fluorescent microscope (Leica).

Mitochondrial membrane potential assay. Mitochondrial membrane potential was measured using Tetramethylrhodamine, methyl ester (TMRM, Life Technology) following the manufacturer's instructions. Briefly, MuSCs were sorted and resuspended in PBS at 1×10^5 cells/ml. Cells were then stained with TMRM at the final concentration of 20nM for 30min at room temperature. Cells were then washed three times with PBS and mitochondrial membrane potentials were analyzed using a LSRII (BD) FACS machine with the excitation and emission wavelengths of 535nm and 610/620nm respectively. MuSCs from the same lot but treated with 10mM FCCP were used as negative control.

β-galactosidase assay. MuSCs were sorted directly on 8 chamber slides (Thermo Scientific). Senescence-associated β-galactosidase activity was detected using the senescence β-galactosidase staining kit (Cell signaling), according to manufacturer's instructions.

Myogenesis assay. Five MuSCs were sorted directly into wells of a Matrigel-coated 96-well cell culture plate, containing MuSC growth medium (F10, 20% FBS, 2.5ng/ml bFGF, 1x pen/strep), using the automated cell deposition unit (ACDU) of the FACSAria II instrument (BD Biosciences). Cells were cultured at 37°C for 5 days. Cell colony formations were counted using the DM IL LED Inverted Microscope (Leica) after fixation in freshly made or defrosted 4% paraformaldehyde (PFA) for 10 min.

Cardiotoxin-induced muscle regeneration. Animals were anesthetized using Isoflurane in oxygen from a precision vaporizer. 50μl of 20μM *Naje mossambica mossambica* cardiotoxin (Sigma) was injected intramuscularly cross the skin and directly into the tibialis anterior (TA) muscle. For SIRT1$^{MuSC-/-}$ mice, cardiotoxin was injected on the third day of the 5 consecutive days of tamoxifen injections, as described above. Mice were sacrificed at 7 and 14 days after injury. TA muscles were immediately embedded in Thermo Scientific™ Shandon™ Cryomatrix™ and frozen in isopentane, cooled in liquid nitrogen, for 2min before being transferred to dry ice and stored at -80°C. Representative wide field images for HE stained cardiotoxin treated muscles are shown in the Supplementary Information Figure 2. 1 (magnified images are seen in Figure 2. 2I).

MuSCs transplantation. Double-sorted MuSCs isolated from 24 months old NR or normal chow diet fed C57B/6J mice were resuspended in 10ul of F10 media with 20% FBS and injected directly into the cardiotoxin pre-injured TA muscle of *mdx* mice 24hrs after the injury. The recipient mice were either 5 weeks (young, 8000 MuSCs transplanted) or 16 months (aged, 15000 MuSCs transplanted) old. The cardiotoxin pre-injury was performed as described above. Recipient mice were sacrificed 4 weeks after transplantation, TA muscle were harvested and prepared for cryosectioning.

***Phb* shRNA lentivirus production and intramuscular *Phb* knockdown.** To make *Phb* shRNA lentivirus, *Phb* shRNA sequences (Forward: 5'-AATTTCTCCCGCTCTCGGAACATCACTCGAGTGATGTTCCGAGAGCGGGAGATTTTTTT AT-3' and reverse: 5'-AAAAAAATCTCCCGCTCTCGGAACATCACTCGAGTGATGTTCCGAGAGCGGGAGA-3', modified from Sigma, TRCN0000313177) or Scramble shRNA sequences (Forward: 5'-AATTCCTAAGGTTAAGTCGCCCTCGCTCGAGCGAGGGCGACTTAACCTTAGGTTTTTTT AT -3' and reverse: 5'-AAAAAAACCTAAGGTTAAGTCGCCCTCGCTCGAGCGAGGGCGACTTAACCTTAGG-3', modified from Addgene, #1864) were sub-cloned into the GFP-containing pLKO 3G vector (Addgene #14748). Subconfluent HEK293T cells were then cotransfected, by calcium phosphate precipitation, with 20 µg of the above described pLKO 3G vectors together with 15 µg of pCMV-R 8.74, and 10 µg of pMD.G, to produce lentiviruses. After 24 hours, the medium was changed. Supernatant containing recombinant lentiviruses was collected at 48h and 72h after transfection and virus was purified by ultracentrifugation. shRNA efficiency was tested in C2C12 cells infected with the above lentiviruses at a MOI of 10. For intramuscular *Phb* knockdown, 24 month old mice were injected with 10^8 TU/ml of either *Phb* or scramble shRNA lentivirus into the tibialis anterior muscle of each leg 24hrs after CTX-induced injury, as previously described (*185*). The CTX injury was performed as described above. Mice were sacrificed 7 days after CTX injury and the TA muscles were harvested and prepared for cryosectioning and histological analysis.

Histology. TA muscles were harvested from anaesthetized mice and immediately frozen in Tissue-TEK® OCT compound (PST). 8-µm cryosections were collected and fixed with 4% paraformaldehyde, which are either stained with haematoxylin/eosin (HE) or antibodies. For immunostainings, heat activated antigen retrieval was performed in pH 6.0 citrate buffer for 10min at 65°C. After washing with PBS-0.1% tween 20 (PBST), the sections were blocked with 10% affinipure Fab goat anti mouse IgG (Jackson Immunoresearch) in PBST for 60min and PBST containing 2% BSA and 5% goat serum for 30min at room temperature. Primary antibodies were then applied over night at 4°C. The following antibodies were used: anti-

eMHC (Developmental Studies Hybridoma Bank, DSHB, University of Iowa), anti-Pax7 (DSHB, University of Iowa), anti-γH2AX Ser 139 (Millipore), anti-Laminin (Sigma), anti-PDGFR (Cell signaling), anti-F4/80 (Sigma), anti-c-KIT (BD Pharmingen), anti-TRP2 (Santa Cruz), anti-activated-caspase3 (Cell signaling). Subsequently, the slides were washed in PBST and incubated with appropriate secondary antibodies and labeling dyes. For immunofluorescence, secondary antibodies were coupled to Alexa-488 or Alexa-568 fluorochromes (Life technology), and nuclei were stained with DAPI (Invitrogen). After washing in PBST, tissue sections were mounted with Dako mounting medium (Dako).

Collected brain samples were taken from mice perfused with PBS and 4% PFA. Harvested whole brains were further fixed in 4% PFA overnight, and thereafter cryoprotected in 30% sucrose for 48 hours prior to embedding in OCT compound (PST) in preparation for cryosectioning. All immunostainings were performed using the same protocol as described for muscle samples. Antibodies used were anti-Ki67 (AbCam) and anti-doublecortin (Santa Cruz).

For cellular immunostaining, freshly isolated MuSCs were sorted directly into 8-chamber slides (Thermo Scientific) and examined immediately after 30min of sedimentation or cultured for 3 generations. Cells were then fixed with either 4%PFA or 3% H_2O_2 in methanol for 10-15min. After 15min permeabilization with 0.5% Triton X-100, cells were blocked and immunostained using a similar protocol to that used for muscle tissue sections. All samples were imaged with a DMI4000 B Inverted Microscope (Leica) or the VS120-S6-W slides scanner (Olympus). Images were analyzed using ImageJ software. For immunofluorescence quantification, positively stained cells were defined as those with an intensity that was higher than a given threshold, which was then applied to all images. The thresholds were set up using sample slides before analyzing experimental data. More than 3 whole muscle cross-section areas, or more than 6 randomly chosen microscope scopes from each animal in all experimental conditions were used for quantification. All *in vitro* cultured or FACS sorted cells (> 500 per condition) were applied for analysis if cell number quantifications were performed.

NAD$^+$ and NADH quantification. MuSCs were isolated from the gastrocnemius, soleus, quadriceps, TA and EDL muscles from both hindlimbs of the control or NR-treated young and aged mice (4 groups). Approximately 5,000-8,000 MuSCs were collected from each animal, with 6 animals in each group, and sorted directly into 200µl of lysis buffer provided by the NAD$^+$/NADH assay kit (Biovision, k337-100)(*55*). NAD$^+$ and NADH concentrations were then measured following the manufacturer's instructions, which were modified by scaling down assay volumes by 50% in all steps. Results were calculated according to the standard curve,

which was created using NADH standards from the kit. Final NAD$^+$ and NADH concentrations for each sample were normalized to the total cell number

Gene expression analyses. Total RNA was extracted from MuSCs by sorting cells directly into TriPure RNA isolation reagent (Roche) or from cultured C2C12 myoblasts using TriPure reagent according to the product manual. Total RNA was transcribed to cDNA using QuantiTect Reverse Transcription Kit (Qiagen). Expression of selected genes was analyzed using the LightCycler480 system (Roche) and LightCycler® 480 SYBR Green I Master reagent (Roche). The acidic ribosomal protein 36b4 gene (ribosomal protein, large, P0, *Rplp0*) was used as house keeping reference.

Proteomics. Protein sample preparation and SWATH mass spectrometry (SWATH-MS) measurements were performed as follows: protein extraction and trypsin (Promega) digestion were done as previously described (*186*). ~20 µg of protein extracts from young, young-NR, aged and aged-NR mouse muscle stem cells were processed respectively. After digestion, the peptide samples were cleaned by Sep-Pak tC18 cartridges (Waters, Milford, MA, USA) and evaporated on a vacuum centrifuge until dry, and re-solubilized in 2% acetonitrile/0.1% formic acid prior to MS measurement. The SWATH and shotgun mass spectrometry were performed on the 5600 TripleTOF mass spectrometer as previously described (*171*). Alternatively, a set of 64 variable isolation windows was consecutively constructed covering the 400 to 1200 m/z precursor range. The spectral library was constructed using the results from shotgun-MS with SpectraST (*187*), as previously described (*188*). The SWATH-MS targeted data extraction was performed using OpenSWATH (*189*), which applies a target-decoy model to estimate the false-discovery rate (FDR) using the mProphet algorithm (*190*). Peptide features were retained to reach the 1% FDR threshold. Protein abundances were estimated using the three most intensive transitions from the three most intensive peptides, and normalized with the total protein abundance in each sample.

Western blotting. C2C12 cells were lysed in a buffer composed of 50 mM Tris, 150 mM KCl, EDTA 1 mM, NP40 1%, nicotinamide 5mM, sodium butyrate 1mM and protease inhibitors cocktail (Roche) at pH 7,4. Proteins were separated by SDS-PAGE and transferred onto nitrocellulose membranes. Blocking and antibody incubations were performed in 3% BSA. The following primary antibodies were used: anti-cleavage caspase 3 (Cell Signaling); Anti-γH2AX (Millipore); anti-HSP60 (Enzo Life Science); anti-β-actin (Sigma); anti-PHB (Biolegend); anti-PHB2 (Santa Cruz); anti-CKD4 (Novus biologicals); anti-CCND1 (Santa Cruz); anti-CCND3 (Santa Cruz); anti-HSP90 (BD Biosciences); HSP70 (Abcam); anti-MT-CO1 (Biolegend); anti-ATP5A (Biolegend); anti-Grp78 (Abcam); anti-α-Tubulin (Sigma); and

anti-CLPP (Sigma). All secondary antibodies were from Jackson Immunoresearch. Antibody detection reactions were developed by enhanced chemiluminescence (Advansta, CA, USA) and imaged using the c300 imaging system (Azure Biosystems). Full images of Western blots are shown in the Supplementary Information Figure 2. 2.

Respirometry on primary MuSCs. Basal and uncoupled oxygen consumption rates (OCRs) and the extracellular acidification rate (ECAR) were measured using the Seahorse extracellular flux bioanalyzer (XF96, Seahorse Bioscience Inc.)(*191*). To uncouple mitochondria, 5µM of FCCP was injected after a basal respiration measurement. All measurements were performed in triplicates and results were normalized to total cell number seeded after FACS sorting.

Bioinformatic analysis. Quadriceps microarray data from young and aged mice MuSCs (*7, 152, 155*) were analyzed for transcript expression using the Kyoto encyclopedia of genes and genomes (KEGG), gene ontology (GO) or gene set enrichment analysis (GSEA) analysis. Raw microarray data are also publicly available on GEO under the accession numbers GSE47177, GSE47401 and GSE47104. All gene expression heat maps were drawn using GENE-E software.

Statistical analysis. The sample size (n) for each experimental group is described in each figure legend. GraphPad Prism software was used for all statistical analyses. Quantitative data displayed as histograms are expressed as means ± standard error of the mean (represented as error bars). Results from each group were averaged and used to calculate descriptive statistics. *Student*'s *t* test was used for comparisons between two groups with statistical significance was set at a *P* value of *$P < 0.05$, **$P < 0.01$ and ***$P < 0.001$. For multiple comparisons, a two-way analysis of variance (ANOVA) was performed followed by a Newman–Keuls post-hoc test. Significance for a main effect of treatment was set at a *P* value of †$P < 0.05$, ††$P < 0.01$ and †††$P < 0.001$, a main effect of age was set at a *P* value of ‡$P < 0.05$, ‡‡$P < 0.01$ and ‡‡‡$P < 0.001$ and an interaction was set at a *P* value of $^{\varepsilon}P < 0.05$, $^{\varepsilon\varepsilon}P < 0.01$ and $^{\varepsilon\varepsilon\varepsilon}P < 0.001$. Survival analyses were performed using the Kaplan-Meier method and the significance of differences between survival curves calculated using the log-rank test. The time-dependent hazard rate was estimated through numerical differentiation of the Kaplan–Meier cumulative hazard estimate. The *p*-value was calculated with the use of a Cox proportional hazards model.

2.6.2 Supplementary figures

figure 2.S 1 Mitochondrial dysfunction in muscle stem cells (MuSCs) during aging

A-B, Gene-set enrichment analysis (GSEA) demonstrates up- or downregulated signaling pathways in MuSCs from two-year-old mice, compared to 4-month-old mice. Analysis was performed on microarray data from the publicly available GEO data sets GSE47104 (*155*) (A) and GSE47401 (*152*) (B) using Kyoto encyclopedia of genes and genomes (KEGG) enrichment. Signaling pathways are ranked on the basis of their normalized enrichment scores (NESs); positive and negative NESs indicate down- or upregulation in aged MuSCs, respectively. Specific pathways related to MuSC function are highlighted in red and blue. **C**, Top 10 ranked

downregulated pathways in MuSCs from aged animals (GSE47177), based on gene ontology (GO) enrichment. Pathways are ranked by family wise error rate (FWER) *p* values. **D,** Area-proportional Venn diagram representing common genes (*P* < 0.05) between the significantly upregulated genes in MuSC transcriptomes originating from aged mice (GSE47177 (*7*) and GSE47401), and genes from the human mitochondrial transcriptome (*165*). **E**, Pie chart illustrating the percent composition of the common 113 mitochondrial genes found in C**.** TXN, transcription, TLN, translation. **F**, Custom gene-set analysis showing enrichment of mitochondrial respiratory chain (OXPHOS), TCA cycle and mitochondrial unfolded protein response (UPR^{mt}) related transcripts from MuSCs of young (Y) and aged (A) mice obtained from three independent data sets (GSE47177, GSE47401 and GSE47104 (*152*)). Roman numerals indicate corresponding OXPHOS complexes. **G**, Gene-set analysis showing enrichment of the mitochondrial transcriptome from MuSCs of young and aged mice obtained from three independent data sets (GSEl7177, GSE47401 and GSE47104). **H**, Oxygen consumption rate (OCR) in isolated primary MuSCs, cultured *in vitro* for three generations. **I**, Gene-set analysis showing enrichment of cell senescence related genes from MuSCs of young and aged mice obtained from three independent data sets (GSE47177, GSE47401 and GSE47104). **J**, Relative expression for cell cycle genes in freshly isolated primary MuSCs, cultured *in vitro* for three generations. **K**, Relative gene expression for cell senescence markers in freshly sorted MuSCs. Data are normalized to *36b4* mRNA transcript levels. All data are shown as mean ± s.e.m. **P* < 0.05, ***P* < 0.01, ****P* < 0.001. Statistical significance was calculated by *Student*'s *t* test. **H, J-K**, n = 6 mice per group.
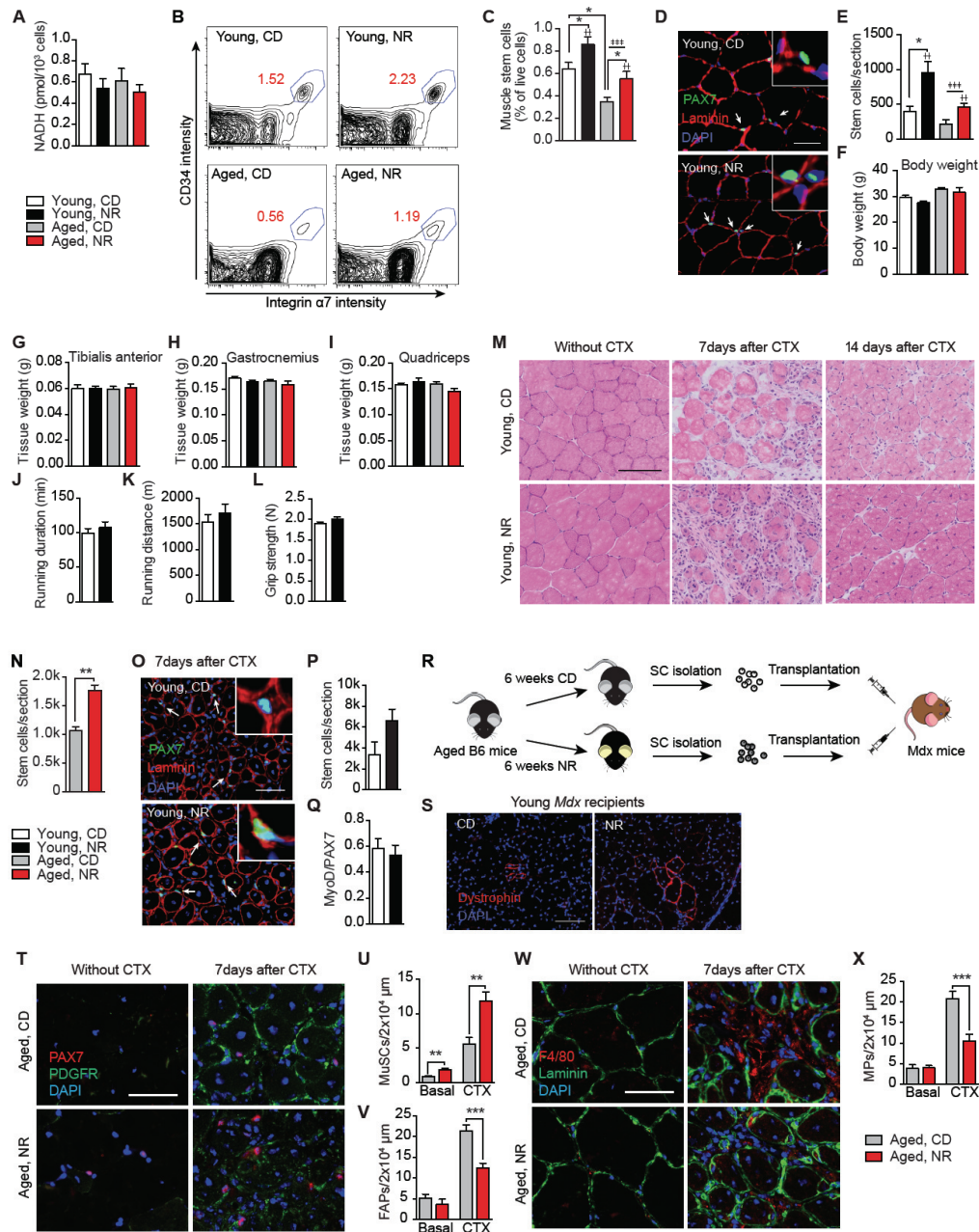
figure 2.S 2 Improved muscle stem cell numbers and muscle function in NR-treated mice

A-X, Young (1 months old) and aged (22-24 months old) C57BL/6J mice received a dietary supplement with NR (400 mg/kg/day) for 6 weeks. **A**, NADH levels in MuSCs freshly isolated from control and NR diet-fed mice. **B**, FACS contour plots of Sca-1⁻, Lin⁻ (CD11b⁻ CD23⁻, CD45⁻) cells isolated from muscle tissue. Percentage of the CD34⁺/integrin α7⁺/Lin⁻/Sca-1⁻ MuSCs were noted in red in contour plots. **C**, Quantification of FACS-sorted CD34⁺/integrin α7⁺/Lin⁻/Sca-1⁻ MuSCs isolated from control and NR diet-fed mice. Cell numbers were normalized to the entire live cell population. **D-E**, Representative image of PAX7 immunostained muscle cross-sections taken from control and NR-treated young mice (D) and the quantification of PAX7⁺ MuSCs of young mice (E). Myofibers were counterstained with Laminin. Arrows point to PAX7-positive SCs. 20 x 20µm insets show single MuSC. Scale bar = 50µm. **F-I**, Body weight (F) and TA (G), gastrocnemius (H), and quadriceps (I) muscle weights for each cohort. **J-L**, Comparison of maximal running duration (J), running distance (K) and grip strength (L) between

control and NR-treated young mice. **M**, TA muscle structure in tissue-sections from control and NR-treated young mice with 7 and 14 days of recovery following CTX induced muscle damage. Images show representative H&E staining of muscle cross sections. Scale bar = 100μm. **N**, quantification of immunostained PAX7-positive MuSCs in TA muscle cross-sections taken from control and NR-treated mice 7 days after CTX-induced muscle damage. **O-P**, Representative images (O) and quantification (P) of PAX7 immunostained muscle cross-sections taken from control and NR-treated young mice 7 days after CTX-induced muscle damage. Myofibers were counterstained with Laminin. Arrows point to PAX7-positive SCs. 20 x 20μm insets show single MuSC. Scale bar = 50μm. **Q**, Quantification of the signal intensity ratio between MYOD1 and PAX7 in PAX7-positive MuSCs, performed on sections isolated 7 days after muscle damage in young mice. Images not shown. **R**, The schema of MuSCs transplantation experiments. MuSCs were double sorted from control and NR diet treated C57BL/6J mice and transplanted into the different hind limbs of the same *mdx* mouse. **S**, Dystrophin immunostaining of TA muscle sections in young (5 weeks old) *mdx* mice 4-weeks after receiving transplantations of MuSCs isolated from control or NR-treated aged C56BL/6J donors. Scale bar = 100μm. **T-V**, Representative images (T) and quantification of PAX7$^+$ MuSCs (U) and PDGFR$^+$ FAPs (V) in immunostained muscle cross-sections taken from control and NR-treated aged mice under basal conditions or 7 days after CTX-induced muscle damage. Scale bar = 50μm. **W-X**, Representative images (W) and quantification of F4/80$^+$ macrophages (MPs) (X) in immunostained muscle cross-sections taken from control and NR-treated aged mice under basal conditions or 7 days after CTX-induced muscle damage. Myofibers were counterstained with Laminin. Scale bar = 50μm. Statistical significance was calculated by *Student*'s *t* test or two-way ANOVA. All data are represented as mean ± s.e.m. *$P < 0.05$, **$P < 0.01$, ***$P < 0.001$. Main effects for treatment or age are denoted as † or ‡, respectively. **A-C**, n = 6 mice per group; **D-I**, **M**-**Q** and **T**-**X**, n = 3-6 mice per group; **J**-**L**, n = 10-12 mice in each group; **S**, n = 12 donor mice, n = 3 recipient mice for each treatment.
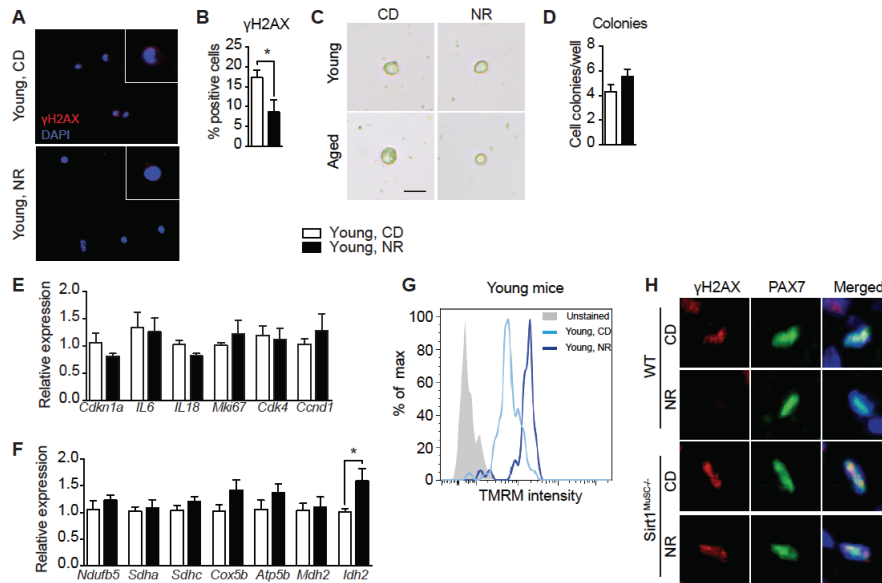
figure 2.S 3 NR treatment prevents muscle stem cell senescence by improving mitochondrial function

Young (1 months old) C57BL/6J mice or 8 months old SIRT1^MuSC-/- mice received a dietary supplement with NR (400 mg/kg/day) for 6 weeks. All results are compared to mice given a control diet. Data of the aged mice (22-24 months old) from the same experiments were mainly presented in Figure 2. 3. **A-B**, Immunostaining (A) and quantification (B) of γH2AX in freshly sorted MuSCs from young mice treated with NR. 20 x 20μm insets show single MuSC. **C**, β-galactosidase staining of freshly sorted MuSCs from young and aged mice given chow or NR supplemented diets. Scale bar = 10μm. **D**, Colony formation ability assay in freshly FACS sorted MuSCs from young mice treated with NR. **E-F**, Quantification of transcript expression for cell cycle and inflammatory secretome genes (E) or mitochondrial OXPHOS and TCA genes (F) in young MuSCs isolated from mice treated with NR. **G**, Mitochondrial membrane potential, measured by TMRM assay, in freshly isolated MuSCs from young NR-treated mice. **H**, Representative images of γH2AX and PAX7-positive cells in immunostained TA muscle cross-sections taken from control and NR-treated mice 7 days after CTX-induced muscle damage. All data are represented as mean ± s.e.m. Statistical significance was calculated by *Student*'s *t* test. *P < 0.05. **A-D**, and **G-H** n = 3-6 mice per group; **E-F**, n = 6 mice per group.
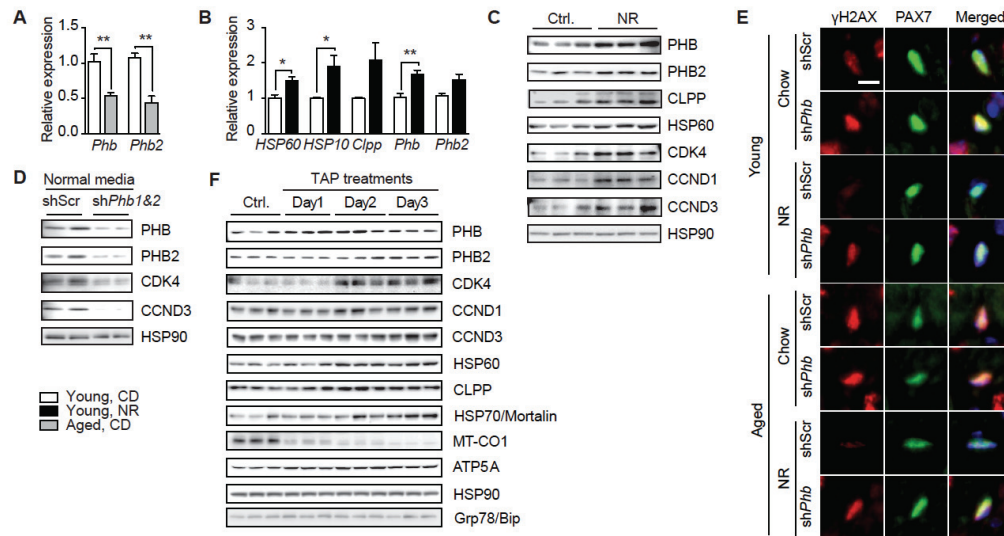
figure 2.S 4 Effects of NR on MuSC senescence are mediated by prohibitin activation of UPR^mt

A, Quantification of transcript expression for prohibitins in MuSCs from young (one-month old) and aged (22-24 months old) mice fed a chow diet (CD). **B**, Quantification of transcript expression for UPR^mt related genes and prohibitins in MuSCs from young (one-month old) C57BL/6J mice fed CD or receiving a dietary supplement with NR (400 mg/kg/day) for 6 weeks. **C**, Western blots showing the expression of prohibitins, UPR^mt markers and cell cycle related proteins in C2C12 myoblasts upon a 6-h NR treatment. **D**, Expression of prohibitins and cell cycle related genes in C2C12 myoblasts after the combined *Phb* and *Phb2* shRNA knockdown in normal DMEM cell growth media. **E**, Representative images of γH2AX and PAX7-positive cells in immunostained TA muscle cross-sections taken from control and NR-treated *Phb* knockdown mice 7 days after CTX-induced muscle damage. **F**, Expression of prohibitins and cell cycle related genes in C2C12 myoblasts treated for the indicated periods with 50 μg/ml thiamphenicol (TAP), which induces a mitonuclear imbalance and UPR^mt. All data are represented as mean ± s.e.m. Statistical significance was calculated by *Student*'s *t* test. *$P < 0.05$, **$P < 0.01$, ***$P < 0.001$. **A-B**, n = 6 per treatment group. **E**, n=3 mice per group.

49
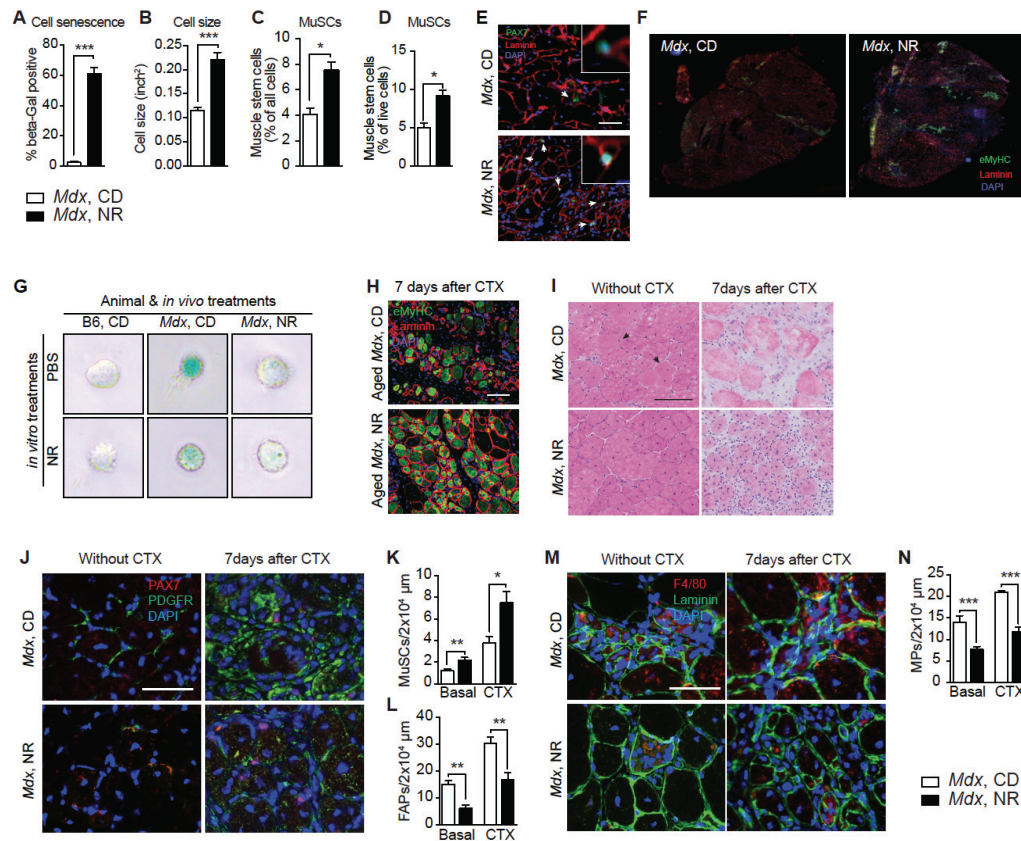
figure 2.S 5 Increased stem cell number and stemness in NR-treated *mdx* mice

mdx mice received a dietary supplement with NR (400 mg/kg/day) for 10 weeks. **A-B**, Quantification of β-galactosidase-positive cells (A) and cell size (B) for primary MuSCs isolated from C57BL/10SnJ or *mdx* mice and cultured *in vitro* for three generations. **C-D**, Quantification of FACS sorted CD34^{+}/integrin α7^{+}/Lin^{-}/Sca-1^{-} MuSCs isolated from control and NR diet-fed *mdx* mice, cell numbers were normalized to the entire cell population (C) or to the entire live cell population (D). **E**, Immunostaining of MuSCs (PAX7^{+}) in tissue-sections of NR-treated *mdx* mice 7 days after CTX-induced muscle damage. Myofibers were counterstained with Laminin. Arrows point to PAX7^{+} MuSCs. 20 x 20μm insets show single MuSC. Scale bar = 50μm. **F**, Immunostaining of neo-regenerated muscle fibers, indicated by eMyHC-positive fibers, in tissue-sections of NR-treated *mdx* mice under basal conditions. Images show the whole TA muscle cross-section. Myofibers were counterstained with Laminin. **G**, Representative images of β-galactosidase staining of FACS-sorted MuSCs from C57BL/6J, untreated (*mdx*) or NR-treated *mdx* (*mdx* with NR) mice challenged with PBS or NR for 6 hours. **H**, Immunostaining of neo-regenerated muscle fibers, indicated by eMyHC-positive fibers, in tissue-sections of NR-treated aged *mdx* mice (16 months old) 7 days after CTX-induced damage. Myofibers were counterstained with Laminin. Scale bar = 50μm. **I**, Muscle structure in tissue-sections from NR-treated young *mdx* mice (14 weeks old) with 7 days of recovery following CTX-induced muscle damage. Images show representative H&E staining of whole TA muscle cross-sections. Scale bar = 100μm. **J-L**, Representative images (J) and quantification of PAX7^{+} MuSCs (K) and PDGFR[+] FAPs (L) in immunostained muscle cross-sections taken from control and NR-treated *mdx* mice under basal conditions or 7 days after CTX-induced muscle damage. Scale bar = 50μm. **M-N**, Representative images (M) and quantification of F4/80[+] macrophages (MPs) (N) in immunostained muscle cross-sections taken from control and NR-treated *mdx* mice without under basal conditions or 7 days after muscle damage. Myofibers were counterstained with Laminin. Scale bar = 50μm. All data are represented as mean ± s.e.m. Statistical significance

was calculated by *Student*'s *t* test. *$P < 0.05$, **$P < 0.01$. ***$P < 0.001$. **A-F** and **H-N** n = 3-6 mice per treatment group. **G**, n = 3 mice and n = 6 *in vitro* treatments. More than 500 cells were quantified in each condition.
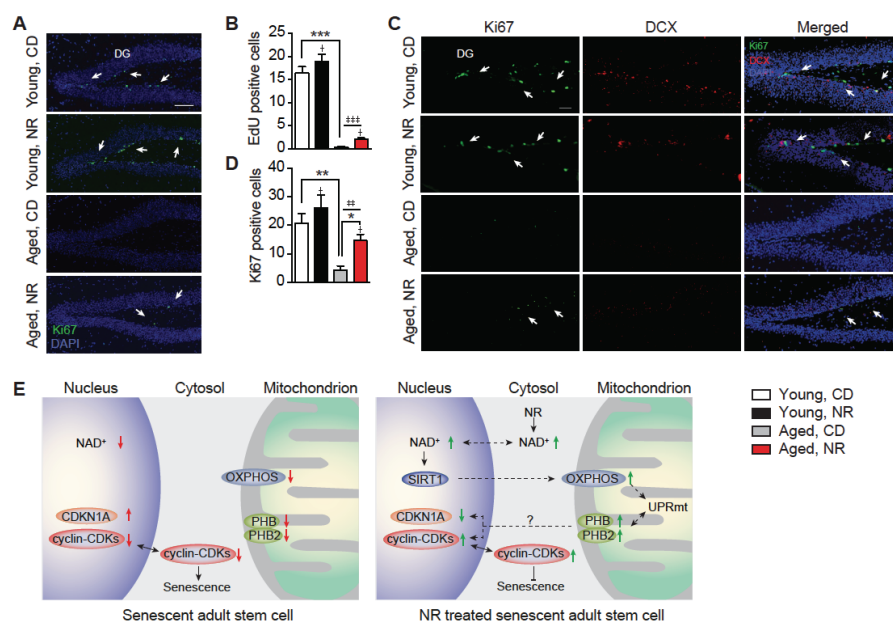
figure 2.S 6 NR improves neural stem cell (NSC) of aged C57BL/6J mice

Aged (22-24 months old) C57BL/6J mice received a dietary supplement with NR (400 mg/kg/day) for 6 weeks, which were then compared to control-diet-fed young or aged mice. **A-B**, Representative images (A) and quantification (B) of proliferating EdU-positive NSCs in the dentate gyrus (DG) of the hippocampus from young and aged mice following NR treatment. Arrows point to EdU-positive NSCs. **C-D**, Representative images (C) and quantification of Ki67-positive NSCs and the neuron regeneration marker, doublecortin (DCX), in the dentate gyrus (DG) of the hippocampus (D) harvested from young and aged mice following NR. Arrows point to Ki67-positive NSCs. **E.** Hypothethical mechanistic scheme showing how NR prevents adult stem cell senescence. Statistical significance was calculated by two-way ANOVA. All data are represented as mean ± s.e.m. *$P < 0.05$, **$P < 0.01$, ***$P < 0.001$. Main effects for treatment or age are denoted as † or ‡, respectively. **A-D**, n = 6 in each group.

2.7 Acknowledgments

Chapter 3. Control of muscle stem cell function by the acetyltransferase KAT2A

Adapted from:

Zhang, H., Luan, P., Ryu, D., Sorrentino, V., Menzies, K. J. Schoonjans, K., & Auwerx, J. Control of muscle stem cell function by the acetyltransferase KAT2A. ***Under preparation***

3.1 Abstract

Muscle stem cells (MuSCs) are essential for skeletal muscle homeostasis and repair. The complete mechanism controlling MuSC maintenance and differentiation, however, remains elusive. We found that KAT2A expression is essential for myogenic differentiation of MuSCs. KAT2A loss-of-function in cells blocks MuSC differentiation, and in mice impairs regeneration after muscle damage. The regulation of KAT2A in MuSCs function might rely on its ability to enzymatically acetylate proteins, a well-known protein modification, such as the MuSC transcription factor PAX7.

3.2 One sentence summary

KAT2A regulates MuSCs function through PAX7 acetylation

3.3 Introduction

Skeletal muscle homeostasis and regeneration relies on functional MuSCs or satellite cells. With muscle stress or damage, quiescent MuSCs are activated to differentiate into new fibers, join existing fibers, or replenish the existing pool of MuSCs through self-renewal. However, these responses are blunted in muscle with aging or with myopathies, such as Duchenne's muscular dystrophy (DMD), and are often a result of the decline in MuSC number and function. Deciphering each of the factors that modulate satellite cell specification, maintenance, proliferation and differentiation will provide the foundation for developing new strategies for the treatment of muscular diseases as well as muscle sarcopenia, which is defined as the loss of muscle mass during aging. Recent reports have begun to indicate the role of posttranslational modifications, such as acetylation, in MuSC activation and function during aging(*7, 192-194*). However, the current knowledge of posttranslational modifications regulating MuSC homeostasis remains rudimentary.

3.4 Results

3.4.1 KAT2A is upregulated in activated MuSCs

To investigate potential acetylation modulators in the control MuSC activation and differentiation, we examined publically available MuSC gene expression datasets of quiescent and activated MuSCs isolated from control and muscle-damaged mice(*7*). We first analyzed transcriptomes from MuSCs that had been identified and isolated using the yellow fluorescent protein (YFP)-conjugated to the MuSC marker PAX7, the well-known transcription factor involved in MuSC maintenance. Expression of most of the known lysine acetyltransferases (KATs) and lysine deacetylases (KDACs), which catalyze posttranslational protein modifications(*2*) are dynamically altered during MuSCs activation

and differentiation (Figure 3.1A). Intriguingly, among all the KATs, *Kat2a* is the only transcript that is upregulated in activated in MuSCs during muscle regeneration (60 hours after muscle damage), which subsequently begins to decline during the differentiation of MuSCs (84 hours after damage), pointing to a possible strict time-dependent necessity for KAT2A expression during MuSCs activation (Figure 3.1A). This was further confirmed in MuSCs isolated using a extensive profile of cell surface markers (VCAM$^+$/CD31$^-$/CD45$^-$/Sca1$^-$) (Figure 3.S1A). Aging on the other hand is accompanied by a decline in MuSC activation(*8*). In line with these observations, *Kat2a* expression is reduced in aged MuSCs (Figure 3.1B and figure 3.S1B). Recently, MuSCs were reported to be in a more activated quiescent state after contralateral leg muscle damage, a state termed G$_{Alert}$ MuSCs(*195*). Interestingly, *Kat2a* is the only KAT that is upregulated in the G$_{Alert}$ phase in MuSCs (Figure 3.1C). Based on these observations, we hypothesized that acetylation likely plays a role in muscle regeneration and that KAT2A upregulation may be considered a biomarker and regulator of MuSCs activation.
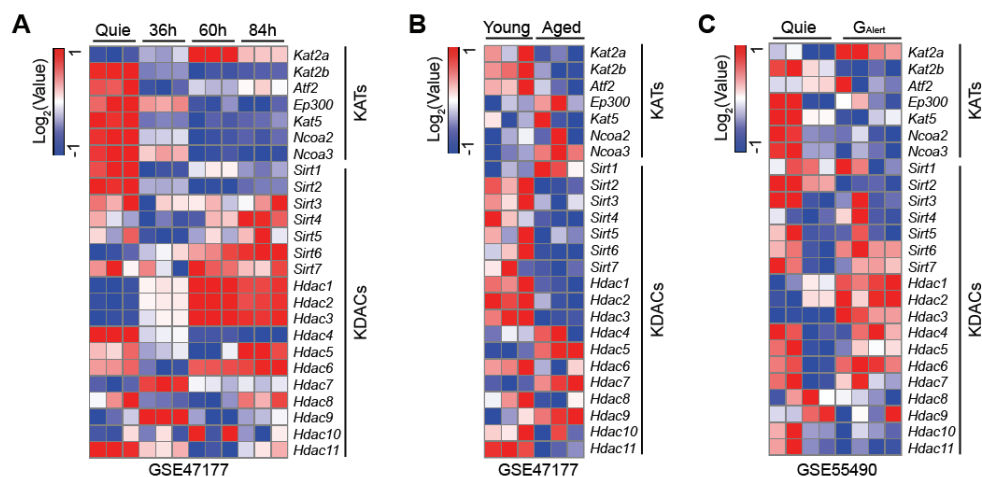
Figure 3. 1 KDAC and KAT gene expression patterns in MuSCs during muscle regeneration

A-C, Clustered heatmap of the gene expression profiles for (A) PAX7$^+$ quiescent and activated MuSCs prior to and 36, 60 and 84hr after BaCl$_2$-induced muscle injury(*7*); (B) MuSCs isolated from young (2-3 months old) and aged (2-years old) mice(*7*); (C) MuSCs isolated from the undamaged control (Quie), and muscles which was contralateral to the leg that received the injury (G$_{Alert}$)(*195*).

3.4.2 KAT2A is essential for the differentiation of MuSCs.

To confirm the function of KAT2A in muscle stem cells, we performed knockdowns (KDs) of *Kat2a* and its ortholog *Kat2b* in isolated primary MuSCs using adenoviral-driven *Kat2a* or *Kat2*b shRNA constructs. Interestingly, MuSCs lacking KAT2A completely lost their ability to differentiate into contracting myotubes. While control myoblasts differentiated into myotubes in a 2% concentration of horse serum medium after 4 days, the *Kat2a* loss-of-function (LOF) primary MuSCs have an altered morphology and exhibit reduced cell numbers (Figure 3.2A). Importantly, *Kat2b* LOF, which was reported to be required for the activity of MYOD1, an

important transcription factor regulating MuSCs differentiation(*194*), shows much less efficiency in blocking MuSCs differentiation (Figure 3.2A). *Kat2a* and *Kat2b* double KD cells show a similar morphology as single *Kat2a* LOF (Figure 3.2A). The necessity of KAT2A in myogenic differentiation was further confirmed at the transcript level of myosin heavy chain I (encoded by gene *Myh7*), IIA (encoded by gene *Myh2*) and IIB (encoded by gene *Myh4*) by real-time qPCR (Figure 3.2B), and at the protein level by immuno-staining for MYH2 (Figure 3.2C). All of these myosin heavy chain proteins can be used as markers for the development of the contractile apparatus. We then tested the function of KAT2A in C2C12 myoblasts, a murine cell line that is derived from satellite cells and whose behavior corresponds to that of progenitor lineage. Cycling C2C12 myoblasts are comparable to activated satellite cells in a muscle fiber(*196*). Upon inducing differentiation, C2C12 myoblast lose their myogenic potential for differentiation when *Kat2a* alone or both *Kat2a* and *Kat2b* are knocked down (figure 3.S2A). Compared to *Kat2a* LOF, *Kat2b* LOF C2C12 myoblasts differentiate more normally after exposure to differentiation medium for 4 days (figure 3.S2A). In normal C2C12 myoblasts, we observe a decrease in PAX7 and MYOD1 expression levels, along with an increase of MYH7 and MYH2 levels under differentiation *in vitro* (Figure 3.2D). Interestingly, KAT2A expression is reduced during the process of C2C12 differentiation while KAT2B maintains a more stable level of expression (Figure 3.2D). This confirms our bioinformatics analyses (Figure 3.1A), which indicated that there is a decline of *Kat2a* expression during MuSCs differentiation. *Kat2a*, but not *Kat*2b, LOF in C2C12 cells caused the loss of expression of MYH7 and MYH2, as well as MYOD1, indicating that KAT2A controls MuSC activation and differentiation by controlling the expression of myogenic transcription factors (Figure 3.2E and figure 3.S2B).
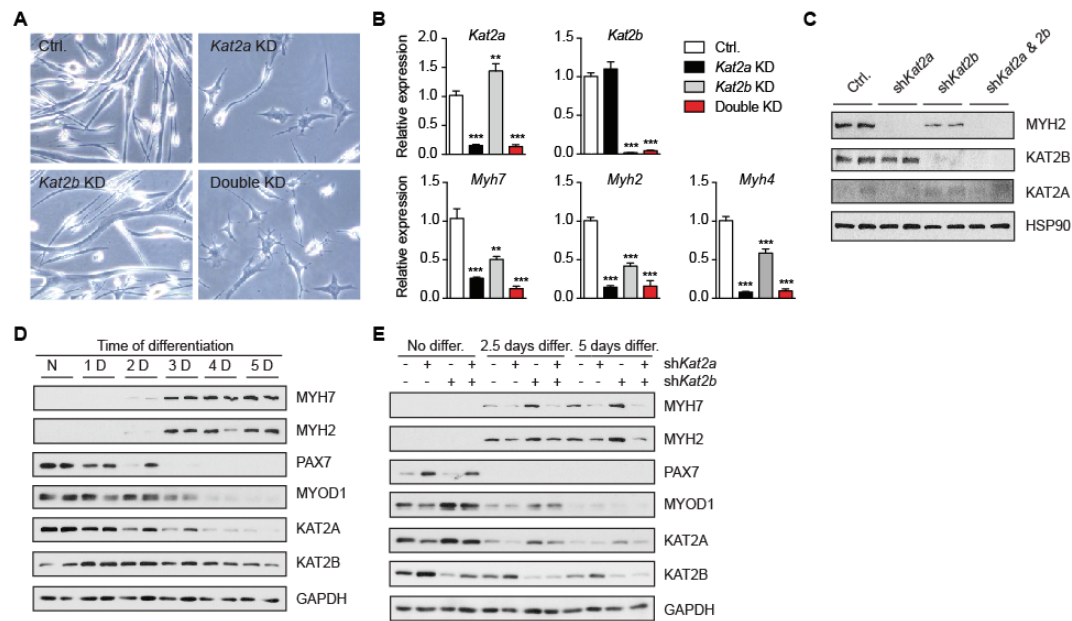
Figure 3. 2 KAT2A controls the myogenic differentiation of MuSCs

A, morphology of primary MuSCs differentiated for 4 days, with or without shRNA inducing *Kat2a* and/or *Kat2b* LOF; **B**, transcript expression of *Kat2a*, *Kat2b* and muscle myosin heavy chain genes after *Kat2a* and/or *Kat2b* LOF and 4 days induction of differentiation, N = 6 per condition. All comparisons are compared to the PBS treated control cells (Ctrl.). Statistical significance was calculated by a one-way ANOVA with a post-hoc dunnett's test. **$P<0.01$, ***$P<0.001$. **C**, protein expression of the myoblast differentiation marker MYH2 in primary MuSCs 4 days after differentiation, with or without *Kat2a* and/or *Kat2b* LOF. **D**, protein expression at different differentiation time points for C2C12 cells, GAPDH served as a loading control; **E**, protein expression at 2.5 and 5 days after differentiation in C2C12 cells with or without *Kat2a* and/or *Kat2b* LOF.

3.4.3 KAT2A is required for the muscle regeneration

Stemming from our bioinformatics analysis (Figure 3.1) and functional assays of KAT2A in MuSCs *in vitro* (Figure 3.2), we decided to analyze the role of KAT2A *in vivo* with a focus on muscle stem cell function and muscle physiology. Conditional MuSC-specific Kat2a LOF mice were created by crossing the B6.129S-*Pax7*^tm1(cre/ERT2)Gaka/J (*Pax7*-Cre) strain with B6.*Kat2a*^flox/flox (*Kat2a*^L2/L2) mice (figure 3.S3). The *Pax7*-Cre:*Kat2a*^L2/L2 mouse has functional KAT2A and PAX7 under normal conditions, yet once given tamoxifen, *Kat2a* is deleted in PAX7-expressing cells, specifically in MuSCs (i.e. *Kat2a*^MuSC-/-). We found, when compared to control adult mice, that *Kat2a*^MuSC-/- mice have reduced MuSCs numbers 5-days after tamoxifen injection (Figure 3.3, A and B). Accompanying this observation, there was a decrease in the muscle fiber size 2-weeks after tamoxifen induced *Kat2a* LOF. This was indicated by both the average size and distribution of muscle fiber cross-sectional areas (Figure 3.3, C and D) and mini-Feret diameters (Figure 3.3, E and F). Muscle regeneration ability is one of the key indicators of MuSCs function(*9, 197*). We therefore examined the role of KAT2A on muscle regeneration with cardiotoxin (CTX)-induced muscle damage. Indeed,

Kat2a LOF mice showed delayed muscle regeneration, as indicated by hematoxylin and eosin (H&E) staining of tibialis anterior muscle cross-sections following 7 days of recovery after muscle damage (Figure 3.3G). Collectively, all the data indicate that KAT2A, as an important regulator of MuSCs function, is also essential for muscle regeneration.
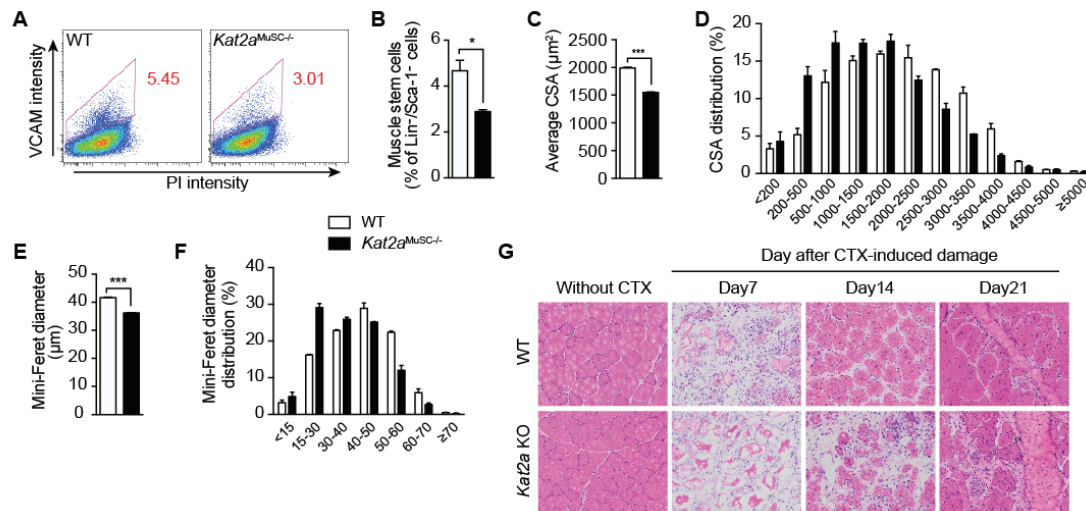
Figure 3. 3 KAT2A controls MuSCs differentiation and muscle regeneration

A, FACS contour plot of Sca-1⁻/Lin⁻/PI⁻ cells isolated from control and *Kat2a*^MuSC-/- mouse limb muscles. Percentage of VCAM⁺/Sca-1⁻/Lin⁻/PI⁻ MuSC populations are noted in red contour blots. **B**, quantified MuSCs relative to the total Sca-1⁻/Lin⁻/PI⁻ cell population. **C-D**, quantification of average (C) and distribution (D) of muscle fiber cross-section area (CSA) for control and *Kat2a*^MuSC-/- mice. **E-F**, quantification of average (E) and distribution (F) of muscle fiber mini-Feret diameter for control and *Kat2a*^MuSC-/- mice. **G**, Hematoxylin and eosin (H&E) staining of tibialis anterior muscle cross sections in control and *Kat2a*^MuSC-/- mice at the indicated days after CTX-induced muscle damage. N = 3 mice per condition. Statistical significance was calculated by *Student t* test. *$P<0.05$, **$P<0.01$, ***$P<0.001$

3.4.4 KAT2A regulates MuSC function through PAX7 acetylation.

PAX7 is a transcription factor that controls muscle stem cell maintenance in adults(*198, 199*). While the activity of many transcription factors is regulated by reversible acetylation, whether or not PAX7 can be acetylated is unknown. Given that PAX7 functions as a transcription factor in myogenesis and that KAT2A also plays essential roles in MuSCs activation/differentiation (demonstrated above), it may be possible that KAT2A regulates the function of PAX7 by changing its acetylation status. To test this hypothesis, C2C12 cells were first transfected with a plasmid to overexpress *Pax7* (PAX7 gain of function; GOF) and/or transduced with an adenoviral vector for the LOF or GOF of *Kat2a*. Indeed we observed the co-immunoprecipitation of KAT2A when performing a pull-down assay with anti-PAX7 (Flag) antibody. This suggests an interaction between these two proteins (Figure 3.4A). Moreover, endogenous PAX7 was induced in *Kat2a* LOF cells, whereas endogenous *Kat2a* levels were increased upon PAX7 overexpression (Figure 3.4B). These data indicate a

reciprocal regulation between KAT2A and PAX7 at the protein level. Importantly, KAT2A overexpression leads to increased PAX7 acetylation (Figure 3.4C), which might affect the activity and/or stability of PAX7.
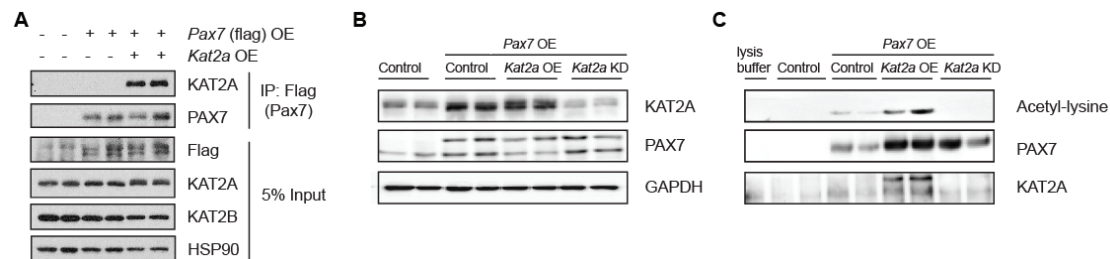
Figure 3. 4 Acetylation of PAX7 by KAT2A

Proteins were extracted 2 days after C2C12 cells were transduced with adenovirus to induce a GOF (OE) or LOF (KD) of *Kat2a* and/or transfected with a plasmid overexpressing *Pax7*. **A**, Interaction between PAX7 and KAT2A was verified by immunoprecipitation of PAX7 conjugated with a Flag-tag followed by the immunoblotting of KAT2A. **B**, Protein expression after *Pax7* GOF and/or with *Kat2a* GOF or LOF. **C**, Acetylation of PAX7 was examined by of Western blot analysis with anti-KAT2A antibody following immunoprecipitation of PAX7 with anti-Flag in C2C12 cell lysates.

3.5 Conclusions

Despite the fact that histone acetylation has been linked to MuSCs activation(*55*) and several myogenic transcription factors, such as MYOD1 and MEF2 have been reported to be acetylated in myogenic differentiation(*193, 194*), the potential role of KAT2A, which catalyzes the acetylation of both histones and transcriptional factors/cofactors, has never been examined. Our work demonstrates the crucial role of KAT2A in MuSC activation and differentiation. *Kat2a*, but not its ortholog *Kat2b*, is upregulated temporarily during the early stages of MuSC activation and is downregulated in MuSC aging. *Kat2a* LOF inhibits myoblast differentiation of both C2C12 myoblasts and primary MuSCs. The essential role of KAT2A in MuSC activation was further demonstrated *in vivo* by observing MuSC-specific *Kat2a* LOF mice, which exhibited delayed muscle regeneration. The effect of KAT2A on MuSC activation and differentiation might be mediated by controlling myogenic transcription factor expression and PAX7 acetylation. Our work therefore identified a new posttranslational modification for PAX7, a major MuSCs regulator, and unveiled KAT2A as a main regulator of PAX7 activity. Therefore our study highlights the existence of a signaling cascade leading to the acetylation of PAX7 during MuSCs activation and differentiation.

3.6 Supplementary materials

3.6.1 Materials and Methods

Animals. $Kat2a^{MuSC-/-}$ mice were created at the EPFL SPF animal core facility by crossing $Kat2a^{flox/flox}$ mice (*157*) with the $Pax7^{creER}$ strain (B6.Cg-Pax7$^{tm1(cre/ERT2)Gaka}$/J, purchased from Jackson laboratory). Animal phenotyping experiments were carried out according to standard operational procedures (SOPs) established and validated within the Eumorphia program (*182*). To induce KAT2A knockout in MuSCs, a 20mg/ml of Tamoxifen/corn oil solution was given to $Kat2a^{flox/flox}$:$Pax7^{creER}$ mice via intraperitoneal injection for 5 consecutive days at 1mg/10g of mouse body weight. $Kat2a^{flox/flox}$ mice were injected at the same dosage of tamoxifen and served as controls. All mice were housed in micro-isolator cages in a room illuminated from 7:00am-7:00pm with *ad libitum* access to normal chow diet (2016S, Harlan Laboratories) and water. Animal experiments were authorized by the local animal experimentation committee of the Canton de Vaud under licenses 2665 and 2890.

Grip strength test. Muscle strength was assessed by a grip strength behavior task after 5 weeks of NR treatment. The grasp strength of each mouse for all four limbs was measured on a pull-grid assembly connected to the grip strength meter (Columbus Instruments). The mouse was drawn along a straight line parallel to the grid until the grip is broken and the peak amount of force in grams was recorded. This was repeated 4 times with 5 minute intervals.

FACS based muscle stem cell isolation. Gastrocnemius, soleus, quadriceps, and tibialis anterior muscles from both limbs were excised and transferred into PBS on ice. All muscles were trimmed, minced and digested with 0.1mg/ml of type II collagenase (Sigma) in PBS for 15 min at 37°C. Samples were then centrifuged at 750g for 5min and further digested in 1 mg/ml of collagenase/dispase (Roche) for 30 min at 37°C. Muscle slurries were sequentially filtered through 100, 70 and 40 µm cell strainers. The isolated cells were then washed in washing buffer (PBS + 2.5% FBS) then resuspended in 200µl of washing buffer and immediately stained with antibodies, including the MuSC markers CD31 (1:800, eBioscience, eFluor450 conjugated); CD34 (1:200, eBioscience, eFluor660 conjugated); CD45 (1:200, eBioscience, eFluor450 conjugated); CD11b (1:400, eBioscience, eFluor450 conjugated); Sca-1 (1:1000, eBioscience, PE-Cy7 conjugated); and α7 integrin (1:300, MBL) for 30 min at 4°C. Secondary staining was performed with a mixture of goat anti-mouse antibody (1:800, Life technologies, Alexa Fluor 488 conjugated) and propidium Iodide (PI, Sigma) for 15 min at 4°C in the dark. Stained cells were analyzed and sorted using the FACSAria II instrument (BD Biosciences). Debris and dead cells were excluded by forward scatter, side scatter and PI gating. Cells were sorted either directly on slides for immunostaining or into lysis buffer for NAD$^+$ measurements and into TriPure (Roche) reagent for RNA extraction.

Cell culture and treatments. FACS sorted MuSCs were grown on a 10% Matrigel (Corning)-coated dish and flasks with Fams F-10 media (Gibco), supplemented with 20%

fetal bovine serum (FBS, Gibco), 2.5ng/ml basic fibroblast growth factor (bFGF, Sigma) and penicillin/streptomycin (1x, Gibco). Dishes were coated with 10% growth factor-free Matrigel solution on ice for 7 min then transferred to a 37°C cell culture incubator overnight before use. Cells were grown for three generations *in vitro* before experiments with cells plated and passaged at 10^3 cells/ml and 50% confluence, respectively. C2C12 mouse myoblasts were grown in DMEM (4.5g/L glucose, Gibco) supplemented with 10% FBS and penicillin/streptomycin (1x, Gibco). Gene expression or knockdown was performed using either adenovirus infection or cell transformations with *Kat2a* shRNA (Santa Cruz) using jetPEI DNA transfection kit (Polyplus), according to manufacturer's instructions. Cells were treated with 1mM NR or PBS for 6 hours before cell harvesting or fixation.

Cardiotoxin-induced muscle regeneration. Animals were anesthetized using Isoflurane in oxygen from a precision vaporizer. 50µl of 20µM *Naje mossambica mossambica* cardiotoxin (Sigma) was injected intramuscularly cross the skin and directly into the tibialis anterior (TA) muscle. For SIRT1$^{MuSC-/-}$ mice, cardiotoxin was injected on the third day of the 5 consecutive days of tamoxifen injections, as described above. Mice were sacrificed at 7 and 14 days after injury. TA muscles were immediately embedded in Thermo Scientific™ Shandon™ Cryomatrix™ and frozen in isopentane, cooled in liquid nitrogen, for 2min before being transferred to dry ice and stored at -80°C.

Histology. TA muscles were harvested from anaesthetized mice and immediately frozen in Tissue-TEK® OCT compound (PST). 8-µm cryosections were collected and fixed with 4% paraformaldehyde, which are either stained with haematoxylin/eosin (HE) or antibodies. For immunostainings, heat activated antigen retrieval was performed in pH 6.0 citrate buffer for 10min at 65°C. After washing with PBS-0.1% tween 20 (PBST), the sections were blocked with 10% affinipure Fab goat anti mouse IgG (Jackson Immunoresearch) in PBST for 60min and PBST containing 2% BSA and 5% goat serum for 30min at room temperature. Primary antibodies were then applied over night at 4°C. The following antibodies were used: anti-eMHC (Developmental Studies Hybridoma Bank, DSHB, University of Iowa), anti-Pax7 (DSHB, University of Iowa), anti-Laminin (Sigma). Subsequently, the slides were washed in PBST and incubated with appropriate secondary antibodies and labeling dyes. For immunofluorescence, secondary antibodies were coupled to Alexa-488 or Alexa-568 fluorochromes (Life technology), and nuclei were stained with DAPI (Invitrogen). After washing in PBST, tissue sections were mounted with Dako mounting medium (Dako).

For cellular immunostaining, freshly isolated MuSCs were sorted directly into 8-chamber slides (Thermo Scientific) and examined immediately after 30min of sedimentation or cultured for 3 generations. Cells were then fixed with either 4%PFA or 3% H$_2$O$_2$ in methanol for 10-15min. After 15min permeabilization with 0.5% Triton X-100, cells were blocked and

immunostained using a similar protocol to that used for muscle tissue sections. All samples were imaged with a DMI4000 B Inverted Microscope (Leica) or the VS120-S6-W slides scanner (Olympus). Images were analyzed using ImageJ software. For immunofluorescence quantification, positively stained cells were defined as those with an intensity that was higher than a given threshold, which was then applied to all images. The thresholds were set up using sample slides before analyzing experimental data. More than 3 whole muscle cross-section areas, or more than 6 randomly chosen microscope scopes from each animal in all experimental conditions were used for quantification. All *in vitro* cultured or FACS sorted cells (> 500 per condition) were applied for analysis if cell number quantifications were performed.

Gene expression analyses. Total RNA was extracted from MuSCs by sorting cells directly into TriPure RNA isolation reagent (Roche) or from cultured C2C12 myoblasts using TriPure reagent according to the product manual. Total RNA was transcribed to cDNA using QuantiTect Reverse Transcription Kit (Qiagen). Expression of selected genes was analyzed using the LightCycler480 system (Roche) and LightCycler® 480 SYBR Green I Master reagent (Roche). The acidic ribosomal protein 36b4 gene (ribosomal protein, large, P0, *Rplp0*) was used as house keeping reference.

Western blotting. C2C12 cells were lysed in a buffer composed of 50 mM Tris, 150 mM KCl, EDTA 1 mM, NP40 1%, nicotinamide 5mM, sodium butyrate 1mM and protease inhibitors cocktail (Roche) at pH 7,4. Proteins were separated by SDS-PAGE and transferred onto nitrocellulose membranes. Blocking and antibody incubations were performed in 3% BSA. The following primary antibodies were used: anti-β-actin (Sigma); anti-KAT2A (cell signaling); anti-KAT2B (cell signaling); anti-HSP90 (BD Biosciences). All secondary antibodies were from Jackson Immunoresearch. Antibody detection reactions were developed by enhanced chemiluminescence (Advansta, CA, USA) and imaged using the c300 imaging system (Azure Biosystems).

Bioinformatic analysis. Quadriceps microarray data from young and aged mice MuSCs (*7, 152, 155*) were analyzed for transcript expression using the Kyoto encyclopedia of genes and genomes (KEGG), gene ontology (GO) or gene set enrichment analysis (GSEA) analysis. Raw microarray data are also publicly available on GEO under the accession numbers GSE47177, GSE47401 and GSE47104. All gene expression heat maps were drawn using GENE-E software.

Statistical analysis. The sample size (n) for each experimental group is described in each figure legend. GraphPad Prism software was used for all statistical analyses. Quantitative data displayed as histograms are expressed as means ± standard error of the mean (represented as error bars). Results from each group were averaged and used to calculate

descriptive statistics. *Student*'s *t* test was used for comparisons between two groups with statistical significance was set at a *P* value of *P < 0.05, **P < 0.01 and ***P < 0.001. For multiple comparisons, a two-way analysis of variance (ANOVA) was performed followed by a Newman–Keuls post-hoc test.

3.6.2 Supplementary figures
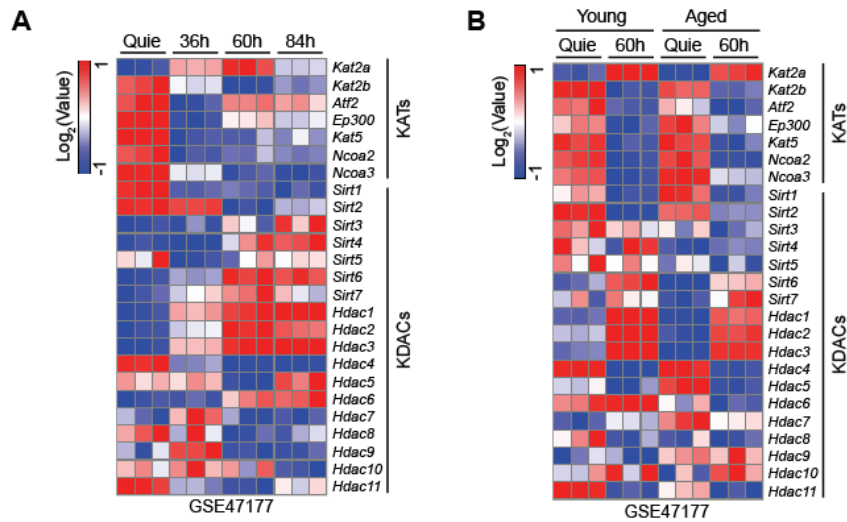
figure 3.S 1 KDAC and KAT gene expression patterns in MuSCs during muscle regeneration

A-B, clustered heatmap of the gene expression profiles for (A) CD34^{+} quiescent and activated MuSCs prior to and 36, 60 and 84hr after $BaCl_2$-induced muscle injury(7); (B) MuSCs isolated from young (2-3 months old) and aged (2-years old) mice(7) in quiescent or activated MuSCs prior to 60 hours after $BaCl_2$-induced muscle injury.
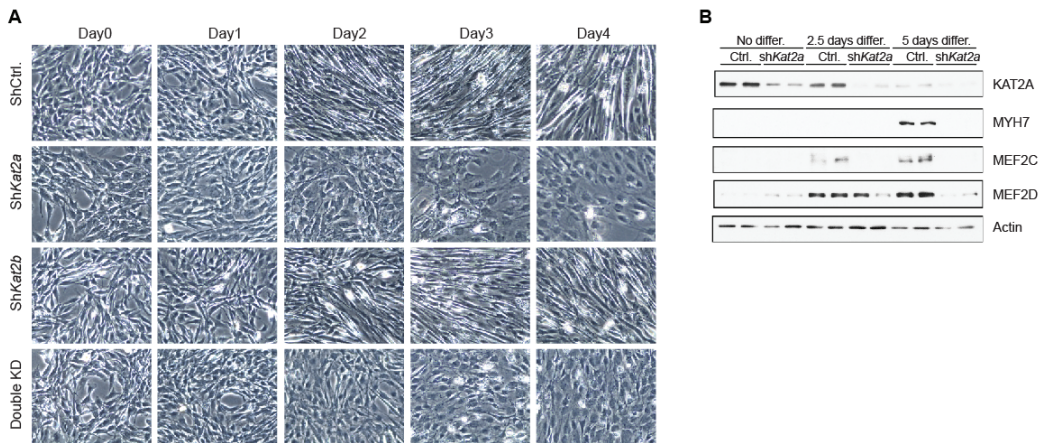
figure 3.S 2 KAT2A controls the myogenic differentiation of MuSCs

A, morphology of C2C12 myoblast differentiated at the indicated days, with or without shRNA induced *Kat2a* and/or *Kat2b* LOF; B, protein levels of the myoblast differentiation marker MYH7 and myogenic differentiation regulators MEF2C and MEF2D, in C2C12 myoblast at the indicated differentiation time points, with or without *Kat2a* and/or *Kat2b* LOF. Actin served as a loading control.

figure 3.S 3 Schema of making *Kat2a*^{MuSC-/-} mice

Kat2a^{MuSC-/-} mice were created by crossing *Kat2a*^{flox/flox} mice with the *Pax7*^{creER} strain (B6.Cg-Pax7^{tm1(cre/ERT2)Gaka}/J), purchased from Jackson laboratory.

Chapter 4. NAD$^+$ repletion improves muscle function in muscular dystrophy

Adapted from :

4.1 Abstract

Duchenne muscular dystrophy (DMD) is caused by inherited mutations in the dystrophin gene that lead to progressive skeletal muscle degeneration. In diverse populations of mice we observe strong correlations between transcripts related to mitochondrial biogenesis, the dystrophin-sarcoglycan complex, and nicotinamide adenine dinucleotide (NAD^+)-synthesis, suggesting a role for the essential cofactor NAD^+ in protecting muscle from metabolic and structural degeneration. Furthermore, human transcriptome data from patients with DMD, and other muscle diseases, exhibit a particular signature of enrichment for various poly ADP-ribose (PAR) polymerases (PARPs) and the nicotinamide N-methyltransferase (*NNMT)* transcript, all major consumers of NAD^+ involved in pleiotropic events, including inflammation. Validating these findings, we reveal that the *mdx* mouse, a model of DMD, is characterized by significant reductions in muscle NAD^+ levels, concurrent to increased PARP activity and reduced expression of nicotinamide phosphoribosyltransferase (NAMPT), the rate-limiting enzyme for NAD^+ biosynthesis. Replenishing NAD^+ stores by dietary nicotinamide riboside supplementation benefits muscle function in *mdx* and *mdx*/*Utr^-/-^* mice, an effect replicated in *C. elegans* models of DMD. The beneficial effects of NAD^+ repletion in muscular dystrophy are pleiotropic and rely on the improvement in mitochondrial function and structural protein expression and on reductions in general PARylation, inflammation and fibrosis. We furthermore validated non-invasive magnetic resonance spectroscopy (MRS) monitoring of NAD^+ levels as a clinical biomarker of disease severity and efficacy of NAD^+ boosting strategies. In combination, these studies suggest that the replenishment of NAD^+ may be of benefit to patients with muscular dystrophies characterized by *PARP/NNMT* gene expression signatures.

4.2 One sentence summary

NAD^+ repletion by NR diet improves muscle function in muscular dystrophy

4.3 Introduction

Muscular dystrophies result from the reduced support network that connects myofilament proteins within the cell to the basal lamina outside the cell, rendering the sarcolemma more susceptible to damage. As an X-linked mutation, DMD affects 1 in 3500 males and often leads to death due to heart or respiratory failure (*200, 201*). With no effective treatment, the deterioration of muscle function and strength results from increased muscle damage, fibrosis and necrosis. DMD symptoms are shared by other pathologies that involve muscle wasting, such as cancer, AIDS and aging, all characterized by declines in metabolic and physiological parameters, with progressive weakness in skeletal muscle. Despite considerable advances in exon skipping and other genetic and pharmacological approaches to treat DMD, there are

still many caveats in the delivery, effectiveness and safety of these therapies (reviewed in (*202*)), thus leaving a necessity for other therapeutic strategies.

Fatigue and muscle weakness, as seen in DMD, are also symptoms of mitochondrial myopathies and metabolic diseases (reviewed in (*203*)). Recent studies have linked SIRT1-dependent mitochondrial biogenesis to reductions in *mdx* mice pathology and muscle atrophy (*204-207*). Interestingly, NAD^+ repletion provides protection from metabolic diseases and mitochondrial dysfunction induced by diet or aging, often in a SIRT1-dependent manner (*101, 157-160*). Sirtuins in general consume NAD^+ as a cofactor for the deacetylation of proteins while also generating nicotinamide (NAM). Similarly, PARP proteins are known to consume NAD^+ during the poly ADP-ribosylation (PARylation) of proteins. As a result, PARP inhibition or genetic loss of function of *PARP1* in mice, increases muscle NAD^+ levels and sirtuin-directed mitochondrial biogenesis (*208, 209*). Initial evidence for an involvement of PARP activity in DMD was revealed with increased PARP1 expression, from 20 patient biopsies, that was correlated to reduced telomere length (*210*). We provide evidence that *PARP* expression in DMD biopsies spans across 10 members of the PARP family, creating a unique signature of expression common with that of other (neuro-)muscular diseases, thus warranting an analysis of NAD^+ metabolism in various models of DMD ranging from *C. elegans* to mice. In addition, NAD^+ can promote the polymerization of laminin and subcellular localization of paxillin, an integrin-associated adaptor protein, improving cell adhesion in a zebra fish models of muscular dystrophy (*211*). Taking these evidences into consideration, we hypothesized that NAD^+ availability, balanced, in part, by the conversion of NAM to nicotinamide mononucleotide (NMN) by the rate limiting salvage enzyme NAMPT, the further conversion of NMN to NAD^+ by NMN adenylyltransferases (NMNATs), and finally NAD^+ consumption by a panel of PARP proteins (Figure 4. 1A; reviewed in (*212*)), could have a multifaceted influence on the development of muscle weakness and fatigue in in DMD and potentially other (neuro-)muscular diseases.

Our study reveals that in a mouse model of DMD, widespread PARylation of proteins leads to severe NAD^+ depletion, which is linked to reduced mitochondrial and structural gene expression. Repleting NAD^+ levels with nicotinamide riboside treatment, an NAD^+ booster, not only restored mitochondrial function but also expression of proteins in the dystrophin-associated glycoprotein complex and improved muscle function in multiple species. We furthermore validate NAD^+ as a biomarker for the diagnosis and treatment of muscle dysfunction that could have broad clinical applications, not only in muscular dystrophy, but also in other muscle diseases characterized by mitochondrial dysfunction or PARP activation.

4.4 Results

4.4.1 Correlations between transcripts related to NAD$^+$ with muscular dystrophy

To evaluate the relationship between muscle NAD$^+$ metabolism and muscle health, we first examined correlations between transcripts of NAD$^+$ salvaging or consuming enzymes and diverse muscle parameters. By assessing natural transcript variance in quadriceps muscles of 42 strains of genetically-diverse BXD mice (described in (*157, 213-215*)) (figure 4. S1, A to B), we observed that *Nampt and Nmnat3* expression levels correlate positively to muscle mass (Figure 4. 1, B and C). *Nampt* also correlates robustly to increased expression of transcripts related to mitochondrial biogenesis (Figure 4. 1D). Using custom-generated gene sets from BXD strains expressing the highest and lowest levels of *Nampt* transcripts, genes related to mitochondrial biogenesis, autophagy and muscle regeneration, along with *Nmnat1*, were found to be enriched with *Nampt* (figure 4. S1C) (*216*). Based on this preliminary analysis, we performed a principal component analyses on these networks now using all 42 BXD strains. In the resulting factor loading plot, we observed that transcripts encoding genes relating to mitochondrial biogenesis, the dystrophin-sarcoglycan complex and muscle regeneration are strongly correlated to expression of *Nampt*, *Nmnat1* and *Nrk1,* an enzyme responsible for converting nicotinamide riboside (NR) into NMN, suggesting a beneficial effect of NAD$^+$-synthesis on several levels of muscle function (Figure 4. 1E). A circular schematic was then plotted using the same set of genes in order to demonstrate the positive and negative correlations amongst each of them (Figure 4. 1F). Interestingly, we found that genes associated with the pathogenesis of muscle dystrophy in *mdx* mice were negatively correlated in this principal component analysis, while genes related to mitochondrial biogenesis and muscle structure and growth correlated positively. We then examined the expression of transcripts involved in NAD$^+$ homeostasis in extant human skeletal muscle datasets from patients with DMD in comparison to controls (*217, 218*). In contrast to the previously described elevation in *PARP1* expression in DMD muscle (*210*), we discovered a consistent enrichment signature of *PARP* transcripts, and of the nicotinamide N-methyltransferase (*NNMT)* transcript, an enzyme known to shunt NAD$^+$ away from biosynthesis through methylation (*219, 220*), with no change in *PARP1* expression (Figure 4. 1G). Surprisingly, this *PARP/NNMT* gene enrichment signature was very well replicated in biopsies from patients with a large variety of muscular dystrophies or (neuro-)muscular disease (figure 4. S2A). Alternatively, genes associated with biosynthesis were not significantly altered in any of these patient datasets (Figure 4. 1H and figure 4. S2B). These findings demonstrated the high likelihood for NAD$^+$ depletion in DMD, but also in other (neuro-)muscular diseases.
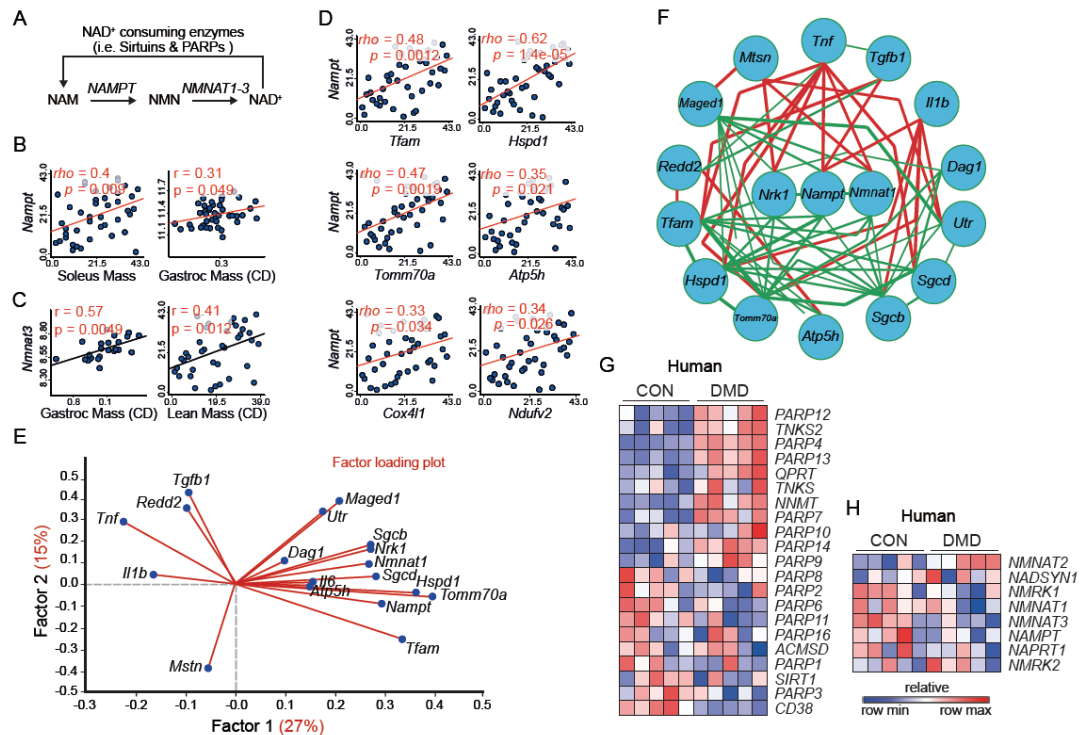
Figure 4. 1 The relationship between transcripts involved in NAD⁺-biosynthesis and consumption with muscular dystrophy in mice and DMD patients

(A) Schematic illustrating NAD⁺ consumption by Sirtuins and PARPs and the salvage of NAD⁺ from NAM via NAMPT and NMNAT enzymes. In 42 strains of genetically-diverse BXD mice (B) *Nampt* and (C) *Nmnat3* transcripts were each positively correlated to various measurements of muscle mass, as a percentage of body weight. (D) *Nampt* transcript expression in the BXD strains was also positively correlated with transcript expression for regulators of mitochondrial transcription and for genes encoding components of the mitochondria. (E) Further analysis of the BXD strains showed that mitochondrial-related transcripts (*Tfam*, *Hspd1*, *Atp5h* and *Tomm70a*) remain positively correlated to NAD⁺-synthesis transcripts (*Nampt*, *Nmnat1* and *Nrk1*), as seen on a factor loading plot (biplot), where angles more than 90° between gene vectors represent negative correlation (and an angle of 180° indicates perfect negative correlation). Also, NAD⁺-synthesis transcripts positively correlate to transcripts of utrophin (*Utr*) and dystrophin-associated glycoproteins (*Dag1*, *Sgcb*, *Sgcd*) and muscle growth (*Maged1* and *Il6*), while they are negatively correlated to genes previously reported to be involved in the pathology of *mdx* mice (*Tgfb1*, *Tnf*, *Mstn*, *Il1b* and *Redd2*). These transcripts were then plotted in a (F) circular schematic using a Pearson's $r \geq |0.2|$ in BXD strains showing negative (red) and positive (green) correlations. The expression of transcripts related to NAD⁺ (G) consumption or (H) biosynthesis show an enrichment signature of *PARP* genes and of the *NNMT* gene in human DMD skeletal muscle datasets (n=5/group) (*217, 218*).

4.4.2 NAD⁺ as a biomarker of elevated PARP activity in *mdx* mice

Given the central role of NAD⁺ in mitochondrial homeostasis and organismal metabolism (*104*), we set out to determine if reduced NAD⁺ levels could explain the attenuation of mitochondrial function in the muscle of *mdx* mice and could be used as an *in vivo* biomarker of muscle damage. Indeed, *in vivo* non-invasive ³¹P MRS measurements of NAD⁺ levels were lower in *mdx* muscle compared to controls (Figure 4. 2A). Reduced NAD⁺ levels were

also confirmed by mass spectrometry measurements (*157*) in postmortem muscle specimens (Figure 4. 2B). From the high expression of PARP transcripts in DMD patients (Figure 4. 1H), we hypothesized that the over-activation of PARPs could underpin the depletion of NAD$^+$ levels in *mdx* mice, an idea further bolstered by our recent data showing the contrasting situation of elevated NAD$^+$ levels in *Parp1*KO mice (*100*) or in PARP inhibitor-treated mice (*157*). As hypothesized, PARP activity and global protein PARylation levels were increased in *mdx* muscle (Figure 4. 2C), which also reinforces the usefulness of the *mdx* model for comparisons to DMD. Furthermore, reduced NAMPT protein levels and NAD$^+$ salvage may also contribute to the reductions in NAD$^+$ levels in *mdx* muscle (Figure 4. 2D). Of note, NMNAT1 and NMNAT3 levels were not changed in *mdx* mice. These results indicate that *mdx*-induced damage leads to PARP activation, attenuated NAD$^+$ salvage and reduced NAD$^+$ levels, which serve as a potential biomarker for muscular dysfunction.
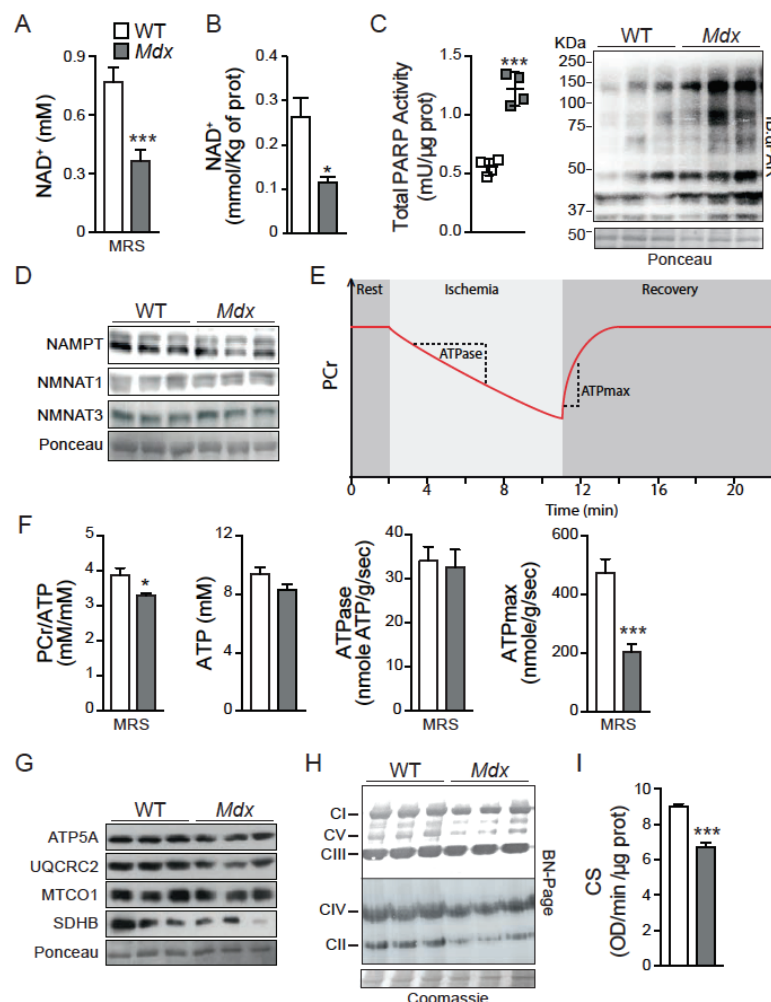
Figure 4. 2 NAD$^+$ as a biomarker and limiting factor for *in vivo* energetics and mitochondrial function in *mdx* mice

Measurements on gastrocnemius from 16-week-old male *mdx* or control mice. As a potential new biomarker for muscular dystrophy, (**A**) NAD$^+$ levels were reduced, as measured by ^{31}P MRS (n=7, WT; n=12, *mdx*). (**B**) These

values paralleled total intracellular NAD$^+$ levels measured by mass spectrometry in tissue extracts (n=5). Reductions in NAD$^+$ levels may be due to augmented NAD$^+$ consumption, evidenced by enhanced (**C**) PARP activity and total PARylation content (n=4), in addition to reduced NAD$^+$ salvage demonstrated by lower (**D**) NAMPT protein, with NMNAT1 and NMNAT3 unchanged, using a Ponceau loading control. (**E**) Schematic of *in vivo* ^{31}P MRS of *mdx* skeletal muscle mitochondrial energetics. Dynamic MR spectra were acquired during the following periods: rest (2 min), ischemia (9 min), and recovery (9 min). (**F**) HPLC and ^{31}P MRS measurements of ATP and Phosphocreatine (PCr), respectively, showing unchanged ATP levels (n=7) and a reduction in the PCr/ATP ratio (n=7, WT; n=5, *mdx*). As the resting ATPase activity did not change (indicating unaltered ATP demand) (n=7 for WT; n=5, *mdx*), *mdx* animals must function at an increased fraction of their now reduced maximal capacity (ATPmax) (n=7, WT; n=5, *mdx*) to meet the unchanged ATP demand, when MRS data is compared to control animals. *mdx* muscle exhibited corresponding reductions in mitochondrial proteins and function in *mdx* muscle, as represented by (**G**) nuclear- and mitochondrial-encoded mitochondrial protein expression, compared to a Ponceau loading control, (**H**) Blue-native PAGE of isolated mitochondria and (**i**) citrate synthase (CS) activity (n=9).

4.4.3 Limited NAD$^+$ affects in vivo energetics and mitochondrial function in mdx mice

To corroborate the known positive relationship between mitochondrial biogenesis and NAD$^+$ metabolism (reviewed in (*212*)), we assessed *mdx* skeletal hindlimb muscles mitochondrial energetics using *in vivo* ^{31}P MRS to measure ATP and phosphocreatine (PCr) fluxes (Figure 4. 2E). PCr buffers cellular ATP levels through the creatine kinase reaction. Therefore the ratio of PCr/ATP reflects the cellular energy state. The lower PCr/ATP ratio in the *mdx* hindlimb is a reflection of energy stress and demonstrates a greater load on the mitochondria to maintain ATP levels (Figure 4. 2F). This greater load on the mitochondria in *mdx* hindlimb muscles is also apparent in the relationship between resting and maximal mitochondrial ATP production. As previously reported in *mdx* mice (*221*), the maximum mitochondrial oxidative phosphorylation rate (ATPmax) was reduced *in vivo* compared to WT mice, while the resting ATPase activity, which reflects resting mitochondria ATP synthesis, was unchanged (Figure 4. 2F). Thus, *mdx* hindlimb mitochondria had to function at a greater fraction of their capacity to meet ATP demand (ATPase), than in the WT mice, and were therefore under a greater energy stress (lower PCr/ATP). Explaining these energetic impairments and reaffirming the role of NAD$^+$ in mitochondria, protein levels for both nuclear- and mitochondrial-encoded OXPHOS subunits, including ATP5A, UQCRC2, MTCO1 and SDHB were lower in *mdx* mice (Figure 4. 2G). A lower abundance of complexes I, II, IV and V in *mdx* skeletal muscles was also evidenced by Blue-native gel electrophoresis (Figure 4. 2H). Coordinately, citrate synthase (CS) activity in *mdx* muscle extracts were reduced compared to control samples (Figure 4. 2I). Together these data confirm that NAD$^+$ levels are attenuated in *mdx* muscles, resulting in impaired tissue energetics and mitochondrial function.

4.4.4 NR enhances muscle function in cells and dys-1;hlh-1 mutant C. elegans

Boosting NAD$^+$ levels using various NAD$^+$ precursors, may hence recover mitochondrial function, potentially improving muscle health (*101, 222*). To test this hypothesis, we first

evaluated the effects of the NAD$^+$-precursor NR on mitochondrial function in mouse skeletal muscle C2C12 cells. Notably, NR increased NAD$^+$ levels (Figure 4. 3A), improving mitochondrial complex abundance in differentiated C2C12 myotubes (Figure 4. 3B). NR also increased the maximal electron transport system (ETS) capacity in C2C12 myotubes, following exposure to the uncoupler, FCCP (Figure 4. 3C). Consistent with the fact that the beneficial impact of NAD$^+$ boosting is reliant on sirtuin-mediated protein deacetylation, global protein acetylation was reduced in NR-treated C2C12 myotubes (Figure 4. 3D). Furthermore, NR modulated myotube mitochondrial protein expression and FOXO1 acetylation in SIRT1-dependent fashion, as evidenced by pharmacological (using the SIRT1 inhibitor EX527) and genetic (using a SIRT1 shRNA) SIRT1 loss of function (LOF) experiments (Figure 4. 3E).

We further ascertained the involvement of SIRT1 in mediating the effect of NR, by studying the mobility of worms carrying mutations for both the dystrophin-like gene *dys-1* and the MyoD homologue *hlh-1* that display time-dependent impairments of locomotion and muscle degeneration during aging (*223*). NR improved the mobility of *dys-1;hlh-1* mutant worms over the course of 6 days of aging, an effect that was completely attenuated upon feeding worms with *sir-2.1* RNAi (RNAi for the worm otholog of SIRT1) (Figure 4. 3F). Following 8 days there was also a *sir-2.1*-dependent improvement in worm paralysis with NR treatment (Figure 4. 3G). Importantly, *dys-1;hlh-1* worms exhibited less muscle degeneration when treated with NR (Figure 4. 3H). This beneficial effect was again lost with *sir-2.1*RNAi (Figure 4. 3H). Altogether, these results suggest that NR enhances mitochondrial function in C2C12 muscle cells and improves mobility and the dystrophy phenotype in *C. elegans*, in a SIRT1-dependent manner.
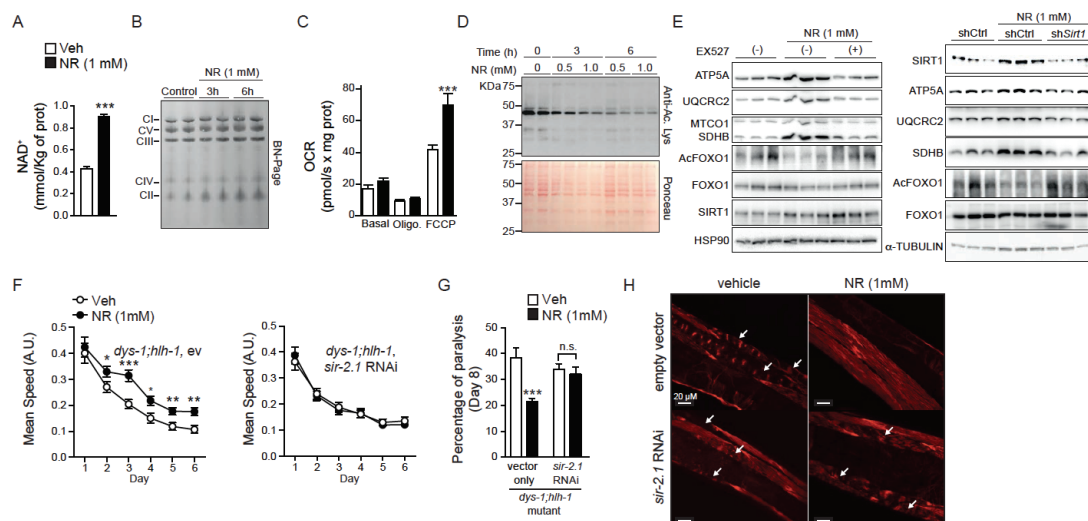
Figure 4. 3 NR enhances mitochondrial function in C2C12 myotubes and increases SIRT1-dependent muscle integrity and function in *dys-1;hlh-1* double mutant *C. elegans*

C2C12 myotubes were treated with 0.5 to 1 mM NR. 12 hrs of NR increases (A) intracellular NAD^+ levels (n=6), inducing (B) mitochondrial biogenesis, as demonstrated by Blue-native PAGE of mitochondrial complexes from isolated mitochondria, and (C) increased OCR in myotubes exposed to the uncoupler FCCP (n=6). (D) Total protein acetyl-lysine levels in myotubes were reduced after 3-6hrs of exposure to 0.5 and 1mM NR. (E) SIRT1 inhibition with EX527 (10 µM) in myotubes or knockdown with an sh*Sirt1* adenovirus attenuated increases in mitochondrial proteins and reductions in FOXO1 acetylation following NR treatment. (F) Improvements in *dys-1;hlh-1* mutant worm fitness on days 2-6 of adulthood following NR, and its *sir-2.1*-dependence shown in animals fed RNAi for *sir-2.1* [R11A8.4], as measured by examining worm motility using the worm tracker (*158*) (n=3, 60 worms per experiment). Reduced worm paralysis (n=3, 60 worms per experiment) (G) and muscle degeneration (n=6, 60 worms per experiment) (H) in *dys-1;hlh-1* mutant worms following NR was not observed in *dys-1;hlh-1* worms fed RNAi for *sir-2.1*. Arrows indicate degenerated muscle fibers.

4.4.5 NR reduces PARylation and improves in vivo muscle energetics in *mdx* mice

These data incited us to determine the efficacy of NR to prevent or delay the onset of mitochondrial dysfunction in muscular dystrophy. Therefore, using a preventive approach we fed a chow diet supplemented with NR (400 mg/kg/day) to 4-week-old *mdx* mice for 12 weeks and assessed NAD^+ levels and mitochondrial energetics *in vivo* using the same ^{31}P MRS approach. NR-treatment enhanced *in vivo* NAD^+ bioavailability in the hindlimb muscles of *mdx* mice (Figure 4. 4A), as again confirmed with postmortem measurements of gastrocnemius biopsies (Figure 4. 4B). Of note, NAD^+ levels were also lower in the livers of *mdx* mice and were restored by NR supplementation, whereas no change was observed in NAD^+ levels in subcutaneous white adipose tissue (figure 4. S3, A and B). In the muscle, this increase in NAD^+ levels occurred concurrent to a reduction in PARP activity and global PARylation (Figure 4. 4C), along with elevated NAMPT, NMNAT1 and NMNAT3 protein expression in *mdx* muscle (Figure 4. 4D). With unchanged ATP levels (Figure 4. 4E), NAD^+ repletion improved the PCr/ATP ratio, indicating less energy stress in NR treated muscles. The reduced energy stress was supported by an elevation in the mitochondrial capacity (higher ATPmax) without a change in resting ATPase activity (Figure 4. 4F). Therefore, as NR-treated *mdx* mice exhibited a higher ATPmax, their hindlimb muscle mitochondria were able to work at a lower fraction of their capacity to meet ATP demand (ATPase) and were therefore under a lower energy stress (higher PCr/ATP). On a mechanistic level, this was accompanied by increased abundance of individual OXPHOS proteins and of mitochondrial complexes II, IV and V (Figure 4. 4, G and H). In addition, CS activity and cytochrome *c* oxidase histochemical staining of gastrocnemius was increased in NR treated *mdx* muscles (Figure 4. 4, I and J). As a result, NR increased the running capacity in *mdx* mice (Figure 4. 4K), in the absence of body weight and lean mass differences (figure 4. S3 C and D). Interestingly, the respiratory exchange ratio (RER) was lower in *mdx* compared to control mice, an effect that was surprisingly attenuated with NR (figure 4. S3 E). NR therefore effectively corrected the mitochondrial profile of *mdx* animals leading to *in vivo* improvements

in muscle energetics and function, all of which correlated well with the measurements of NAD$^+$ as a biomarker for disease severity and treatment effectiveness.
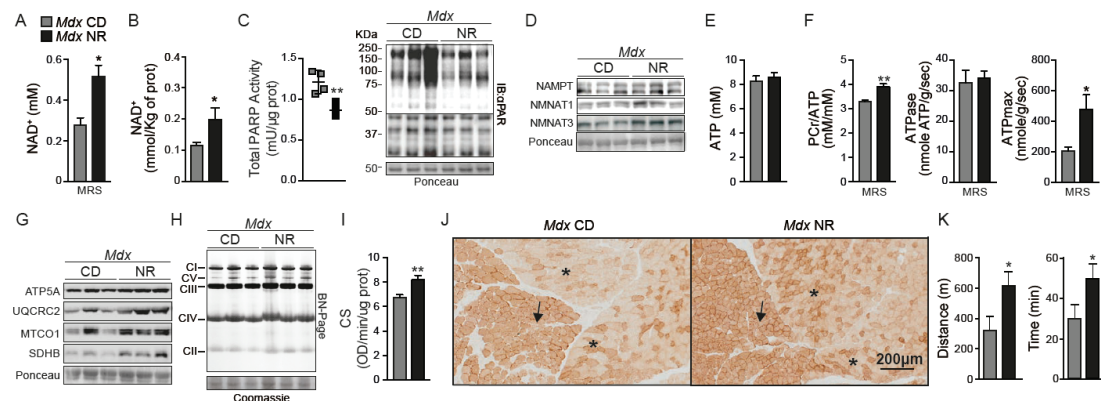
Figure 4. 4 *In vivo* **monitoring of NAD$^+$ provides an efficacy biomarker for improvements in the phenotype of NR-treated *mdx* mice**

16-week-old *mdx* mice received a dietary supplement with NR (400 mg/kg/day) for 12 weeks. (**A**) ^{31}P MRS measurements of increasing NAD$^+$ levels upon NR treatment in *mdx* mice (n=5, *mdx*; n=10, *mdx* NR). (**B**) The recovery of *mdx* muscle NAD$^+$ levels was verified by the analysis of gastrocnemius extracts by MS (n=5). (**C**) PARP activity and total protein PARylation was reduced (n=4), while (**D**) NAMPT, NMNAT1 and NMNAT3 content increased, following NR treatment of *mdx* mice. (**E**) Unchanged ATP levels were measured by HPLC in gastrocnemius (n=7, *mdx*; n=10, *mdx* NR). (**F**) *in vivo* ^{31}P MRS measurements of mitochondrial energetics revealed an improvement in the PCr/ATP ratio (n=5, *mdx*; n=10, *mdx* NR), unchanged resting ATPase activity (n=5, *mdx*; n=10, *mdx* NR), and a recovery of ATPmax (n=5, *mdx*; n=10, *mdx* NR) in NR treated *mdx* mice. NR treated *mdx* animals hence function at a reduced fraction of their capacity (ATPmax) to meet ATP demand. The enhancement of NAD$^+$ metabolism with NR prevented improved (**G**) ATP5A, UQCRC2, MTCO1 and SDHB protein levels, using a Ponceau loading control, (**H**) mitochondrial complexes as evidenced by Blue-native PAGE of isolated gastrocnemius mitochondria, using a Coomassie loading control, (**I**) CS activity in frozen gastrocnemius extracts (n=9, *mdx*; n=6, *mdx* NR), and (**J**) cytochrome *c* oxidase staining of soleus (arrow) and gastrocnemius (asterisks) muscle fibers. (**K**) NR increased the running distance and time during an endurance treadmill test in *mdx* mice (n=9, *mdx*; n=12, *mdx* NR).

4.4.6 NAD$^+$ repletion protects *mdx* muscle from damage, inflammation and fibrosis

As the transcripts of the dystrophin-sarcoglycan complex and muscle regeneration are strongly correlated to *Nampt*, *Nmnat1* and *Nrk1* expression in the BXD reference population (Figure 4. 1, E and F), we next determined if changes in NAD$^+$ altered muscle integrity in *mdx* mice. Indeed, this positive correlation was consistent with the robust increase in α-dystrobrevin and δ-sarcoglycan protein in the gastrocnemius of *mdx* mice treated in a preventive mode with NR (Figure 4. 5A). The NR treated *mdx* mice, furthermore, displayed less susceptibility to muscle damage, evidenced by reduced permeability to Evans Blue (Figure 4. 5, B-D), decreased plasma creatine kinase levels (Figure 4. 5E) and increased grip strength (figure 4. S4A). More importantly, the susceptibility to injury was reduced in *mdx* animals during repeated lengthening contractions, from a loss of 64% (SEM = ±15) loss to a

34% (SEM = ±12) in animals treated with NR (Figure 4. 5F). These mice also showed a reduced number of centralized nuclei in tibialis anterior muscles (Figure 4. 5, G). The average minimal Feret's diameter, and corresponding distribution, showed an increase in fiber size with NR treatment in *mdx* mice (Figure 4. 5, G and H and figure 4. S4B). This was confirmed in these same mice by quantifying the average and distribution of cross-sectional area of muscle fibers (Figure 4. 5, G and H and figure 4. S4C). In conjunction with the improved muscle function and the reduced level of muscle damage with NR, muscle inflammation was decreased in NR treated *mdx* mice. This was reflected by the ability of NR treatment to reduce macrophage infiltration in the skeletal muscle of *mdx* animals (figure 4. S4D) and to attenuate *Tnfα* transcript levels in *mdx* mice (figure 4. S4E), with no effect on the expression of anti-inflammatory genes *Il13* and *Il4* (data not shown). The reduction of skeletal muscle inflammation following NR was also recapitulated in the diaphragm, as demonstrated by reductions in staining for CD45 in muscle transverse- and longitudinal-sections (Figure 4. 5I and figure 4. S4F). Closely related to inflammation and damage, a population of muscle resident cells expressing mesenchymal PDGF receptor alpha (PDGFRα), capable of differentiating *in vitro* to fibrogenic or adipogenic lineages and named fibro/adipogenic precursors (FAPs) (*224, 225*), were examined following NR treatment in *mdx* mice. The number of FAP cells is known to be higher in both *mdx* and *mdx*/*Utr*^{-/-} mice, causing the deposition of both skeletal muscle fat and connective tissues (*226, 227*). Importantly, FAP cell numbers were lower in both the TA (figure 4. S4, G and H) and in transverse- and longitudinal-sections of the diaphragm (Figure 4. 5J and figure 4. S4, I and J) of *mdx* mice given an NR supplement. In line with the reduction of FAP cell numbers, NR treatment reduced the appearance of fibrosis in both transverse- and longitudinal-sections of the diaphragm of *mdx* mice (Figure 4. 5J and figure 4. S4 K).

Importantly, using a therapeutic approach, a 12-week NR treatment starting at 3.5 weeks of age in the more severe and already symptomatic *mdx*/*Utr*^{-/-} double mutant mouse model also improved grip strength (Figure 4. 5K). This suggests that NR treatment can slow and potentially reverse components of muscular dysfunction in two separate mouse models of muscular dystrophy.
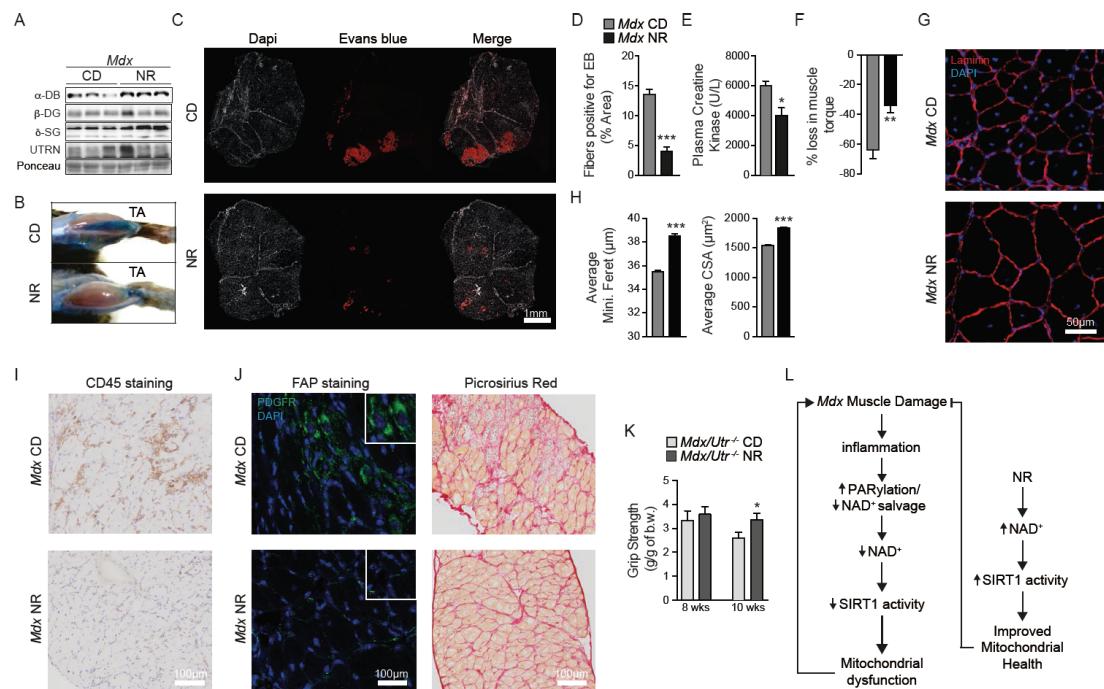
Figure 4. 5 NAD$^+$ repletion causes compensatory increases in the expression of structural proteins and protects muscle from damage and fibrosis

16-week-old *mdx* mice received a dietary supplement with NR (400 mg/kg/day) for 12 weeks. (A) NR-treated *mdx* mice exhibited increased α-dystrobrevin and δ-sarcoglycan protein expression in gastrocnemius extracts. NR attenuated *mdx* muscle damage as evidenced through (B) Evans Blue staining of both TA muscle and (C) sections of gastrocnemius and soleus muscles (Evans Blue - red and dapi - white), (D) quantified using ImageJ software (n=6, *mdx*; n=12, *mdx* NR). NR also (E) reduced basal plasma creatine kinase levels (n=5, *mdx*; n=6, *mdx* NR). (F) mdx mice treated with NR demonstrated an attenuation in the percent loss of torque in quadriceps, following muscle damage induced by lengthening contractions (n=7, *mdx*; n=6, *mdx* NR). (G) Representative images stained with dapi and laminin used to quantify (H) increases in the average minimal Feret's diameter (in µm) and cross-sectional area (in µm^2) of tibialis anterior muscle fibers, indicating increases in fiber size with NR treatment in *mdx* mice (8 weeks of NR treatment, n=5). Quantification of images was performed with ImageJ software. (I) Similarly, reduced CD45 staining was seen in diaphragms of *mdx* mice treated with NR. (J) Fibro/adipogenic precursors (FAPs) expressing mesenchymal PDGF receptor alpha (PDGFRα) were decreased in diaphragms of *mdx* mice treated with NR (n=3). Also, reductions in the fibrosis of *mdx* diaphragms were observed with less Picrosirius red staining in transverse muscle sections of NR treated mice. (K) As evidence for the therapeutic effectiveness of NR treatment, mdx/*Utr$^{-/-}$* mice grip strength was improved from 8 weeks (n=4, *mdx*/*Utr$^{-/-}$*; n=7, *mdx*/*Utr$^{-/-}$* NR) to 10 weeks of age (n=3, *mdx*/*Utr$^{-/-}$*; n=5, *mdx*/*Utr$^{-/-}$* NR). These mice received 5 and 7 weeks of NR treatment (400 mg/kg/day), respectively. (L) Scheme summarizing the SIRT1-dependent effects of NR on *mdx* mouse muscle.

4.5 Discussion and conclusions

We demonstrate here that muscular dystrophy in *mdx* mice is associated with muscle NAD$^+$ depletion, which can be monitored as an *in vivo* biomarker of disease severity using MRS. Reduced NAD$^+$ levels are likely the result of PARP activation and reduced NAD$^+$ salvage (Figure 4. 5L), as postulated from the robust *PARP*/*NNMT* gene enrichment signature in

human dystrophy patients (Figure 4. 1G and figure 4. S2A). PARP activation was previously shown to have a negative correlation to energy expenditure; hence reducing PARP activity improves metabolism by increasing intracellular NAD^+ levels in animals (*157, 228*). NAD^+ repletion in *mdx* animals using NR exploits an alternative NAD^+ synthesis pathway to counter increased PARP consumption of NAD^+, leading to the recovery of NAD^+-dependent sirtuin signaling. This effect attenuates the loss of mitochondrial function and the susceptibility for muscle degeneration and necrosis in *mdx* mice, which may in turn be responsible for the reduced necessity for global PARP activation. Despite elevations in NAD^+ there are reductions of global PARylation owing to the fact that PARP activity is dependent on various other factors for activation, such as inflammation to which PARPs are responsive, as has been shown in liver inflammation and fibrosis (*229*). As inflammation is attenuated in *mdx* mice following NR treatment, we propose that this beneficial effect, that in turn lowers the level of PARP activation in muscle, may slow the development of fibrosis. These data underscore the importance of NR as an alternative substrate for NAD^+ biosynthesis that can be exploited in *mdx* mice to increase muscle strength and decrease susceptibility to mechanical damage, while reducing plasma creatine kinase levels and fibrosis. We also demonstrate the potential for NR to improve muscle function and muscle strength in *mdx*/*Utr$^{-/-}$* mice. Our data therefore suggests that the use of other NAD^+ precursors, such as NMN and NA analogs, and/or inhibitors of NAD^+ consumption, such as PARP inhibitors, could be effective for treating muscular dystrophy. Indeed, all of these different compounds have been shown to improve respiratory capacity in diet or age-related mitochondrial dysfunction (*157, 159, 230*). Finally, these data confirm the importance of SIRT1 as a target for treating the *mdx* phenotype (*204*) and to prevent FOXO-directed muscle degeneration (*207, 231*). More importantly, our work highlights the potential for NAD^+ to act as a biomarker that responds to NAD^+ boosting strategies as an effective adjunct therapy for muscular dystrophy. Our observations may furthermore have broad implications for other (neuro-)muscular diseases, injuries or forms of muscle denervation, that are characterized by mitochondrial dysfunction or general PARP activation.

4.6 Supplementary materials

4.6.1 Materials and Methods

Animal experiments. Three weeks old male C57BL/10SnJ mice or C57BL/10ScSn-*Dmd^{mdx}*/J, purchased from The Jackson Laboratory, were fed with pellets containing vehicle or NR (400 mg/kg/day) for 8 weeks beginning at 3.5 weeks of age. The *mdx*/*Utr$^{-/-}$* double mutant strain was generated by crossing C57BL/10ScSn-*Dmd^{mdx}*/J mice with *Utrn^{tm1Ked}*/J mice from The Jackson Laboratory. Experiments with *mdx*/*Utr$^{-/-}$* mice included both male and females fed with pellets containing vehicle or NR (400 mg/kg/day) up to 13 weeks, beginning

at 3.5 weeks of age. The pellets were prepared by mixing the powder chow diet (D12450B, Research Diets Inc.) with NR dissolved in water. Pellets were dried under a laminar flow hood at least over night. Control pellets without NR were made similarly. Most clinical tests were carried out according to standard operational procedures (SOPs) established and validated within the Eumorphia program (*182*). Body composition was determined by Echo-MRI (Echo Medical Systems) and oxygen consumption (VO_2), food intake and activity levels were monitored during the indirect calorimetry tests using the comprehensive laboratory animal monitoring system (CLAMS, Columbus Instruments) after 3 weeks of treatment. Endurance capacity test was performed as published (*80, 232*) after 7 weeks of treatment. All animals were sacrificed after an overnight fast and 4 to 6hr refed conditions. Blood was collected upon sacrifice, while tissues were collected, weighed and flash-frozen in liquid nitrogen.

Ethical approval: These experiments were authorized by the Veterinary office of the Canton of Vaud, Switzerland (Authorization n°2665).

Cell culture. The C2C12 mosue muscle derived cell line was obtained from ATCC (CRL-1772TM). C2C12 myoblasts were cultured in Dulbecco's modified Eagle's medium (DMEM) including 4.5 g/L glucose, 20% fetal calf serum and 50 μg/ml gentamicin. Differentiation of C2C12 cells into myotubes was induced over four days in Dulbecco's modified Eagle's medium (DMEM) including 4.5 g/L glucose, 2% horse serum and 50 μg/ml gentamicin. Cells were tested for mycoplasma using Mycoprobe (#CUL001B, R&D systems, MN, USA), following the manufacturer's instructions.

Grip strength test. Muscle strength was assessed by a grip strength behavior task after 5 weeks of NR treatment. The grasp strength of each mouse for all four limbs was measured on a pull-grid assembly connected to the grip strength meter (Columbus Instruments). The mouse was drawn along a straight line parallel to the grid until the grip is broken and the peak amount of force in grams was recorded. This was repeated 4 times with 5 minute intervals.

Creatine Kinase. Collected plasma was used for creatine kinase measurements using the CKI Flex® reagent cartridge (Siemens Healthcare Diagnostics AG) on the Dimension®Xpand Plus instrument (Siemens Healthcare Diagnostics AG).

Histology. Muscles prepared for histology were placed in Thermo Scientific™ Shandon™ Cryomatrix™ embedding resin and then frozen in isopentane cooled in liquid nitrogen for 2 min before being placed on dry ice.

5-µm cryosections were stained for succinate dehydrogenase or cytochrome *c* oxidase activity as previously described (*232*), or with picrosirius red to assess fibrosis.

Immunohistochemistry and immunofluorescence was performed on 5-µm cyrosections fixed with 4% paraformaldehyde, which were stained with various antibodies. Heat activated antigen retrieval was performed in pH 6.0 citrate buffer for 10min at 65°C. After washing with PBS-0.1% tween 20 (PBST), sections were blocked with 10% affinipure Fab goat anti mouse IgG (Jackson Immunoresearch) in PBST for 60min followed by PBST containing 2% BSA and 5% goat serum for 30min. Sections were then incubated over night at 4°C with primary antibodies, including anti-Laminin (Sigma), anti-CD45 (Life Technology), anti-F4/80 antigen (AbD Serotec) and anti-PDGF Receptor alpha (cell signaling). Subsequently, the slides were washed in PBST and incubated with appropriate secondary antibodies and labeling dyes. For immunofluorescence, secondary antibodies were coupled to Alexa-488 or Alexa-568 fluorochromes (Life technology), and nuclei were stained with DAPI (Invitrogen). After washing in PBST, tissue sections were mounted with Dako mounting medium (Dako). For immunohistochemistry HRP-tagged secondary antibodies were used and visualized using diaminobenzidine staining, while Mayer's Hematoxylin was used to visualize the nuclei.

Muscle damage was assessed with a 1% solution Evans Blue Dye (EBD), which is injected into the peritoneal cavity, using 1% volume to body weight, 24hrs before sacrifice. EBD is dissolved in PBS (0.15 M NaCl, 10 mM phosphate buffer, pH 7.4) and sterilized by passage through membrane filters with a 0.2 µm pore size. Upon sacrifice, the hind leg skin of the mice is removed, and the animals are photographed for dye uptake into skeletal muscles, indicated by blue coloration. Muscle sections from EBD-injected animals are incubated in ice-cold acetone at −20°C for 10 min, washed 3×10 min with PBS, counterstained with 4',6-diamidino-2-phenylindole (DAPI) and mounted with Vectashield mounting medium. Microscopy images of red emission fluorescence from EBD-positive muscle fibers were analyzed using ImageJ software.

We determined the minimal Feret's diameter and cross-sectional area in tibialis anterior muscles of CD and NR fed *mdx* mice using the ImageJ software quantification of laminin stained muscle images. We analyzed a minimum of 3,000 fibers for each condition and measurement. The minimal Feret's diameter is defined as the minimum distance between two parallel tangents at opposing borders of the muscle fiber. This measure has been found to be resistant to deviations away from the optimal cross-sectioning profile during the sectioning process(*233*).

Enzyme activity measurements. Total poly(ADP-ribose) polymerase activity was analyzed in tissue homogenates using the HT Colorimetric PARP Apoptosis Assay Kit (Trevigen). This

PARP activity assay kit is sensitive to PARylation of proteins that are 2 units of poly-ADP-ribosyl units of length and larger. Citrate synthase activity was determined in tissue homogenates using a commercial CS Assay kit (Sigma).

Tissue and C2C12 cell NAD$^+$ quantification. NAD$^+$ was extracted using acidic extraction method and analyzed with mass-spectrometry. Frozen muscle tissues or cultured cells taken from the -80 freezer were immediately extracted in 1M perchloric acid and neutralized in 3M K2CO3 on ice. After centrifugation, the supernatant was mixed with Buffer A (H2O + 20mM ammonium acetate, pH 9.4) and loaded on to a column (Kintex EVO C18, 100A, 150x2.1mm). The HPLC was run for 2 min at a flow rate of 300ul/min with 100% Buffer A. Then a linear gradient to 100% Buffer B (Methanol + 5mM ammonium acetate, pH 8.5) was performed (from min. 2 to min. 11). 100% Buffer B was maintained for 4min (11 to 15min), then a linear gradient back to 100% Buffer A (from min15 to min 17) began. Buffer A was then maintained at 100% until the end (from min17 to min 25). NAD+ eluted as a sharp peak at and was quantitated based on the peak area compared to a standard curve and normalized to tissue weight or protein of frozen muscle tissues or to protein content of cultured cells.

Identification of Nampt and Parp1-correlated genes and parameters. Quadriceps microarray data (Affymetrix Mouse Gene 1.0 ST) and phenotyping data from a BXD mouse genetic reference population (*157, 213*) were analyzed for correlations with *Nampt* or *Parp1* transcript expression using the GeneNetwork program (http://www.genenetwork.org). Raw microarray data are also publicly available on GEO under the accession number GSE60151. Raw phenotype data are available on GeneNetwork by setting the Group to BXD, type to Phenotype, and searching for the relevant phenotype trait named in Figure 1. Trait 15676 describes soleus muscle mass, as a percentage of body weight, in chow diet fed BXD male mice.

Gene expression analyses. Muscle total RNA was extracted using Trizol extraction. Total RNA was transcribed to cDNA using QuantiTect Reverse Transcription Kit (Qiagen). Expression of selected genes was analyzed using The LightCycler480 System (Roche) and SYBR Green chemistry. All qPCR results were presented relative to the mean of *36b4*, *b2m* and *gapdh*. Primer sets for both quantitative real-time PCR analyses are shown below:

Table S4. 1 Realtime-qPCR primers list

Gene	Description	Forward Primer	Reverse Primer
36b4	ribosomal protein, large, P0	AGATTCGGGATATGCTGTTGG	AAAGCCTGGAAGAAGGAGGTC
b2m	beta-2 microglobulin	TTCTGGTGCTTGTCTCACTG	TATGTTCGGCTTCCCATTCT

gapdh	glyceraldehyde-3-phosphate dehydrogenase	TGTGTCCGTCGTGGATCTGA	CCTGCTTCACCACCTTCTTGAT
tnfα	tumor necrosis factor	GTA GCC CAC GTC GTA GCA AAC	GCA GAC TTA CTG ACC AGC TCA GA
Il13	interleukin 13	CACACTCCATACCATGCTGC	TGTGTCTCTCCCTCTGACCC
Il4	interleukin 4	ACAGGAGAAGGGACGCCAT	GAAGCCCTACAGACGAGCTCA

Western blotting. Samples were lysed in lysis buffer (50 mM Tris, 150 mM KCl, EDTA 1 mM, NP40 1%, nicotinamide 5mM, sodium butyrate 1mM, protease inhibitors pH 7,4). Proteins were separated by SDS-PAGE and transferred onto nitrocellulose membranes. Blocking and antibody incubations were performed in 5% BSA. SIRT1 antibody was from Abcam; Anti-FOXO1 antibody was from Cell Signaling; PAR antibody was from Millipore; anti-acetyl-FRKH(FOXO) antibody was from Santa Cruz Inc. Antibody cocktail (the Mitoprofile Total OXPHOS Rodent WB Antibody Cocktail) for mitochondrial subunits was purchased from Mitosciences. Antibody detection reactions were developed by enhanced chemiluminescence (Advansta, CA, USA) using x-ray films or imaged using the c300 imaging system (Azure Biosystems).

Respirometry on C2C12 myotubes. C2C12 myotubes in suspension were used to measure basal respiration rates using high resolution respirometry (Oroboros Oxygraph-2k; Oroboros Instruments, Austria). Then, oligomycin (2.5 µM), a complex V inhibitor, was injected to measure proton leak, then the protonophore agent FCCP (0.2 mM) was titrated to achieve maximum electron transfer flux. O_2 flux obtained in each step of the protocol was normalized by the protein content of the sample used for the analysis.

Blue-native Page. Blue-native Page on isolated mitochondria from muscle or C2C12 cells was performed using the Native-PAGE™ Novex® Bis-Tris Gel system (Invitrogen). In short, 50ug of isolated mitochondria was solubilized using Native-PAGE sample buffer with 0.5% n-dodecyl-β-D-maltoside (Invitrogen) and complexes were separated using a Native-PAGE Novex 3–12% BisTris gel (Invitrogen). After running, the gel was transferred to a PVDF membrane using the iBlot ™ Gel Transfer System (Invitrogen). The membrane was fixed with 8% acetic acid. After overnight drying, the membrane was destained with methanol. To detect OXPHOS complex, the Mitoprofile Total OXPHOS Rodent WB Antibody Cocktail (Mitosciences) was used. After incubation in the primary antibody dilution, the membrane was washed and detected using the Western Breeze® Chromogenic Western Blot Immunodetection Kit (Invitrogen).

In vivo spectroscopy and data analysis.

MRS methods: A Bruker 14T magnet was used to study the mouse hindlimb muscles (*234*). Briefly, mice were fasted overnight and then given food ad lib 2 hours prior to performing MRS and optical spectroscopy. Mice were anesthetized using 0.01 ml/g of 2.5% tribromoethanol. Left distal hindlimbs are shaved and cleared of dander and mice are situated in place using flexible hook and loop fastening straps to the inside of a custom-built MR/optics probe for the vertical bore 14T spectrometer (Bruker Billerica, MA) as previously described (*234*). Shaved distal hindlimbs were centered inside a horizontal MR solenoid coil with fiber optic wires situation to either side of the hindlimb. The MR solenoid coil was tuned and matched to ^{1}H and ^{31}P and MR was optimized by shimming the ^{1}H signal of tissue H_2O. ^{31}P spectra were then acquired using fully relaxed conditions with proton decoupling (80 transients, 4096 complex points, 20 kHz sweep width, 30 s interpulse delay). Dynamic MR (45° flip angle, 4 transients, 4096 complex points, 20 kHz sweep width, 1.5 s interpulse delay) were acquired in the following periods: rest (2 min), ischemia (9 min), and recovery (9 min). 100% O_2 was administered starting after 1 min of rest during the dynamic phase and continued throughout the experiment. All fully relaxed spectra were Fourier transformed with apodization of 40 HZ, baseline corrected.

Peak simulations: Solutions emulating in vivo conditions were prepared with NAD$^+$ and NADP$^+$ using binding constants taken from the USA National Institute of Standards and Technology (NIST) Critically Selected Stability Constants of Metal Complexes Database (see (*235*)). All solutions contained (in mmol/L): EGTA 15, MOPS 80, free Mg^{2+} 1, Na$^+$ 83 and K$^+$ 52. The following were varied in individual solutions: ATP, ADP, P$_i$, Creatine Phosphate (PCr), ADP, NAD$^+$, NADH, NADP$^+$, or UDP-Glucose. The ionic strength was maintained at 0.175M, pH = 7.0 (36°C) in all solutions. High-resolution MR spectra of solutions in an NMR tube were taken at 4.7T (sweep width=10,000 Hz, 16K complex points, 128 FIDs, 5 s delay between pulses). The Spin Simulation feature of the Mnova software provided the NAD$^+$ (-10.74 ppm and J coupling, 20.03 Hz) and NADP$^+$(-10.83 ppm and J coupling, 18.03 Hz) resonances at each field based on the spin parameters and chemical shifts at 4.7T as described (*236*).

Metabolite Concentrations: Mice were euthanized within 20 minutes of the end of the MRS experiment. Gastrocnemius muscles were removed and frozen from anesthetized mice within 20 minutes of the end of the MRS experiments. Concentration of ATP was measured in the gastrocnemius muscle by HPLC (Waters, Milford, MA) using a protocol described in detail elsewhere (*237*).

Analyses of in vivo *ATP Fluxes:* ^{31}P MR spectra were exponentially multiplied (40Hz at 14T), fourier transformed, and manually phase corrected using Bruker TopSpin (14T) software.

Fully relaxed and dynamic phase spectra were then analyzed with custom written MATLAB software (Mathworks, Natick, MA).

The method used for analyzing MR spectra is described in detail elsewhere(*234*). Peak areas relative to gamma ATP peak area from fully relaxed spectra were used to calculate the resting inorganic phosphate P_i/ATP and PCr/ATP ratios. Three consecutive dynamic spectra were summed to improve signal-to-noise ratio before using the Fit-to-Standard algorithm (*238*) to determine PCr and P_i peak magnitudes throughout dynamic acquisition, relative to rest. Absolute PCr and P_i concentrations were calculated using the ATP concentration measured by HPLC. The chemical shift between the P_i and PCr peaks was used to calculate the cellular pH during the dynamic phase (*239*). Experiments where end of ischemia pH fell below 6.8 were excluded from analyses of ATPmax.

NAD$^+$ and NADP$^+$ in vivo: The NAD(P) region (-10.4 to -11.3 ppm) was extracted from the fully relaxed spectra by fitting a Lorenztian line shape to the a-ATP peak. The NAD$^+$ and NADP$^+$ peaks were estimated by a least squares fit of the simulated peaks to the -10.4 to -11.0 ppm portion of the extracted region.

In vivo measurement of isometric torque and induction of muscle injury. These experiments were performed as described (*240*). Briefly, animals were anesthetized using ~2% isoflurane inhalation and sterile ophthalmic cream was applied to each eye. Under a heat lamp, a needle (25 G) is manually placed through the distal femur to stabilize the femur onto the rig. The ankle is then secured to a custom-machined adjustable lever arm with adhesive tape. The ankle rod should be adjusted so that it lies anteriorly on the distal leg just above the foot. The position of the ankle rod should not be altered between age-matched animals of the same species so that the lever is constant between tests. The lever arm is attached to a stepper motor (model T8904, NMB Technologies, Chatsworth, CA) and a torque sensor (model QWFK-8M, Sensotec, Columbus, OH). Subcutaneous electrodes (J05 Needle Electrode Needles, 36BTP, Jari Electrode Supply) are used to stimulate the femoral nerve. To obtain maximal isometric torque, the pulse amplitude is adjusted to optimize twitch tension and the optimal position of the leg is determined by measuring twitches at different lengths of the quadriceps. Using commercial software (LabView version 2013, National Instruments) each experiment synchronizes contractile activation, the onset of knee rotation, and torque data collection. To assess injury during force lengthening contractions, stimulation of the quadriceps muscles is performed while a computer-controlled motor simultaneously moves the lever arm against the direction of knee extension. This leads to a lengthening (eccentric) contraction. The loss of force production during maximal and repeated lengthening contractions is a result of muscle injury. A maximal tetanic contraction

is then obtained to determine maximal contractile tension (P_0). Maximal tetanic contractions can be performed repeatedly over time with the final tension expressed as percentage of P_0.

C. elegans studies. *C. elegans* movement was recorded for 45 seconds at days 1-8 of adulthood using a Nikon DS-L2 / DS-Fi1 camera and controller setup, attached to both a computer and a standard bright field microscope. The movement of worms during aging was calculated by following worm centroids using a modified version of the freely-available software Parallel Worm Tracker for MATLAB (*158, 241*). These experiments were repeated at least three times.

Treatments were performed by adding the NAD^+ precursor NR at 1mM dissolved in water just before pouring the plates. Worms were exposed to NR during the full life from eggs until death. To ensure a permanent exposure to the compound, plates were changed twice a week. Worm paralysis was assessed as previously described (*242*).

Muscle degeneration experiments were performed on 90 mm Petri dishes containing Nematode Growth Medium (NGM) agar. Plates were induced overnight at room temperature with 4mM IPTG and seeded with HT115 bacteria expressing either empty vector RNAi L4440 or *sir-2.1* RNAi clone [R11A8.4, clone purchased from GeneService and sequenced] grown in Luria broth with 100µg/ml ampicilin and 12,5µg/ml tetracycline until reaching an optic density between 0.6 and 0.8. Synchronized egg populations of *dys-1(cx18);hlh-1(cc561ts)* double mutant animals (*223*) were cultured at 15°C during 8 days and harvested for a 25 min fixation in 1ml PBS supplemented with 20µl of 37% formaldehyde. Samples were then permeabilized by cold methanol during 2 minutes and stained by rhodamine-coupled phalloidin, a marker of filamentous actin, as described previously (*243*). Using a Zeiss Axioplan microscope (x40), the 2 most visible muscle quadrants of each animal were scored for missing cells or cells showing actin fibers fragmented, aggregated or destroyed (40 cells per animal and at least 60 worms per condition were examined per experiment). All experiments were performed blindly three times and compared using a Student's t-test. Illustrative images of the actin network for each condition were recorded using a Zeiss LSM 510 meta fluorescence confocal microscope (objective x40) and analyzed using ImageJ.

Statistics. Differences between two groups were assessed using two-tailed t-tests. GraphPad Prism 5 (GraphPad Software, Inc.) for all statistical analyses. All p-values <0.05 were considered significant. *$p \leq 0.05$; **$p \leq 0.01$; ***$p \leq 0.001$. All animal experiments were performed once.

Sample size determination: For all experiments, sample size was estimated based on the known variability of the assay.

4.6.2 Supplementary Figures
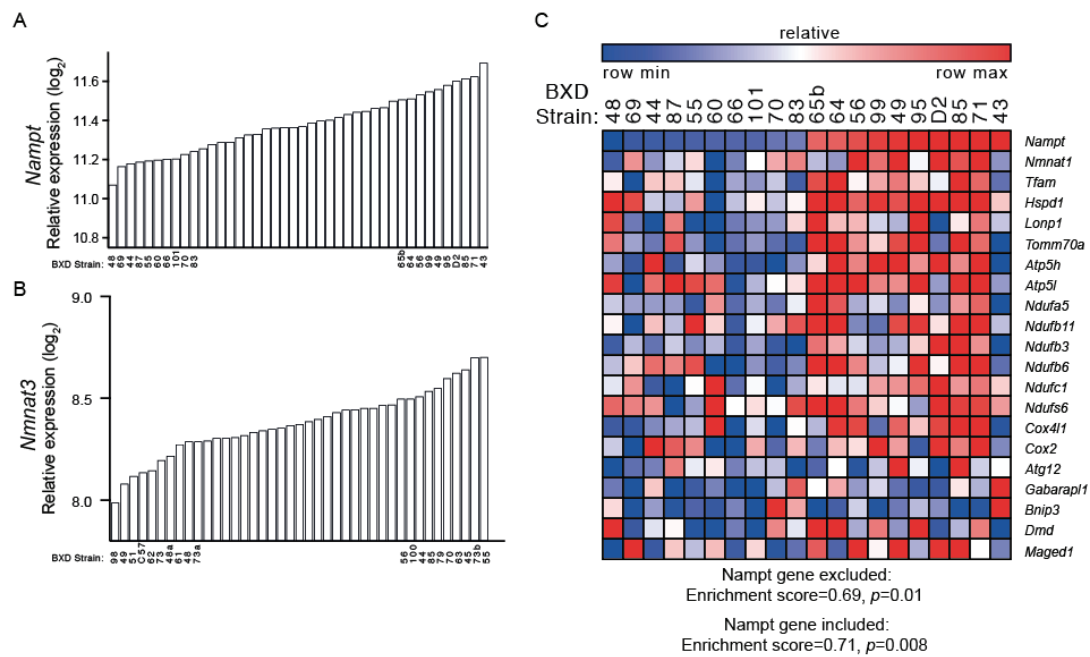
figure 4.S 1 The relationship between transcripts involved in NAD$^+$-biosynthesis and consumption with muscular dystrophy in mice

Expression of (**A**) *Nampt* and (**B**) *Nmnat3* in the quadriceps of 42 strains of the BXD mouse genetic reference population. Each bar represents mRNA from a pool of 5 animals per strain. Extreme strains are labeled. Custom gene set analysis showing enrichment of mitochondrial-related transcripts with (**C**) *Nampt* in data from strains with the 10 highest and 10 lowest transcript levels from 42 strains of the BXDs (*157*). Using gene set enrichment analysis we found a positive correlation to *Nampt* transcript expression with an enrichment score=0.69 and *p*=0.01, with the *Nampt* gene excluded from the analysis.
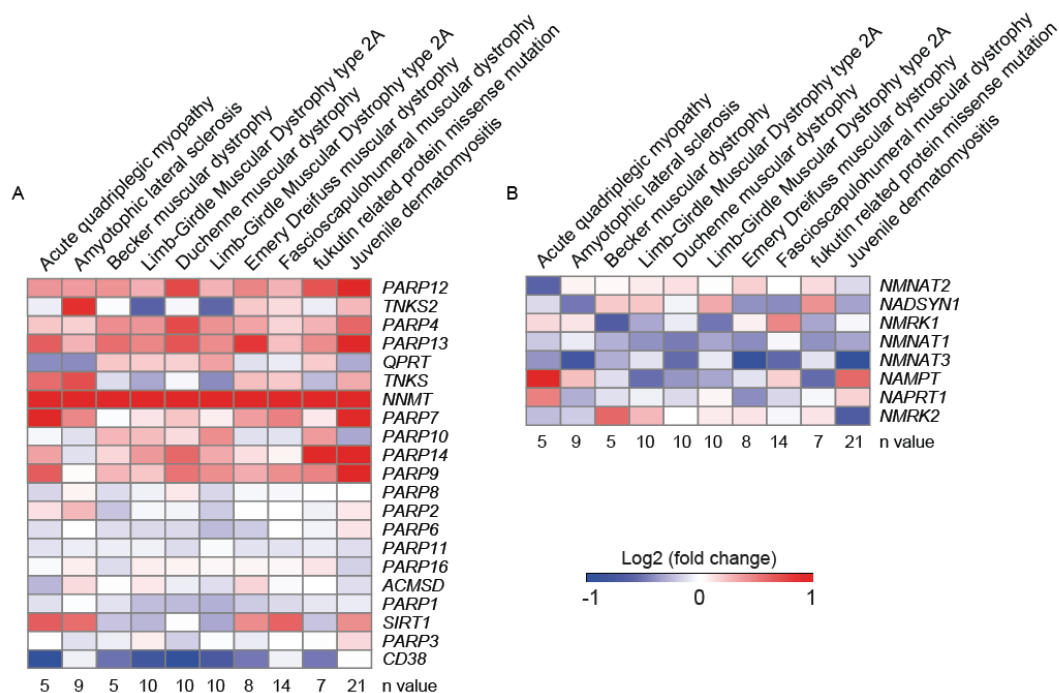
figure 4.S 2 The relationship between transcripts involved in NAD$^+$-biosynthesis and consumption with muscular dystrophy in patients

The expression of transcripts related to NAD$^+$ (**A**) consumption or (**B**) biosynthesis exhibit an enrichment signature of *PARP* genes and the *NNMT* gene that is consistent across skeletal muscle datasets (*217, 218*) from a variety of muscular dystrophies and in patients with (neuro)-muscular diseases. All results for a given condition are averaged from a group of datasets and expressed in relationship to the average of the control patient values (n value for each disease is indicated at the bottom of the heatmap; n=18 for the control group).
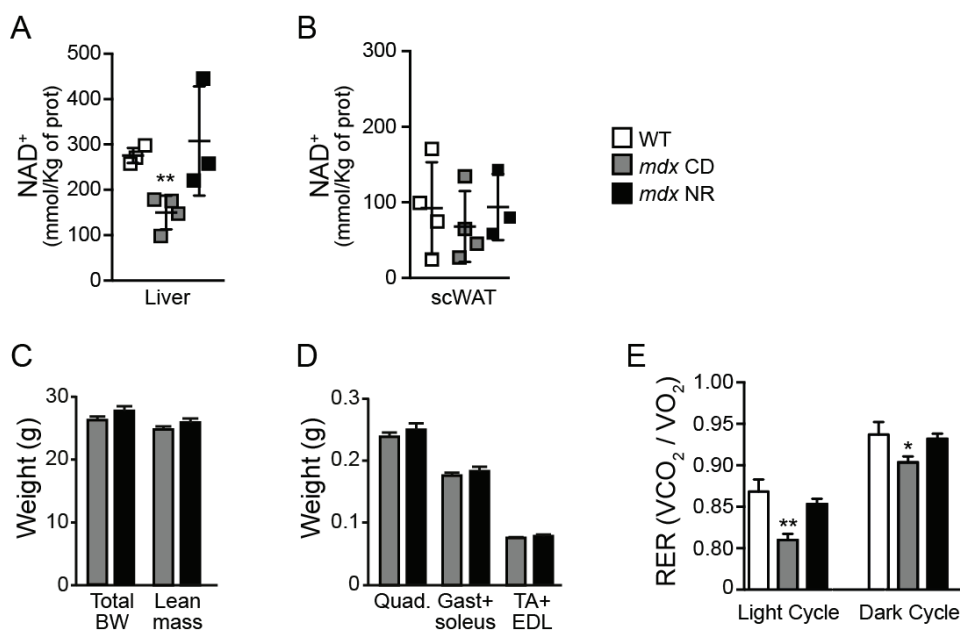
figure 4.S 3 *In vivo* monitoring of NAD$^+$ provides an efficacy biomarker for improvements in the phenotype of NR-treated *mdx* mice

mdx mice treated for 12 weeks with NR demonstrated (**A**) restored NAD$^+$ levels in liver (n=4 for WT and *mdx* CD, n=3 for *mdx* NR) yet (**B**) no changes in subcutaneous WAT (n=4 for WT and *mdx* CD, n=3 for *mdx* NR). NR treated mdx mice also showed no significant changes in (**C**) total body weight, lean mass (n=6) or (**D**) wet weights of quadriceps, gastrocnemius and soleus or tibialis anterior and extensor digitorum longus muscles (n=5). (**E**) Energy expenditure was evaluated through calculation of the respiratory exchange ratio (RER) over a 24 hr period for *mdx* mice with or without NR treatment compared to WT mice (n=6).
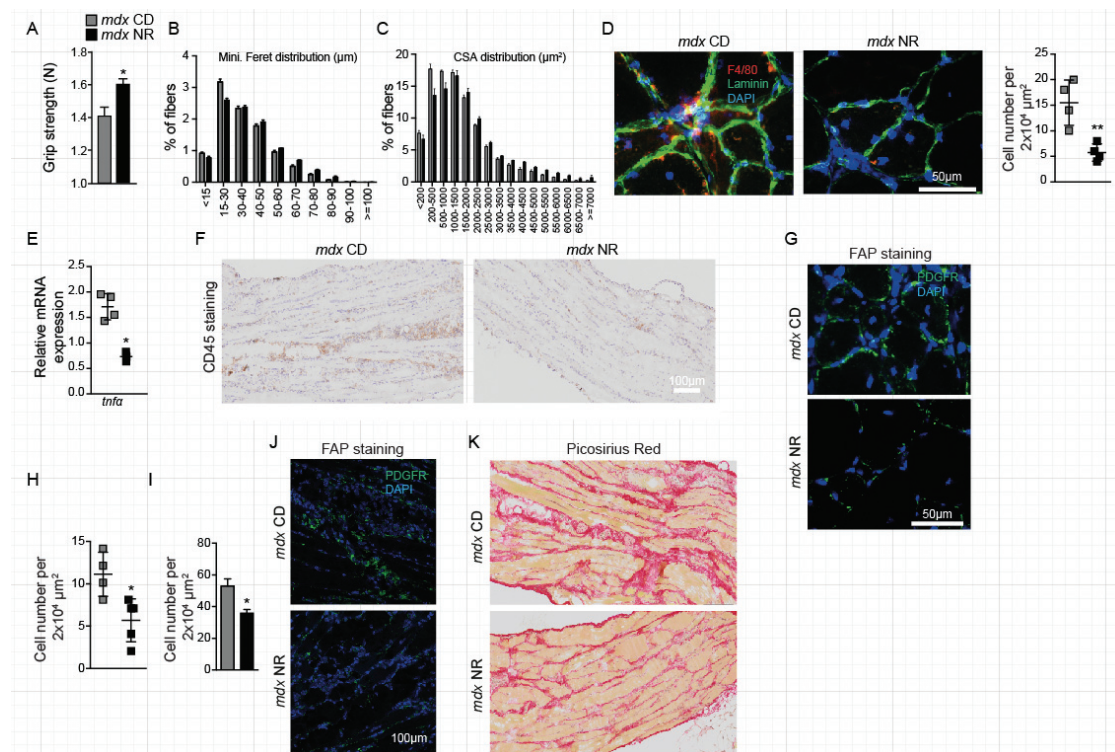
figure 4.S 4 NAD$^+$ repletion improves muscle function and protects muscle from damage and fibrosis

mdx mice treated for 12 weeks with NR exhibited (**A**) increased limb grip strength in *mdx* mice (Newtons of force, n=6). Analysis of the (**B**) minimal Feret's diameter (in μm) and the (**C**) cross-sectional area (in μm^2) of *mdx* tibialis anterior muscle fibers show an increase in fiber size with NR treatment (8 weeks of NR treatment, n=5). Quantification of images was performed with ImageJ software. NR-treated *mdx* mice also demonstrated (**D**) reduced macrophage content, quantified by counting F40/80-positive stained cells in *mdx* tibialis anterior muscles (n=4). Quantification of images was performed with ImageJ software. (**E**) mRNA levels of *tnfα,* a mediator of inflammation in *mdx* mice, was attenuated with NR treatment in gastrocnemius muscle (n=3). (**F**) CD45 positive cells were reduced in the longitudinal-sections of NR-treated *mdx* mouse diaphragms. PDGFR positive cells were reduced following NR in both (**G**) transverse-sections of TA muscle and in (**H**) quantified transverse-sections of diaphragms in *mdx* mice. Quantification of images was performed with ImageJ software (n=4 for *mdx* CD, n=5 for *mdx* NR). (**I**) Reduced PGDFR staining of longitudinal-sections of the diaphragm (**J**) quantified using ImageJ software (n=6 for *mdx* CD, n=5 for *mdx* NR). (**K**) Fibrosis was reduced in longitudinal sections of the diaphragm in *mdx* animals given an NR supplemented diet, as seen with less picosirius red staining.

4.7 Acknowledgements

Chapter 5. Discussion and conclusions

5.1 Why NAD$^+$ and mitochondria are important for quiescent stem cells?

Quiescent adult stem cells, such as MuSCs, are thought to rely predominantly on mitochondrial-independent glycolysis for energy, a process that would reduce cellular concentrations of NAD$^+$ (*161*). Following this theory, mitochondrial function in MuSC and other quiescent stem cells might be not as important as the most types of full-differentiated tissue, which largely relay on mitochondrial oxidative respiration for energy production. However, mitochondrial function has been recently linked to SCs maintenance and activation (*55, 162-164*), which indicates that mitochondria might be actually important in stem cell quiescence, and fate decision. Our work in Chapter 2 shows that modulation of the NAD$^+$ levels and mitochondrial function are essential for muscle, neural and melanocyte stem cell senescence in aging. Therefore our work shed light on a new intrinsic stem cell senescence regulatory pathway, and unveiled the importance of NAD$^+$ levels and mitochondria in stem cell maintenance. This research work also brings to light several interesting questions around the role of mitochondrial homeostasis in stem cell function and aging.

One fundamental question is why the NAD$^+$ pool and the mitochondrial activity decline in the senescent stem cell in both natural aging mice and in the *mdx* muscular dystrophy mouse strain? There are several reasons that might explain the decline in NAD$^+$ in MuSC senescence, which occurs in both aged and *mdx* mice(*8*). One possible reason is the reduction of NAD$^+$ synthesis due to the dysfunction of the key enzymes involved in NAD$^+$ biosynthesis, such as the decline of NAMPT (*159*). Another possibility is the increased expression and/or activity of NAD$^+$ consuming enzymes, such as PARP(*133*) or CD38(*244*) enzymes, in the aged mice. PARPs transfer ADP-ribose from NAD$^+$ to histones and other proteins at sites of DNA damage to facilitate DNA repair. Considering the requirements of DNA repair in the aged mice, the hyper-activation of PARPs in MuSCs of aged mice could be the mechanism of the NAD$^+$ reduction in these cells. As for CD38, levels of this enzyme might be induced by lipopolysaccharides and inflammatory cytokines, such as TNF-α(*244*). The reduction in NAD$^+$ levels could further deactivate sirtuins, especially the SIRT1 and SIRT3, which is linked to the reduction of mitochondrial biogenesis and function (*8*). Nevertheless, neither the decrease of NAD$^+$ synthesis nor super-activation of PARPs or CD38 has been tested in stem cell aging(*8*). Moreover, we can not rule out other scenarios, such as that the metabolic change in aged stem cells might cause an imbalance in the

NAD$^+$/NADH ratio by hyper-activation of glycolysis. More studies will be necessary to unveil the processes leading to NAD$^+$ decline and mitochondrial dysfunction in aged stem cells.

Another related question is how can NAD$^+$ boosting and improvement of mitochondrial function prevent stem cell aging? One possible reason might reside in the fact that mitochondria may provide stem cells with the essential energy that cannot be sufficiently obtained from glycolysis. Additionally, mitochondria may be involved in several signaling pathways that are crucial for stem cell maintenance. Importantly, our research showed that the UPR^{mt} might be one of the important signaling pathways responsible for preserving stem cell health in aged mice. In particular, UPR^{mt} activation by NAD$^+$ boosting inhibits expression of the senescent regulator CDKN1A in MuSCs (Chapter 2). More work will be needed to understand how UPR^{mt} activation represses CDKN1A expression and the downstream activation of cell cycle genes (Figure 2.3 F-I).

In the work presented here, we examined the beneficial effect of NAD$^+$ boosting in muscle, neural and melanocyte stem cell aging. An interesting question is whether NR-treatment can also benefit other stem cell types. It is important to note that different stem cell types have totally different characteristics during the process of aging(245-248). For instance, even though most of the stem cell types exhibit altered proliferation and differentiation in aging, the change in cell proliferation frequency can be either increased (such as intestinal and hematopoietic stem cells) or decreased (such as MuSCs and Neural stem cells) (245, 247, 248). We have shown that the muscle, neural and melanocyte stem cells all decline in proliferation with aging. However, other stem cells, such as hematopoietic and intestinal stem cells, have been reported to show an increase in proliferation in aged mice. Therefore, it will be important to test whether NAD$^+$ boosters, such as NR, could also reduce senescence of these stem cells during aging. Another interesting stem cell type is the cancer stem cell. These cells can be quiescent for long time, and once activated, they possess high proliferation capacity(159). It will be very interesting to test the role of mitochondria in cancer stem cell function. Recently, NR has shown to be effective in the prevention of liver cancer, probably through reduction of DNA damage(249). Meanwhile, NAD$^+$ depletion might also inhibit the growth of several cancers (reviewed in (181)). All together, whether NR has potential effects on cancer stem cell activation and proliferation is still unknown.

Moreover, It would be interesting to test whether other strategies aimed at increasing NAD$^+$ levels or improving mitochondrial activity also could similarly prevent stem cell senescence in aging and diseases. Nicotinamide mononucleotide (NMN), one NAD$^+$ salvage synthesis substrate and therefore another NAD$^+$ booster, has been shown to rescue the decline in neural stem cell number during aging(163). However, it is unknown whether the beneficial effect of NMN administration is occurring by inhibiting stem cell senescence. Besides, It

would be interesting to test whether NMN also prevents other stem cells from aging. Moreover, it will be necessary to evaluate whether PARP inhibitors, which have been repeatedly proven to boost NAD$^+$ levels in adult tissue and diseases, could also benefit stem cells in aging and disease conditions. Likewise the impact of CD38 inhibitors would be interesting to test. Evaluating the effect of other mitochondrial biogenesis or functional activators, and UPR^{mt} activators, in stem cell aging and function will be another interesting research topic.

5.2 Anti-aging and muscular dystrophy: how important the stem cells are?

The beneficial effect of NR on *mdx* mice might be pleiotropic. NR treatment improves mitochondrial function, increases muscle structural protein expression and reduces general PARylation, inflammation and fibrosis (Chapter 4). All these effects are mainly on muscle fibers. NR also prevents MuSC aging in normal and *mdx* mice, and therefore improves muscle regeneration ability in the *mdx* mice (Chapter 2). The decline of MuSC numbers in *mdx* mice has been shown at ages as early as 12 weeks(*250*), and apoptosis/senescence of MuSCs has been reported in young *mdx* mice throughout the ages of 4 to 23 weeks(*251-254*). Therefore, the beneficial effects of NR might relay on both muscle fibers and MuSCs. Similarly, NAD$^+$ boosters have been reported to show stem cell-independent beneficial effects on aged animals(*133, 159*). The question is, how much the stem cell pool contributed to the anti-aging and muscular dystrophy effect provided by NR?

To address this question, we have performed MuSC-specific *Sirt1* and *Phb1* deficiency experiments. We found that the anti-senescence effect of NR-treatment was blocked in either SIRT1 or PHB1 deficient mice. Additionally, the SIRT1 and PHB1 deficient mice have compromised MuSC activation and muscle regeneration after muscle damage. Our results indicate that the effect of NR at least partly depend on improved MuSC function. However, to establish the contribution of stem cells in ameliorating aging and disease with NR, more work is required. First, MuSC-specific *Sirt1* or *Phb1* LOF mice might be helpful in addressing this question. Systemic phenotyping of skeletal muscle function and longevity of NR treated aged *Sirt1* and *Phb1* MuSC-specific LOF mice will help us to answer whether the physiological beneficial effect of NR is dependent on these particular proteins in aging MuSC function. Second, genetically modified mice that specifically improve mitochondrial biogenesis or activity in MuSCs, such as MuSC-specific SIRT1 overexpression mice, might be useful in investigating the contribution of stem cell mitochondrial activity on MuSC aging and muscle physiological function. Third, serial transplantation of fluorescent/luciferase labeled MuSCs isolated from control and NR treated aged mice can be performed in either aged wild type or *mdx* mice(*5, 154*). With this experiment, MuSC function with or without NR treatment can be

truly evaluated without the additional impact of NR on the stem cell niche. Moreover, the endogenous MuSCs of the pre-injured recipient mice can be radiation-ablated, therefore serving as a clean system to examine the regeneration activity of the transplanted MuSCs during aging and muscular dystrophy.

5.3 Acetylation of histone *vs.* transcription regulators, what are their respective roles?

KAT2A, as well as other HATs, can acetylate both histones and transcriptional factors/cofactors(*2*). For both protein groups, acetylation can have significant effect on their function and therefore on gene expression efficiency(*2*). Histone acetylation is an epigenetic modification that can strongly affect gene expression, because of its role in the direct modification of chromatin, both through local relaxation of chromatin structure and recruitment of chromatin remodeling complexes. Acetylated histone tails are generally associated with active chromatin, whereas deacetylated histone tails are associated with silent parts of the genome. Whereas, acetylation of transcription factors or cofactors can change their protein structure, binding ability and biological activity. Importantly, numerous transcription factors or cofactors possess acetyltransferases or deacetylases activity themselves, such as SRCs, TAFII250 and CLOCK (Table 1.4), which further highlights the importance of protein acetylation in gene expression control.

Considering the occurrence of acetylation on both histones and non-histone proteins, one fundamental question is how can they be regulated and what is the "combined" impact of their acetylation in MuSC maintenance and activation?

One possibility is that different KATs and KDACs have a different affinity for histones and non-histone transcription regulators. Therefore, even though most of them acetylate both histone and other proteins, each of the KATs or KDACs has it's own preferred targets, which can be either histones or transcriptional factors/cofactors. Thus, histones and non-histone transcription factors/cofactors are mainly (de-) acetylated by different specific KDACs and KATs. However, it is also known that the specificity of KATs and KDACs can also rely on their binding proteins. As such, KATs and KDACs can be recruited to specific areas of chromatin in a manner that is dependent on their binding to transcriptional regulators. At a specific chromatin location, KATs and KDACs can acetylate and deacetylate both histones and transcription factors/cofactors. While histone acetylation controls the general relaxation of chromatin along with the recruitment of transcriptional factors/cofactors, the acetylation of transcriptal factors/cofactors can further fine-tune the transcriptional activity of given gene at this chromatin location. Therefore the general gene transcription level determined by more

global histone acetylation levels combined with the acetylation status of specific transcriptional regulators will ultimately govern the unique expression levels of select genes.

In the case of KAT2A in MuSCs, our experimental results unveiled acetylation as a new PTM of PAX7, and highlighted the importance of this acetylation in MuSC function regulation (chapter 3). It is easy to understand the significant impact of PAX7 acetylation in MuSC function considering the key role of PAX7 in MuSC maintenance. However, we cannot rule out the possibility that KAT2A also regulates MuSCs function by histone acetylation. Further work will be needed to investigate the role of KAT2A mediated PAX7 acetylation in MuSC function. To do this, KAT2A-acetylated PAX7 lysine(s) will be identified using nano liquid chromatography tandem mass spectrometry (LC-MS/MS). PAX7 mutant proteins will be generated to mimic constitutively acetylated and deacetylated lysines by converting an existing lysine to glutamine or arginine, respectively. Secondly, the DNA binding ability, acetylation activity, the activity of downstream signaling cascade and resulting alterations in MuSC function will be evaluated for constitutively acetylated and deacetylated PAX7 mutant proteins, both *in vitro* in C2C12 cell lines and *in vivo* using adenovirus-introduced PAX7 GOF and LOF experiments in mice. Finally, to explore the possible involvement of histone acetylation in MuSC function, histone acetylation status will be examined in C2C12 cells with KAT2A GOF and LOF and *in vivo* using in KAT2A MuSC-specific LOF mice. Importantly, one of the key histones, H4K16, has been shown to activate myogenic gene transcription in MuSC when acetylated, driving the transition from MuSC quiescence to proliferation. The acetylation of H4K16 during MuSC activation may partially be due to the decline of NAD$^+$ levels and in turn the deactivation of SIRT1 driven deacetylation(*55*). However, knowing that KAT2A is activated in early MuSC activation, it would be interesting to check whether KAT2A mediates H4K16 acetylation.

5.4 How far are we from clinical treatment?

Our work highlights the tremendous potential of NAD$^+$ boosting and subsequent improvements in mitochondrial function in preventing the senescence of multiple types of stem cells in aged mice. More importantly, NAD$^+$ boosting by NR treatment extends mouse lifespan even in mice treated at the late stage of life (chapter 2). The decline of NAD$^+$ levels has also been found in human aging(*255*). It is therefore reasonable to expect that NAD$^+$ boosters might also benefit healthy human aging. In the *mdx* mice, NR not only improves MuSC function, but also reduces general PARylation, inflammation and fibrosis in muscle fibers in muscular disease (chapter 4). Overall, NR benefits muscular diseases through effects on both MuSCs and myofibers. NR hence could be a nutritional intervention that benefits human muscular dystrophy (and potentially other neuro-muscular diseases) and aging. The investigation of PTM in MuSC regulation also brought the relevance of KAT2A

into the light. KAT2A is important for MuSC function and maintenance. More importantly, *Kat2a* expression declines in MuSCs during the process of aging (chapter 3). We therefore hypothesize that increasing the expression of KAT2A may therefore prove beneficial for MuSC aging. With all these promising results, one question is how far are we from translating these results to the clinic?

To use NR in the clinical treatment of muscular dystrophy diseases or aging-related diseases, we need to first test its toxicity in human beings. Preliminary studies have been started in humans from both the industrial and academic sides. For instance, preliminary results from ChromaDex, a natural products company, did not reveal safety issues with NR(*256*). And recently the company announced that their initial results from the first human clinical study for NR met their primary endpoint. The results demonstrated that a single dose of NR resulted in statistically significant increases in the co-enzyme NAD^+ in healthy human volunteers (http://investors.chromadex.com/). This study showed for the first time that NR converted into elevated tissue NAD^+ levels, as has been shown in animal studies.

After confirming that NR was non-toxic, the preventative or curative benefits of NR will need further confirmation in humans. From our data and other publications, NR may show benefits in diseases that include muscular dystrophy and aging-related diseases, including obesity and diabetes, non-alcoholic fatty liver disease (NAFLD) and liver cancer. NR has been shown beneficial effects on all of these diseases in mouse models(*101, 249, 257, 258*). Moreover, animal and clinical work will be required to test whether NR and other NAD^+ boosters also benefit other muscular diseases and aged related diseases, such as Alzheimer's disease (AD) and other dementias, including Parkinson's disease (PD) and PD-related disorders, Huntington's disease (HD) *etc*.

Research on KATs and KDACs covers broad clinical application, such as cancer, rheumatoid arthritis, Alzheimer's disease, stroke, and heart disease(*259*). In humans, several HDAC inhibitors, such as Vorinostat, Romidepsin, Chidamide and Belinostat have been approved by the U.S Food and Drug Administration (FDA) for the treatment of T cell lymphoma. Panobinostat, another pan-HDAC inhibitor, was licensed for the treatment of multiple myelomas. In addition, there are several HDAC inhibitors under different phases of clinical trials(*260, 261*). Considering the decline of KAT2A levels in the MuSCs during aging, HDAC inhibitors or KAT2A activators might also benefits aged MuSCs. It is therefore important to test this hypothesis in both aged and dystrophic animals, and, thereafter, human patients. One of the limitations for using KDAC inhibitors and KAT activators for clinical application is the availability of specific inhibitors and activators. Therefore, finding more specific HDACs and HATs inhibitors and activators might largely improve the use of protein acetylation modulators when it comes to chromatin specific modulation. However, this approach must be

taken cautiously as the potential for affecting multiple chromatin locations is very likely, which could lead to various unexpected side effects in the clinic. The wide array of signaling pathways affected by KDAC and KAT inhibitors or activators will hence be one a major pharmaceutical challenge to overcome.

Altogether, in spite of the high potential for clinical usage of both NAD^+ boosters and KDACs and KATs modulators as novel therapeutics, more investigations, both in basic research as well as in clinical tests, will be necessary before approval for a wide and secure application of these compounds.

5.5 Conclusion

Skeletal muscle serves crucial roles in locomotion and energy metabolism. However, its function can be compromised in disease and in aging. Within my thesis projects, we explored a link between cellular energy metabolism and muscle and MuSCs function. By controlling the concentration of key cellular metabolites, such as NAD^+ and Acetyl-CoA, we can control energy metabolism to directly regulate muscle metabolic and structural homeostasis, and MuSCs activation and senescence, through modulation of mitochondrial activity, PARylation, KAT and KDAC activity.

We found that NAD^+ depletion may act as a biomarker for the progression of muscular dystrophy and MuSC aging. In patients with Duchenne's muscular dystrophy and in the *mdx* mouse model, we found a particular signature of enrichment for various PARPs and the NNMT transcript, all major consumers of NAD^+ involved in pleiotropic events, including inflammation. Replenishing NAD^+ stores with dietary NR supplementation benefits muscle function in *mdx* and *mdx*/*Utr*$^{-/-}$ mice, an effect replicated in a *C. elegans* model of DMD.

Interestingly, NAD^+ decline is also found during MuSC senescence in both aged and *mdx* mice, a quiescent and specific stem cell that was thought to rely predominantly on mitochondrial-independent glycolysis for energy. NR treatment prevents MuSC senescence and also improves neural and melanotyce stem cell function in aged mice, and extends mouse healthspan and lifespan.

We found that the acetyl-CoA-dependent KAT2A acetyltransferase is an important MuSC function regulator. By acetylating the MuSC transcription factor PAX7, KAT2A supports MuSC activation and differentiation. KAT2A deficient MuSCs lose their myogenic differentiation ability and MuSC–specific KAT2A LOF mice have compromised muscle regeneration after muscle damage.

Our research therefore not only answers basic biological questions, such as the molecular mechanisms that regulate MuSC activation, differentiation, and senescence; as well as the fundamentals concerning the pathogenesis of muscular dystrophy in DMD patients, but also provides evidence for potential treatments for human muscular diseases and healthy aging by replenishing the cellular NAD$^+$ pool during aging and disease.

References

1.   M. Tabebordbar, E. T. Wang, A. J. Wagers, Skeletal muscle degenerative diseases and strategies for therapeutic muscle repair. *Annual review of pathology* **8**, 441 (Jan 24, 2013).
2.   K. J. Menzies, H. Zhang, E. Katsyuba, J. Auwerx, Protein acetylation in metabolism - metabolites and cofactors. *Nature reviews. Endocrinology* **12**, 43 (Jan, 2016).
3.   B. K. Pedersen, M. A. Febbraio, Muscles, exercise and obesity: skeletal muscle as a secretory organ. *Nature reviews. Endocrinology* **8**, 457 (Aug, 2012).
4.   J. V. Chakkalakal, K. M. Jones, M. A. Basson, A. S. Brack, The aged niche disrupts muscle stem cell quiescence. *Nature* **490**, 355 (Oct 18, 2012).
5.   B. D. Cosgrove *et al.*, Rejuvenation of the muscle stem cell population restores strength to injured aged muscles. *Nature medicine* **20**, 255 (Mar, 2014).
6.   N. A. Dumont *et al.*, Dystrophin expression in muscle stem cells regulates their polarity and asymmetric division. *Nature medicine* **21**, 1455 (Dec, 2015).
7.   L. Liu *et al.*, Chromatin modifications as determinants of muscle stem cell quiescence and chronological aging. *Cell Rep* **4**, 189 (Jul 11, 2013).
8.   H. Zhang *et al.*, NAD+ repletion improves mitochondrial and stem cell function and enhances life span in mice. *Science*, (Apr 28, 2016).
9.   Y. X. Wang, M. A. Rudnicki, Satellite cells, the engines of muscle repair. *Nature reviews. Molecular cell biology* **13**, 127 (Feb, 2012).
10.   E. Zalewska, S. D. Nandedkar, I. Hausmanowa-Petrusewicz, A method for determination of muscle fiber diameter using single fiber potential (SFP) analysis. *Medical & biological engineering & computing* **50**, 1309 (Dec, 2012).
11.   F. Rahimov, L. M. Kunkel, The cell biology of disease: cellular and molecular mechanisms underlying muscular dystrophy. *J Cell Biol* **201**, 499 (May 13, 2013).
12.   T. A. Rando, The dystrophin-glycoprotein complex, cellular signaling, and the regulation of cell survival in the muscular dystrophies. *Muscle & nerve* **24**, 1575 (Dec, 2001).
13.   J. Ehmsen, E. Poon, K. Davies, The dystrophin-associated protein complex. *Journal of cell science* **115**, 2801 (Jul 15, 2002).
14.   C. Moorwood, Syncoilin, an intermediate filament-like protein linked to the dystrophin associated protein complex in skeletal muscle. *Cellular and molecular life sciences : CMLS* **65**, 2957 (Oct, 2008).
15.   K. M. Bushby, Making sense of the limb-girdle muscular dystrophies. *Brain : a journal of neurology* **122 (Pt 8)**, 1403 (Aug, 1999).
16.   J. T. den Dunnen, E. Bakker, E. G. Breteler, P. L. Pearson, G. J. van Ommen, Direct detection of more than 50% of the Duchenne muscular dystrophy mutations by field inversion gels. *Nature* **329**, 640 (Oct 15-21, 1987).
17.   E. P. Hoffman, R. H. Brown, Jr., L. M. Kunkel, Dystrophin: the protein product of the Duchenne muscular dystrophy locus. *Cell* **51**, 919 (Dec 24, 1987).
18.   M. Koenig *et al.*, Complete cloning of the Duchenne muscular dystrophy (DMD) cDNA and preliminary genomic organization of the DMD gene in normal and affected individuals. *Cell* **50**, 509 (Jul 31, 1987).
19.   A. H. Burghes *et al.*, A cDNA clone from the Duchenne/Becker muscular dystrophy gene. *Nature* **328**, 434 (Jul 30-Aug 5, 1987).
20.   A. P. Monaco *et al.*, Isolation of candidate cDNAs for portions of the Duchenne muscular dystrophy gene. *Nature* **323**, 646 (Oct 16-22, 1986).
21.   B. J. Petrof, J. B. Shrager, H. H. Stedman, A. M. Kelly, H. L. Sweeney, Dystrophin protects the sarcolemma from stresses developed during muscle contraction. *Proceedings of the National Academy of Sciences of the United States of America* **90**, 3710 (Apr 15, 1993).
22.   M. T. Tierney, A. Sacco, Satellite Cell Heterogeneity in Skeletal Muscle Homeostasis. *Trends in cell biology* **26**, 434 (Jun, 2016).

23. R. J. Fairclough, M. J. Wood, K. E. Davies, Therapy for Duchenne muscular dystrophy: renewed optimism from genetic approaches. *Nature reviews. Genetics* **14**, 373 (Jun, 2013).

24. C. S. Young *et al.*, A Single CRISPR-Cas9 Deletion Strategy that Targets the Majority of DMD Patients Restores Dystrophin Function in hiPSC-Derived Muscle Cells. *Cell Stem Cell* **18**, 533 (Apr 7, 2016).

25. A. Mauro, Satellite cell of skeletal muscle fibers. *J Biophys Biochem Cytol* **9**, 493 (Feb, 1961).

26. M. H. Snow, Myogenic cell formation in regenerating rat skeletal muscle injured by mincing I. A fine structural study. *Anatomical Record* **188**, 181 (1977).

27. A. S. Brack, I. M. Conboy, M. J. Conboy, J. Shen, T. A. Rando, A Temporal Switch from Notch to Wnt Signaling in Muscle Stem Cells Is Necessary for Normal Adult Myogenesis. *Cell Stem Cell* **2**, 50 (1/10/, 2008).

28. V. G. Punch, A. E. Jones, M. A. Rudnicki, Transcriptional networks that regulate muscle stem cell function. *Wiley Interdisciplinary Reviews: Systems Biology and Medicine* **1**, 128 (2009).

29. N. Chi, J. A. Epstein, Getting your Pax straight: Pax proteins in development and disease. *Trends in Genetics* **18**, 41 (2002).

30. D. Horst *et al.*, Comparative expression analysis of Pax3 and Pax7 during mouse myogenesis. *International journal of developmental biology* **50**, 47 (2006).

31. M. Buckingham, F. Relaix. (2007), vol. 23, pp. 645-673.

32. B. W. Schäfer, T. Czerny, M. Bernasconi, M. Genini, M. Busslinger, Molecular cloning and characterization of a human PAX-7 cDNA expressed in normal and neoplastic myocytes. *Nucleic acids research* **22**, 4574 (1994).

33. S. Oustanina, G. Hause, T. Braun, Pax7 directs postnatal renewal and propagation of myogenic satellite cells but not their specification. *EMBO Journal* **23**, 3430 (2004).

34. M.-C. Sincennes, C. E. Brun, M. A. Rudnicki, Concise Review: Epigenetic Regulation of Myogenesis in Health and Disease. *Stem Cells Translational Medicine*, (January 21, 2016, 2016).

35. M. Buckingham, F. Relaix, PAX3 and PAX7 as upstream regulators of myogenesis. *Seminars in Cell and Developmental Biology* **44**, 115 (2015).

36. R. Frédéric, R. Didier, M. Ahmed, B. Margaret, A Pax3/ Pax7- dependent population of skeletal muscle progenitor cells. *Nature* **435**, 948 (2005).

37. E. Bober, H.-H. Arnold, T. Franz, P. Gruss, P. Tremblay, Pax- 3 is required for the development of limb muscles: A possible role for the migration of dermomyotomal muscle progenitor cells. *Development* **120**, 603 (1994).

38. A. G. Borycki, J. Li, F. Jin, C. P. Emerson, J. A. Epstein, Pax3 functions in cell survival and in pax7 regulation. *Development (Cambridge, England)* **126**, 1665 (1999).

39. S. Kuang, S. B. Charge, P. Seale, M. Huh, M. A. Rudnicki, Distinct roles for Pax7 and Pax3 in adult regenerative myogenesis.(Author Abstract). *The Journal of Cell Biology* **172**, 103 (2006).

40. F. Relaix, D. Rocancourt, A. Mansouri, M. Buckingham, Divergent functions of murine Pax3 and Pax7 in limb muscle development. *Genes & development* **18**, 1088 (2004).

41. H. C. Olguin, B. B. Olwin, Pax-7 up-regulation inhibits myogenesis and cell cycle progression in satellite cells: a potential mechanism for self-renewal. *Developmental Biology* **275**, 375 (2004).

42. P. S. Zammit *et al.*, Muscle satellite cells adopt divergent fates: a mechanism for self-renewal? *The Journal of cell biology* **166**, 347 (2004).

43. D. D. W. Cornelison, B. J. Wold, Single- Cell Analysis of Regulatory Gene Expression in Quiescent and Activated Mouse Skeletal Muscle Satellite Cells. *Developmental Biology* **191**, 270 (1997).

44. R. L. S. Perry, Molecular mechanisms regulating myogenic determination and differentiation. *Front Biosci* **5**, d750 (2000).

45. L. Bajard *et al.*, A novel genetic hierarchy functions during hypaxial myogenesis: Pax3 directly activates Myf5 in muscle progenitor cells in the limb. *Genes & development* **20**, 2450 (Sep 1, 2006).

46. M. Lagha, D. Rocancourt, F. Relaix, [Pax3/Pax7-dependent population of skeletal muscle progenitor cells]. *Medecine sciences : M/S* **21**, 801 (Oct, 2005).

47. M. A. Rudnicki, F. Le Grand, I. McKinnell, S. Kuang. (2008), vol. 73, pp. 323-331.

48. M. Kitzmann *et al.*, The muscle regulatory factors MyoD and myf- 5 undergo distinct cell cycle- specific expression in muscle cells. *The Journal of cell biology* **142**, 1447 (1998).

49. M. O. Ott, E. Bober, G. Lyons, H. Arnold, M. Buckingham, Early expression of the myogenic regulatory gene, myf- 5, in precursor cells of skeletal muscle in the mouse embryo. *Development (Cambridge, England)* **111**, 1097 (1991).

50. H. C. Olguin, Z. Yang, S. J. Tapscott, B. B. Olwin, Reciprocal inhibition between Pax7 and muscle regulatory factors modulates myogenic cell fate determination. *J Cell Biol* **177**, 769 (Jun 4, 2007).

51. L. Megeney, M. A. Rudnicki, in *Biochem. Cell Biol.* (1995), vol. 73, pp. 723-732.

52. C. A. Berkes, S. J. Tapscott, MyoD and the transcriptional control of myogenesis. *Seminars in Cell and Developmental Biology* **16**, 585 (2005).

53. S. Alessandra, D. Regis, K. Peggy, V. Stefan, M. B. Helen, Self- renewal and expansion of single transplanted muscle stem cells. *Nature* **456**, 502 (2008).

54. C. A. Collins *et al.*, Stem Cell Function, Self- Renewal, and Behavioral Heterogeneity of Cells from the Adult Muscle Satellite Cell Niche. *Cell* **122**, 289 (2005).

55. J. G. Ryall *et al.*, The NAD-Dependent SIRT1 Deacetylase Translates a Metabolic Switch into Regulatory Epigenetics in Skeletal Muscle Stem Cells. *Cell Stem Cell*, (Jan 13, 2015).

56. M. L. Johnson, M. M. Robinson, K. S. Nair, Skeletal muscle aging and the mitochondrion. *Trends in endocrinology and metabolism: TEM* **24**, 247 (May, 2013).

57. K. Iizuka, T. Machida, M. Hirafuji, Skeletal muscle is an endocrine organ. *Journal of pharmacological sciences* **125**, 125 (2014).

58. A. Marette, Y. Liu, G. Sweeney, Skeletal muscle glucose metabolism and inflammation in the development of the metabolic syndrome. *Reviews in endocrine & metabolic disorders* **15**, 299 (Dec, 2014).

59. J. G. Ryall, Metabolic reprogramming as a novel regulator of skeletal muscle development and regeneration. *The FEBS journal* **280**, 4004 (Sep, 2013).

60. E. E. Spangenburg, F. W. Booth, Molecular regulation of individual skeletal muscle fibre types. *Acta physiologica Scandinavica* **178**, 413 (Aug, 2003).

61. R. Bottinelli, C. Reggiani, Human skeletal muscle fibres: molecular and functional diversity. *Progress in biophysics and molecular biology* **73**, 195 (2000).

62. H. Westerblad, J. D. Bruton, A. Katz, Skeletal muscle: energy metabolism, fiber types, fatigue and adaptability. *Exp Cell Res* **316**, 3093 (Nov 1, 2010).

63. D. Pette, R. S. Staron, Myosin isoforms, muscle fiber types, and transitions. *Microscopy research and technique* **50**, 500 (Sep 15, 2000).

64. J. R. Zierath, J. A. Hawley, Skeletal muscle fiber type: influence on contractile and metabolic properties. *PLoS biology* **2**, e348 (Oct, 2004).

65. H. Yin, F. Price, M. A. Rudnicki, Satellite cells and the muscle stem cell niche. *Physiological reviews* **93**, 23 (Jan, 2013).

66. D. E. Kelley, B. Goodpaster, R. R. Wing, J. A. Simoneau, Skeletal muscle fatty acid metabolism in association with insulin resistance, obesity, and weight loss. *The American journal of physiology* **277**, E1130 (Dec, 1999).

67. F. Demontis, R. Piccirillo, A. L. Goldberg, N. Perrimon, The influence of skeletal muscle on systemic aging and lifespan. *Aging cell* **12**, 943 (Dec, 2013).

68. A. C. McPherron, Metabolic Functions of Myostatin and Gdf11. *Immunology, endocrine & metabolic agents in medicinal chemistry* **10**, 217 (Dec, 2010).

69. H. Ellingsgaard *et al.*, Interleukin-6 enhances insulin secretion by increasing glucagon-like peptide-1 secretion from L cells and alpha cells. *Nature medicine* **17**, 1481 (2011).

70.   S. Y. Roth, J. M. Denu, C. D. Allis, Histone acetyltransferases. *Annual review of biochemistry* **70**, 81 (2001).

71.   M. Doi, J. Hirayama, P. Sassone-Corsi, Circadian regulator CLOCK is a histone acetyltransferase. *Cell* **125**, 497 (Jun 05, 2006).

72.   A. Ruiz-Carrillo, L. J. Wangh, V. G. Allfrey, Processing of newly synthesized histone molecules. *Science* **190**, 117 (Oct 10, 1975).

73.   M. Haberland, R. L. Montgomery, E. N. Olson, The many roles of histone deacetylases in development and physiology: implications for disease and therapy. *Nature reviews. Genetics* **10**, 32 (Jan, 2009).

74.   M. J. Carrozza, R. T. Utley, J. L. Workman, J. Cote, The diverse functions of histone acetyltransferase complexes. *Trends in genetics : TIG* **19**, 321 (Jun, 2003).

75.   R. H. Houtkooper, E. Pirinen, J. Auwerx, Sirtuins as regulators of metabolism and healthspan. *Nature reviews. Molecular cell biology* **13**, 225 (Apr, 2012).

76.   X. Liu *et al.*, Transcriptional repression by histone deacetylases in plants. *Molecular plant* **7**, 764 (Jun, 2014).

77.   S. Imai, C. M. Armstrong, M. Kaeberlein, L. Guarente, Transcriptional silencing and longevity protein Sir2 is an NAD-dependent histone deacetylase. *Nature* **403**, 795 (Feb 17, 2000).

78.   S. J. Lin, P. A. Defossez, L. Guarente, Requirement of NAD and SIR2 for life-span extension by calorie restriction in Saccharomyces cerevisiae. *Science* **289**, 2126 (Sep 22, 2000).

79.   J. A. Hall, J. E. Dominy, Y. Lee, P. Puigserver, The sirtuin family's role in aging and age-associated pathologies. *The Journal of clinical investigation* **123**, 973 (Mar 1, 2013).

80.   M. Lagouge *et al.*, Resveratrol improves mitochondrial function and protects against metabolic disease by activating SIRT1 and PGC-1alpha. *Cell* **127**, 1109 (Dec 15, 2006).

81.   J. T. Rodgers *et al.*, Nutrient control of glucose homeostasis through a complex of PGC-1alpha and SIRT1. *Nature* **434**, 113 (Mar 3, 2005).

82.   C. Canto *et al.*, Interdependence of AMPK and SIRT1 for metabolic adaptation to fasting and exercise in skeletal muscle. *Cell metabolism* **11**, 213 (Mar 3, 2010).

83.   M. C. Motta *et al.*, Mammalian SIRT1 represses forkhead transcription factors. *Cell* **116**, 551 (Feb 20, 2004).

84.   X. Li *et al.*, SIRT1 deacetylates and positively regulates the nuclear receptor LXR. *Molecular cell* **28**, 91 (Oct 12, 2007).

85.   J. T. Rodgers, P. Puigserver, Fasting-dependent glucose and lipid metabolic response through hepatic sirtuin 1. *Proceedings of the National Academy of Sciences of the United States of America* **104**, 12861 (Jul 31, 2007).

86.   Y. Liu *et al.*, A fasting inducible switch modulates gluconeogenesis via activator/coactivator exchange. *Nature* **456**, 269 (Nov 13, 2008).

87.   L. Qiang *et al.*, Brown remodeling of white adipose tissue by SirT1-dependent deacetylation of Pparγ. *Cell* **150**, 620 (Aug 03, 2012).

88.   W. C. Hallows, S. Lee, J. M. Denu, Sirtuins deacetylate and activate mammalian acetyl-CoA synthetases. *Proceedings of the National Academy of Sciences of the United States of America* **103**, 10230 (Jul 5, 2006).

89.   K. J. Menzies, K. Singh, A. Saleem, D. A. Hood, Sirtuin 1-mediated Effects of Exercise and Resveratrol on Mitochondrial Biogenesis. *Journal of Biological Chemistry* **288**, 6968 (Apr 08, 2013).

90.   N. L. Price *et al.*, SIRT1 Is Required for AMPK Activation and the Beneficial Effects of Resveratrol on Mitochondrial Function. *Cell metabolism* **15**, 675 (Jun, 2012).

91.   C. Canto *et al.*, AMPK regulates energy expenditure by modulating NAD+ metabolism and SIRT1 activity. *Nature* **458**, 1056 (Apr 23, 2009).

92.   C. Lerin *et al.*, GCN5 acetyltransferase complex controls glucose metabolism through transcriptional repression of PGC-1alpha. *Cell metabolism* **3**, 429 (Jun, 2006).

93.   J. E. Dominy, Jr. *et al.*, The deacetylase Sirt6 activates the acetyltransferase GCN5 and suppresses hepatic gluconeogenesis. *Molecular cell* **48**, 900 (Dec 28, 2012).

94. Y. Lee *et al.*, Cyclin D1-Cdk4 controls glucose metabolism independently of cell cycle progression. *Nature*, (May 25, 2014).

95. M. Sakai *et al.*, CITED2 links hormonal signaling to PGC-1alpha acetylation in the regulation of gluconeogenesis. *Nature medicine* **18**, 612 (Apr, 2012).

96. A. Coste *et al.*, The genetic ablation of SRC-3 protects against obesity and improves insulin sensitivity by reducing the acetylation of PGC-1{alpha}. *Proceedings of the National Academy of Sciences of the United States of America* **105**, 17187 (Nov 4, 2008).

97. C. Sun *et al.*, PCAF Improves Glucose Homeostasis by Suppressing the Gluconeogenic Activity of PGC-1α. *Cell reports* **9**, 2250 (Dec 24, 2014).

98. K. Ravnskjaer *et al.*, Glucagon regulates gluconeogenesis through KAT2B- and WDR5-mediated epigenetic effects. *The Journal of clinical investigation* **123**, 4318 (Oct 1, 2013).

99. W. Xu *et al.*, Loss of Gcn5l2 leads to increased apoptosis and mesodermal defects during mouse development. *Nature genetics* **26**, 229 (Oct, 2000).

100. P. Bai *et al.*, PARP-1 Inhibition Increases Mitochondrial Metabolism through SIRT1 Activation. *Cell metabolism* **13**, 461 (2011).

101. C. Canto *et al.*, The NAD(+) precursor nicotinamide riboside enhances oxidative metabolism and protects against high-fat diet-induced obesity. *Cell metabolism* **15**, 838 (Jun 6, 2012).

102. C. C. Alano, W. Ying, R. A. Swanson, Poly(ADP-ribose) polymerase-1-mediated cell death in astrocytes requires NAD+ depletion and mitochondrial permeability transition. *The Journal of biological chemistry* **279**, 18895 (May 30, 2004).

103. J. R. Revollo, A. A. Grimm, S. Imai, The NAD biosynthesis pathway mediated by nicotinamide phosphoribosyltransferase regulates Sir2 activity in mammalian cells. *The Journal of biological chemistry* **279**, 50754 (Dec 3, 2004).

104. R. H. Houtkooper, C. Canto, R. J. Wanders, J. Auwerx, The secret life of NAD+: an old metabolite controlling new metabolic signaling pathways. *Endocrine reviews* **31**, 194 (Apr, 2010).

105. L. R. Stein, S. Imai, The dynamic regulation of NAD metabolism in mitochondria. *Trends in endocrinology and metabolism: TEM* **23**, 420 (Sep, 2012).

106. C. W. van Roermund, Y. Elgersma, N. Singh, R. J. Wanders, H. F. Tabak, The membrane of peroxisomes in Saccharomyces cerevisiae is impermeable to NAD(H) and acetyl-CoA under in vivo conditions. *EMBO J* **14**, 3480 (Jul 17, 1995).

107. M. Barile, S. Passarella, G. Danese, E. Quagliariello, Rat liver mitochondria can synthesize nicotinamide adenine dinucleotide from nicotinamide mononucleotide and ATP via a putative matrix nicotinamide mononucleotide adenylyltransferase. *Biochemistry and molecular biology international* **38**, 297 (Mar, 1996).

108. F. Berger, C. Lau, M. Dahlmann, M. Ziegler, Subcellular compartmentation and differential catalytic properties of the three human nicotinamide mononucleotide adenylyltransferase isoforms. *The Journal of biological chemistry* **280**, 36334 (Oct 28, 2005).

109. H. Yang *et al.*, Nutrient-sensitive mitochondrial NAD+ levels dictate cell survival. *Cell* **130**, 1095 (Sep 21, 2007).

110. T. Zhang *et al.*, Regulation of Poly(ADP-ribose) Polymerase-1-dependent Gene Expression through Promoter-directed Recruitment of a Nuclear NAD(+) Synthase. *The Journal of biological chemistry* **287**, 12405 (2012).

111. T. Nakagawa, D. J. Lomb, M. C. Haigis, L. Guarente, SIRT5 Deacetylates carbamoyl phosphate synthetase 1 and regulates the urea cycle. *Cell* **137**, 560 (Jun 01, 2009).

112. F. Di Lisa, R. Menabo, M. Canton, M. Barile, P. Bernardi, Opening of the mitochondrial permeability transition pore causes depletion of mitochondrial and cytosolic NAD+ and is a causative event in the death of myocytes in postischemic reperfusion of the heart. *The Journal of biological chemistry* **276**, 2571 (Jan 26, 2001).

113. M. Pittelli *et al.*, Inhibition of nicotinamide phosphoribosyltransferase: cellular bioenergetics reveals a mitochondrial insensitive NAD pool. *The Journal of biological chemistry* **285**, 34106 (Oct 29, 2010).

114. C. C. Alano *et al.*, Differences among cell types in NAD(+) compartmentalization: a comparison of neurons, astrocytes, and cardiac myocytes. *Journal of neuroscience research* **85**, 3378 (Nov 15, 2007).

115. M. E. Tischler, D. Friedrichs, K. Coll, J. R. Williamson, Pyridine nucleotide distributions and enzyme mass action ratios in hepatocytes from fed and starved rats. *Archives of biochemistry and biophysics* **184**, 222 (Nov, 1977).

116. M. Pittelli *et al.*, Pharmacological effects of exogenous NAD on mitochondrial bioenergetics, DNA repair, and apoptosis. *Molecular pharmacology* **80**, 1136 (Dec, 2011).

117. K. L. Bogan, C. Brenner, Nicotinic acid, nicotinamide, and nicotinamide riboside: a molecular evaluation of NAD+ precursor vitamins in human nutrition. *Annu Rev Nutr* **28**, 115 (2008).

118. A. Rongvaux, F. Andris, F. Van Gool, O. Leo, Reconstructing eukaryotic NAD metabolism. *BioEssays : news and reviews in molecular, cellular and developmental biology* **25**, 683 (Jul, 2003).

119. Y. Chi, A. A. Sauve, Nicotinamide riboside, a trace nutrient in foods, is a vitamin B3 with effects on energy metabolism and neuroprotection. *Current Opinion in Clinical Nutrition and Metabolic Care* **16**, 657 (Oct 31, 2013).

120. D. A. Bender, Biochemistry of tryptophan in health and disease. *Mol Aspects Med* **6**, 101 (1983).

121. A. Rongvaux *et al.*, Pre-B-cell colony-enhancing factor, whose expression is up-regulated in activated lymphocytes, is a nicotinamide phosphoribosyltransferase, a cytosolic enzyme involved in NAD biosynthesis. *European journal of immunology* **32**, 3225 (Nov, 2002).

122. M. Emanuelli *et al.*, Molecular cloning, chromosomal localization, tissue mRNA levels, bacterial expression, and enzymatic properties of human NMN adenylyltransferase. *The Journal of biological chemistry* **276**, 406 (Jan 5, 2001).

123. J. A. Yalowitz *et al.*, Characterization of human brain nicotinamide 5'-mononucleotide adenylyltransferase-2 and expression in human pancreas. *The Biochemical journal* **377**, 317 (Jan 15, 2004).

124. X. Zhang *et al.*, Structural characterization of a human cytosolic NMN/NaMN adenylyltransferase and implication in human NAD biosynthesis. *The Journal of biological chemistry* **278**, 13503 (Apr 11, 2003).

125. J. R. Revollo *et al.*, Nampt/PBEF/Visfatin regulates insulin secretion in beta cells as a systemic NAD biosynthetic enzyme. *Cell metabolism* **6**, 363 (Nov, 2007).

126. M. Fulco *et al.*, Glucose Restriction Inhibits Skeletal Myoblast Differentiation by Activating SIRT1 through AMPK-Mediated Regulation of Nampt. *Developmental Cell* **14**, 661 (2008).

127. E. van der Veer *et al.*, Extension of Human Cell Lifespan by Nicotinamide Phosphoribosyltransferase. *Journal of Biological Chemistry* **282**, 10841 (2007).

128. A. Rongvaux *et al.*, Nicotinamide phosphoribosyl transferase/pre-B cell colony-enhancing factor/visfatin is required for lymphocyte development and cellular resistance to genotoxic stress. *J Immunol* **181**, 4685 (Oct 1, 2008).

129. S. P. Lu, M. Kato, S. J. Lin, Assimilation of endogenous nicotinamide riboside is essential for calorie restriction-mediated life span extension in Saccharomyces cerevisiae. *The Journal of biological chemistry* **284**, 17110 (Jun 19, 2009).

130. A. Nikiforov, C. Dolle, M. Niere, M. Ziegler, Pathways and subcellular compartmentation of NAD biosynthesis in human cells: from entry of extracellular precursors to mitochondrial NAD generation. *The Journal of biological chemistry* **286**, 21767 (Jun 17, 2011).

131. P. Belenky *et al.*, Nicotinamide riboside promotes Sir2 silencing and extends lifespan via Nrk and Urh1/Pnp1/Meu1 pathways to NAD+. *Cell* **129**, 473 (May 4, 2007).

132. P. Bieganowski, C. Brenner, Discoveries of nicotinamide riboside as a nutrient and conserved NRK genes establish a Preiss-Handler independent route to NAD+ in fungi and humans. *Cell* **117**, 495 (Jun 14, 2004).

133. L. Mouchiroud *et al.*, The NAD(+)/Sirtuin Pathway Modulates Longevity through Activation of Mitochondrial UPR and FOXO Signaling. *Cell* **154**, 430 (Jul 18, 2013).

134. Y. Sasaki, T. Araki, J. Milbrandt, Stimulation of nicotinamide adenine dinucleotide biosynthetic pathways delays axonal degeneration after axotomy. *J Neurosci* **26**, 8484 (Aug 16, 2006).

135. N. A. Khan *et al.*, Effective treatment of mitochondrial myopathy by nicotinamide riboside, a vitamin B3. *EMBO Mol Med*, n/a (2014).

136. R. Cerutti *et al.*, NAD(+)-Dependent Activation of Sirt1 Corrects the Phenotype in a Mouse Model of Mitochondrial Disease. *Cell metabolism* **19**, 1042 (Jul 03, 2014).

137. L. Liu *et al.*, Chromatin Modifications as determinants of muscle stem cell quiescence and chronological aging. **4**, 189 (2013).

138. H. Munerah, K. Saadia, C. Jihong, L. Qiao, Stepwise acetyltransferase association and histone acetylation at the Myod1 locus during myogenic differentiation. *Scientific Reports* **3**, (2013).

139. P. L. Puri *et al.*, Differential Roles of p300 and PCAF Acetyltransferases in Muscle Differentiation. *Molecular cell* **1**, 35 (1997).

140. V. Sartorelli *et al.*, Acetylation of MyoD directed by PCAF is necessary for the execution of the muscle program. *Molecular cell* **4**, 725 (1999).

141. W. Xu, D. G. Edmondson, S. Y. Roth, Mammalian GCN5 and P/ CAF acetyltransferases have homologous amino- terminal domains important for recognition of nucleosomal substrates. *Molecular and cellular biology* **18**, 5659 (1998).

142. T. P. Yao *et al.*, Gene dosage- dependent embryonic development and proliferation defects in mice lacking the transcriptional integrator p300. *Cell* **93**, 361 (1998).

143. P. Bu, S. Y. R. Dent, Y. A. Evrard, G. Lozano, Loss of Gcn5 acetyltransferase activity leads to neural tube closure defects and exencephaly in mouse embryos. *Molecular and Cellular Biology* **27**, 3405 (2007).

144. W. Lin *et al.*, Developmental potential of Gcn5 −/− embryonic stem cells in vivo and in vitro. *Developmental Dynamics* **236**, 1547 (2007).

145. Y. C. Chen *et al.*, Gcn5 loss-of- function accelerates cerebellar and retinal degeneration in a SCA7 mouse model. *Human Molecular Genetics* **21**, 394 (2012).

146. V. Martínez-Cerdeño *et al.*, N- Myc and GCN5 Regulate Significantly Overlapping Transcriptional Programs in Neural Stem Cells (N- Myc and GCN5 Share Transcriptional Functions). *PLoS ONE* **7**, e39456 (2012).

147. A. J. Wagers, I. L. Weissman, Plasticity of adult stem cells. *Cell* **116**, 639 (Mar 5, 2004).

148. T. Kuilman, C. Michaloglou, W. J. Mooi, D. S. Peeper, The essence of senescence. *Genes & development* **24**, 2463 (Nov 15, 2010).

149. C. Lopez-Otin, M. A. Blasco, L. Partridge, M. Serrano, G. Kroemer, The hallmarks of aging. *Cell* **153**, 1194 (Jun 6, 2013).

150. Y. C. Jang, M. Sinha, M. Cerletti, C. Dall'Osso, A. J. Wagers, Skeletal muscle stem cells: effects of aging and metabolism on muscle regenerative function. *Cold Spring Harbor symposia on quantitative biology* **76**, 101 (2011).

151. C. S. Fry *et al.*, Inducible depletion of satellite cells in adult, sedentary mice impairs muscle regenerative capacity without affecting sarcopenia. *Nature medicine* **21**, 76 (Jan, 2015).

152. F. D. Price *et al.*, Inhibition of JAK-STAT signaling stimulates adult satellite cell function. *Nature medicine* **20**, 1174 (Oct, 2014).

153. I. M. Conboy *et al.*, Rejuvenation of aged progenitor cells by exposure to a young systemic environment. *Nature* **433**, 760 (Feb 17, 2005).

154. P. Sousa-Victor *et al.*, Geriatric muscle stem cells switch reversible quiescence into senescence. *Nature* **506**, 316 (Feb 20, 2014).

155. J. D. Bernet *et al.*, p38 MAPK signaling underlies a cell-autonomous loss of stem cell self-renewal in skeletal muscle of aged mice. *Nature medicine* **20**, 265 (Mar, 2014).

156. M. T. Tierney *et al.*, STAT3 signaling controls satellite cell expansion and skeletal muscle repair. *Nature medicine* **20**, 1182 (Oct, 2014).

157. E. Pirinen *et al.*, Pharmacological Inhibition of poly(ADP-ribose) polymerases improves fitness and mitochondrial function in skeletal muscle. *Cell metabolism* **19**, 1034 (Jun 3, 2014).

158. L. Mouchiroud *et al.*, The NAD(+)/Sirtuin Pathway Modulates Longevity through Activation of Mitochondrial UPR and FOXO Signaling. *Cell* **154**, 430 (Jul 18, 2013).

159. J. Yoshino, K. F. Mills, M. J. Yoon, S. Imai, Nicotinamide mononucleotide, a key NAD(+) intermediate, treats the pathophysiology of diet- and age-induced diabetes in mice. *Cell metabolism* **14**, 528 (Oct 5, 2011).

160. A. P. Gomes *et al.*, Declining NAD(+) induces a pseudohypoxic state disrupting nuclear-mitochondrial communication during aging. *Cell* **155**, 1624 (Dec 19, 2013).

161. K. Ito, T. Suda, Metabolic requirements for the maintenance of self-renewing stem cells. *Nature reviews. Molecular cell biology* **15**, 243 (Apr, 2014).

162. M. Cerletti, Y. C. Jang, L. W. Finley, M. C. Haigis, A. J. Wagers, Short-term calorie restriction enhances skeletal muscle stem cell function. *Cell Stem Cell* **10**, 515 (May 4, 2012).

163. L. R. Stein, S. Imai, Specific ablation of Nampt in adult neural stem cells recapitulates their functional defects during aging. *EMBO J* **33**, 1321 (Jun 17, 2014).

164. P. Katajisto *et al.*, Stem cells. Asymmetric apportioning of aged mitochondria between daughter cells is required for stemness. *Science* **348**, 340 (Apr 17, 2015).

165. T. R. Mercer *et al.*, The human mitochondrial transcriptome. *Cell* **146**, 645 (Aug 19, 2011).

166. A. Sickmann *et al.*, The proteome of Saccharomyces cerevisiae mitochondria. *Proceedings of the National Academy of Sciences of the United States of America* **100**, 13207 (Nov 11, 2003).

167. D. J. Pagliarini *et al.*, A mitochondrial protein compendium elucidates complex I disease biology. *Cell* **134**, 112 (Jul 11, 2008).

168. S. Sartore, L. Gorza, S. Schiaffino, Fetal myosin heavy chains in regenerating muscle. *Nature* **298**, 294 (Jul 15, 1982).

169. D. R. Lemos *et al.*, Nilotinib reduces muscle fibrosis in chronic muscle injury by promoting TNF-mediated apoptosis of fibro/adipogenic progenitors. *Nature medicine* **21**, 786 (Jul, 2015).

170. E. Hara *et al.*, Regulation of p16CDKN2 expression and its implications for cell immortalization and senescence. *Mol Cell Biol* **16**, 859 (Mar, 1996).

171. L. C. Gillet *et al.*, Targeted data extraction of the MS/MS spectra generated by data-independent acquisition: a new concept for consistent and accurate proteome analysis. *Molecular & cellular proteomics : MCP* **11**, O111 016717 (Jun, 2012).

172. P. Rimmele *et al.*, Mitochondrial metabolism in hematopoietic stem cells requires functional FOXO3. *EMBO reports* **16**, 1164 (Sep, 2015).

173. P. J. Coates *et al.*, Mammalian prohibitin proteins respond to mitochondrial stress and decrease during cellular senescence. *Experimental cell research* **265**, 262 (Jun 01, 2001).

174. P. J. Coates, D. J. Jamieson, K. Smart, A. R. Prescott, P. A. Hall, The prohibitin family of mitochondrial proteins regulate replicative lifespan. *Current biology : CB* **7**, 607 (Aug 1, 1997).

175. M. Artal-Sanz, N. Tavernarakis, Prohibitin couples diapause signalling to mitochondrial metabolism during ageing in C. elegans. *Nature* **461**, 793 (Oct 8, 2009).

176. C. Osman, C. Merkwirth, T. Langer, Prohibitins and the functional compartmentalization of mitochondrial membranes. *Journal of cell science* **122**, 3823 (Nov 1, 2009).

177. M. Fulco *et al.*, Sir2 regulates skeletal muscle differentiation as a potential sensor of the redox state. *Molecular cell* **12**, 51 (Jul, 2003).

178. K. P. Quinn *et al.*, Quantitative metabolic imaging using endogenous fluorescence to detect stem cell differentiation. *Sci Rep* **3**, 3432 (2013).

179. E. K. Nishimura, S. R. Granter, D. E. Fisher, Mechanisms of hair graying: incomplete melanocyte stem cell maintenance in the niche. *Science* **307**, 720 (Feb 4, 2005).

180. C. D. Folmes, P. P. Dzeja, T. J. Nelson, A. Terzic, Metabolic plasticity in stem cell homeostasis and differentiation. *Cell Stem Cell* **11**, 596 (Nov 2, 2012).

181. C. Canto, K. J. Menzies, J. Auwerx, NAD(+) Metabolism and the Control of Energy Homeostasis: A Balancing Act between Mitochondria and the Nucleus. *Cell metabolism* **22**, 31 (Jul 7, 2015).

182. M. F. Champy *et al.*, Genetic background determines metabolic phenotypes in the mouse. *Mammalian genome : official journal of the International Mammalian Genome Society* **19**, 318 (May, 2008).
183. P. Rebora, A. Salim, M. Reilly, bshazard: A Flexible Tool for Nonparametric Smoothing of the Hazard Function. *R J* **6**, 114 (Dec, 2014).
184. T. M. Therneau, P. M. Grambsch, *Modeling Survival Data: Extending the Cox Model* (Springer, New York, 2000).
185. E. Kimura, S. Li, P. Gregorevic, B. M. Fall, J. S. Chamberlain, Dystrophin delivery to muscles of mdx mice using lentiviral vectors leads to myogenic progenitor targeting and stable gene expression. *Molecular therapy : the journal of the American Society of Gene Therapy* **18**, 206 (Jan, 2010).
186. Y. Wu *et al.*, Multilayered genetic and omics dissection of mitochondrial activity in a mouse reference population. *Cell* **158**, 1415 (Sep 11, 2014).
187. H. Lam *et al.*, Development and validation of a spectral library searching method for peptide identification from MS/MS. *Proteomics* **7**, 655 (Mar, 2007).
188. B. C. Collins *et al.*, Quantifying protein interaction dynamics by SWATH mass spectrometry: application to the 14-3-3 system. *Nature methods* **10**, 1246 (Dec, 2013).
189. H. L. Rost *et al.*, OpenSWATH enables automated, targeted analysis of data-independent acquisition MS data. *Nature biotechnology* **32**, 219 (Mar, 2014).
190. L. Reiter *et al.*, mProphet: automated data processing and statistical validation for large-scale SRM experiments. *Nature methods* **8**, 430 (May, 2011).
191. M. Watanabe *et al.*, Bile acids induce energy expenditure by promoting intracellular thyroid hormone activation. *Nature* **439**, 484 (Jan 26, 2006).
192. K. Ma, J. K. Chan, G. Zhu, Z. Wu, Myocyte enhancer factor 2 acetylation by p300 enhances its DNA binding activity, transcriptional activity, and myogenic differentiation. *Mol Cell Biol* **25**, 3575 (May, 2005).
193. V. Sartorelli *et al.*, Acetylation of MyoD directed by PCAF is necessary for the execution of the muscle program. *Molecular cell* **4**, 725 (Nov, 1999).
194. P. L. Puri *et al.*, Differential roles of p300 and PCAF acetyltransferases in muscle differentiation. *Molecular cell* **1**, 35 (Dec, 1997).
195. J. T. Rodgers *et al.*, mTORC1 controls the adaptive transition of quiescent stem cells from G0 to G(Alert). *Nature* **510**, 393 (Jun 19, 2014).
196. N. Yoshida, S. Yoshida, K. Koishi, K. Masuda, Y. Nabeshima, Cell heterogeneity upon myogenic differentiation: down-regulation of MyoD and Myf-5 generates 'reserve cells'. *Journal of cell science* **111 (Pt 6)**, 769 (Mar, 1998).
197. A. J. Wagers, I. M. Conboy, Cellular and molecular signatures of muscle regeneration: current concepts and controversies in adult myogenesis. *Cell* **122**, 659 (Sep 9, 2005).
198. M. Buckingham, F. Relaix, The role of Pax genes in the development of tissues and organs: Pax3 and Pax7 regulate muscle progenitor cell functions. *Annual review of cell and developmental biology* **23**, 645 (2007).
199. F. Relaix *et al.*, Pax3 and Pax7 have distinct and overlapping functions in adult muscle progenitor cells. *J Cell Biol* **172**, 91 (Jan 2, 2006).
200. S. J. Moat, D. M. Bradley, R. Salmon, A. Clarke, L. Hartley, Newborn bloodspot screening for Duchenne muscular dystrophy: 21 years experience in Wales (UK). *European journal of human genetics : EJHG* **21**, 1049 (Oct, 2013).
201. J. R. Mendell *et al.*, Evidence-based path to newborn screening for Duchenne muscular dystrophy. *Annals of neurology* **71**, 304 (Apr, 2012).
202. R. J. Fairclough, M. J. Wood, K. E. Davies, Therapy for Duchenne muscular dystrophy: renewed optimism from genetic approaches. *Nature reviews. Genetics* **14**, 373 (Jul, 2013).
203. P. Bonaldo, M. Sandri, Cellular and molecular mechanisms of muscle atrophy. *Disease models & mechanisms* **6**, 25 (Feb, 2013).
204. A. Chalkiadaki, M. Igarashi, A. S. Nasamu, J. Knezevic, L. Guarente, Muscle-specific SIRT1 gain-of-function increases slow-twitch fibers and ameliorates pathophysiology

in a mouse model of duchenne muscular dystrophy. *PLoS Genetics* **10**, e1004490 (Jul, 2014).

205. C. Handschin *et al.*, PGC-1alpha regulates the neuromuscular junction program and ameliorates Duchenne muscular dystrophy. *Genes & development* **21**, 770 (May 01, 2007).

206. M. Sandri *et al.*, PGC-1alpha protects skeletal muscle from atrophy by suppressing FoxO3 action and atrophy-specific gene transcription. *Proceedings of the National Academy of Sciences of the United States of America* **103**, 16260 (Oct 31, 2006).

207. D. Lee, A. L. Goldberg, SIRT1 protein, by blocking the activities of transcription factors FoxO1 and FoxO3, inhibits muscle atrophy and promotes muscle growth. *Journal of Biological Chemistry* **288**, 30515 (Oct 18, 2013).

208. P. Bai *et al.*, PARP-1 inhibition increases mitochondrial metabolism through SIRT1 activation. *Cell Metabolism* **13**, 461 (2011).

209. E. Pirinen *et al.*, Pharmacological Inhibition of poly(ADP-ribose) polymerases improves fitness and mitochondrial function in skeletal muscle. *Cell metabolism* **19**, 1034 (Jul 03, 2014).

210. M. H. Aguennouz *et al.*, Telomere shortening is associated to TRF1 and PARP1 overexpression in Duchenne muscular dystrophy. *Neurobiology of Aging* **32**, 2190 (Dec 01, 2011).

211. M. F. Goody *et al.*, NAD+ biosynthesis ameliorates a zebrafish model of muscular dystrophy. *PLoS biology* **10**, e1001409 (2012).

212. C. Cantó, K. J. Menzies, J. Auwerx, NAD(+) Metabolism and the Control of Energy Homeostasis: A Balancing Act between Mitochondria and the Nucleus. *Cell metabolism*, (Jul 24, 2015).

213. E. G. Williams *et al.*, An evolutionarily conserved role for the aryl hydrocarbon receptor in the regulation of movement. *PLoS Genetics* **10**, e1004673 (Sep, 2014).

214. P. A. Andreux *et al.*, Systems genetics of metabolism: the use of the BXD murine reference panel for multiscalar integration of traits. *Cell* **150**, 1287 (Sep 14, 2012).

215. Y. Wu *et al.*, Multilayered genetic and omics dissection of mitochondrial activity in a mouse reference population. *Cell* **158**, 1415 (Sep 11, 2014).

216. A. Subramanian, From the Cover: Gene set enrichment analysis: A knowledge-based approach for interpreting genome-wide expression profiles. *Proceedings of the National Academy of Sciences* **102**, 15545 (Oct 25, 2005).

217. M. Bakay *et al.*, Nuclear envelope dystrophies show a transcriptional fingerprint suggesting disruption of Rb-MyoD pathways in muscle regeneration. *Brain : a journal of neurology* **129**, 996 (May, 2006).

218. S. Dadgar *et al.*, Asynchronous remodeling is a driver of failed regeneration in Duchenne muscular dystrophy. *The Journal of cell biology* **207**, 139 (Oct 13, 2014).

219. D. Kraus *et al.*, Nicotinamide N-methyltransferase knockdown protects against diet-induced obesity. *Nature* **508**, 258 (May 10, 2014).

220. S. Aksoy, C. L. Szumlanski, R. M. Weinshilboum, Human liver nicotinamide N-methyltransferase. cDNA cloning, expression, and biochemical characterization. *The Journal of biological chemistry* **269**, 14835 (Jun 20, 1994).

221. J. M. Percival *et al.*, Sildenafil reduces respiratory muscle weakness and fibrosis in the mdx mouse model of Duchenne muscular dystrophy. *The Journal of pathology* **228**, 77 (Sep, 2012).

222. P. Belenky *et al.*, Nicotinamide riboside promotes Sir2 silencing and extends lifespan via Nrk and Urh1/Pnp1/Meu1 pathways to NAD+. *Cell* **129**, 473 (Jun 04, 2007).

223. K. Gieseler, K. Grisoni, L. Ségalat, Genetic suppression of phenotypes arising from mutations in dystrophin-related genes in Caenorhabditis elegans. *Current biology : CB* **10**, 1092 (Sep 21, 2000).

224. A. W. B. Joe *et al.*, Muscle injury activates resident fibro/adipogenic progenitors that facilitate myogenesis. *Nature cell biology* **12**, 153 (Mar, 2010).

225. J. E. Heredia *et al.*, Type 2 innate signals stimulate fibro/adipogenic progenitors to facilitate muscle regeneration. *Cell* **153**, 376 (May 11, 2013).

226. C. Sciorati, E. Clementi, A. A. Manfredi, P. Rovere-Querini, Fat deposition and accumulation in the damaged and inflamed skeletal muscle: cellular and molecular players. *Cellular and Molecular Life Sciences* **72**, 2135 (Jul, 2015).

227. N. Cordani, V. Pisa, L. Pozzi, C. Sciorati, E. Clementi, Nitric oxide controls fat deposition in dystrophic skeletal muscle by regulating fibro-adipogenic precursor differentiation. *Stem cells (Dayton, Ohio)* **32**, 874 (May, 2014).

228. P. Bai *et al.*, PARP-1 inhibition increases mitochondrial metabolism through SIRT1 activation. *Cell Metab* **13**, 461 (Apr 6, 2011).

229. P. Mukhopadhyay *et al.*, Poly (ADP-ribose) polymerase-1 is a key mediator of liver inflammation and fibrosis. *Hepatology (Baltimore, Md.)* **59**, 1998 (Jun, 2014).

230. T. van de Weijer *et al.*, Evidence for a direct effect of the NAD+ precursor Acipimox on muscle mitochondrial function in humans. *Diabetes*, (Oct 28, 2014).

231. A. Brunet *et al.*, Stress-dependent regulation of FOXO transcription factors by the SIRT1 deacetylase. *Science* **303**, 2011 (Mar 26, 2004).

232. H. Yamamoto *et al.*, NCoR1 Is a Conserved Physiological Modulator of Muscle Mass and Oxidative Function. *Cell* **147**, 827 (Nov, 2011).

233. R. D. Cohn *et al.*, Angiotensin II type 1 receptor blockade attenuates TGF-beta-induced failure of muscle regeneration in multiple myopathic states. *Nature medicine* **13**, 204 (Mar, 2007).

234. M. P. Siegel *et al.*, Impaired adaptability of in vivo mitochondrial energetics to acute oxidative insult in aged skeletal muscle. *Mech Ageing Dev* **133**, 620 (Sep-Oct, 2012).

235. M. J. Kushmerick *et al.*, 31P NMR spectroscopy, chemical analysis, and free Mg2+ of rabbit bladder and uterine smooth muscle. *J Biol Chem* **261**, 14420 (1986).

236. M. Lu, X. H. Zhu, Y. Zhang, W. Chen, Intracellular redox state revealed by in vivo (31) P MRS measurement of NAD(+) and NADH contents in brains. *Magn Reson Med* **71**, 1959 (Jun, 2014).

237. R. W. Wiseman, T. S. Moerland, P. B. Chase, R. Stuppard, M. J. Kushmerick, High-performance liquid chromatographic assays for free and phosphorylated derivatives of the creatine analogues BETA-guanidopropionic acid and 1-carboxy-methyl-2-iminoimidazolidine (Cyclocreatine). *Anal Biochem* **204**, 383 (1992).

238. F. W. Heineman, J. Eng, B. A. Berkowitz, R. S. Balaban, NMR spectral analysis of kinetic data using natural lineshapes. *Magnetic Resonance in Medicine* **13**, 490 (1990).

239. D. J. Taylor, P. J. Bore, P. Styles, D. G. Gadian, G. K. Radda, Bioenergetics of intact human muscle a [31]P Nuclear Resonance Study. *Molecular Biology and Medicine* **1**, 77 (1983).

240. S. J. P. Pratt, R. M. Lovering, A stepwise procedure to test contractility and susceptibility to injury for the rodent quadriceps muscle. *Journal of biological methods* **1**, (2014).

241. D. Ramot, B. E. Johnson, T. L. Berry, L. Carnell, M. B. Goodman, The Parallel Worm Tracker: a platform for measuring average speed and drug-induced paralysis in nematodes. *PloS one* **3**, e2208 (2008).

242. D. J. Klionsky *et al.* (2012), vol. 8, pp. 445-544.

243. R. H. Waterston, D. Hirsh, T. R. Lane, Dominant mutations affecting muscle structure in Caenorhabditis elegans that map near the actin gene cluster. *Journal of molecular biology* **180**, 473 (Dec 15, 1984).

244. J. Camacho-Pereira *et al.*, CD38 Dictates Age-Related NAD Decline and Mitochondrial Dysfunction through an SIRT3-Dependent Mechanism. *Cell metabolism* **23**, 1127 (Jun 14, 2016).

245. R. A. Signer, S. J. Morrison, Mechanisms that regulate stem cell aging and life span. *Cell Stem Cell* **12**, 152 (Feb 7, 2013).

246. M. B. Schultz, D. A. Sinclair, When stem cells grow old: phenotypes and mechanisms of stem cell aging. *Development* **143**, 3 (Jan 1, 2016).

247. J. Oh, Y. D. Lee, A. J. Wagers, Stem cell aging: mechanisms, regulators and therapeutic opportunities. *Nature medicine* **20**, 870 (Aug 6, 2014).

248. P. Sousa-Victor, L. Garcia-Prat, A. L. Serrano, E. Perdiguero, P. Munoz-Canoves, Muscle stem cell aging: regulation and rejuvenation. *Trends in endocrinology and metabolism: TEM* **26**, 287 (Jun, 2015).

249. K. S. Tummala *et al.*, Inhibition of de novo NAD(+) synthesis by oncogenic URI causes liver tumorigenesis through DNA damage. *Cancer cell* **26**, 826 (Dec 8, 2014).

250. M. Cerletti *et al.*, Highly efficient, functional engraftment of skeletal muscle stem cells in dystrophic muscles. *Cell* **134**, 37 (Jul 11, 2008).

251. L. Heslop, J. E. Morgan, T. A. Partridge, Evidence for a myogenic stem cell that is exhausted in dystrophic muscle. *Journal of cell science* **113 (Pt 12)**, 2299 (Jun, 2000).

252. J. Smith, G. Fowkes, P. N. Schofield, Programmed cell death in dystrophic (mdx) muscle is inhibited by IGF-II. *Cell death and differentiation* **2**, 243 (Oct, 1995).

253. J. Smith, C. Goldsmith, A. Ward, R. LeDieu, IGF-II ameliorates the dystrophic phenotype and coordinately down-regulates programmed cell death. *Cell death and differentiation* **7**, 1109 (Nov, 2000).

254. J. G. Tidball, D. E. Albrecht, B. E. Lokensgard, M. J. Spencer, Apoptosis precedes necrosis of dystrophin-deficient muscle. *Journal of cell science* **108 (Pt 6)**, 2197 (Jun, 1995).

255. H. Massudi *et al.*, Age-associated changes in oxidative stress and NAD+ metabolism in human tissue. *PLoS One* **7**, e42357 (2012).

256. D. B. Conze, J. Crespo-Barreto, C. L. Kruger, Safety assessment of nicotinamide riboside, a form of vitamin B3. *Human & experimental toxicology*, (Jan 20, 2016).

257. K. Gariani *et al.*, Eliciting the mitochondrial unfolded protein response by nicotinamide adenine dinucleotide repletion reverses fatty liver disease in mice. *Hepatology* **63**, 1190 (Apr, 2016).

258. R. Cerutti *et al.*, NAD(+)-dependent activation of Sirt1 corrects the phenotype in a mouse model of mitochondrial disease. *Cell metabolism* **19**, 1042 (Jun 3, 2014).

259. Y. Wang *et al.*, Dysregulation of histone acetyltransferases and deacetylases in cardiovascular diseases. *Oxidative medicine and cellular longevity* **2014**, 641979 (2014).

260. A. C. West, R. W. Johnstone, New and emerging HDAC inhibitors for cancer treatment. *The Journal of clinical investigation* **124**, 30 (Jan, 2014).

261. J. M. Wagner, B. Hackanson, M. Lubbert, M. Jung, Histone deacetylase (HDAC) inhibitors in recent clinical trials for cancer therapy. *Clinical epigenetics* **1**, 117 (Dec, 2010).

List of abbreviations

BMD	Becker muscular dystrophy
CCND1	Insulin-induced cyclin D1
CDK4	Cyclin-dependent kinase 4
CDKN2A	Cyclin-dependent kinase inhibitor 2A
CITED2	CBP/p300-interacting transactivator 2
CK	Creatine kinase
CLOCK	circadian locomotor output cycles kaput
CR	Caloric restriction
CREB	cAMP response element-binding protein
CRTC2	CREB regulated transcription coactivator 2
CTX	Cardiotoxin
DAPC	Dystrophin associated protein complex
DAPI	4',6-diamidino-2-phenylindole
DCX	Doublecortin
DMD	Duchenne muscular dystrophy
DMD	Duchenne's muscular dystrophy
DMEM	Dulbecco's modified Eagle's medium
EBD	Evans Blue Dye
ECM	Extracellular matrix
EdU	5-ethynyl-2-deoxyuridine
ETC	Electron transport chain
FAP	Fibro-adipogenic progenitors
FDA	U.S Food and Drug Administration
FOXO1	Forkhead box protein O 1
GCN5	General control of amino acid synthesis 5
GNAT	Gcn5-related N-acetyltransferase
GO	Gene ontology
GSEA	Gene Set Enrichment Analysis
H&E	Hematoxylin and eosin
HD	Homeobox DNA-binding domain
IGF-1	Insulin-like growth factor-1
IGFBP	IGF-binding protein
IL-6	Interleukin -6
KAT	Lysine acetyltransferase
KDAC	Lysine deacetylases
KEGG	Kyoto encyclopedia of genes and genomes
LXR	Liver X receptors
MAPK14	Mitogen-activated protein kinase 14
McSCs	Melanocyte SCs
MEF2	Myocyte Enhancer Factor 2
MNMAT1	NMN adenylyltransferase 1
MRF	Myogenic regulatory factor
MRS	Magnetic resonance spectroscopy

MuSC	Muscle stem cell
MYF5	Myogenic Factor 5
MYH	Myosin heavy chain
MYOD	Myoblast Determination Protein
MYST	MOZ, YBF2, SAS2 and TIP60
NA	Nicotinic acid
NAD$^+$	Nicotinamide adenine dinucleotide
NAFLD	Non-alcoholic fatty liver disease
NAM	Nicotinamide
NAMPT	Nicotinamide phosphoribosyltransferase
NCOA	Nuclear receptor coactivator
NES	Normalized enrichment score
NMN	Nicotinamide mononucleotide
NNMT	Nicotinamide N-methyltransferase
NR	Nicotinamide riboside
NSC	Neural SC
OCR	Oxygen consumption rate
OP	Octapeptide motif
OXPHOS	Oxidative phosphorylation
PAR	Poly ADP-ribose
PARP	Poly ADP-ribose (PAR) polymerase
PARylation	Poly ADP-ribosylation
PCAF	p300/CBP associated factor
PD	Paired Domain
PDC	Pyruvate dehydrogenase complex
PGC-1α	Peroxisome proliferator-activated receptor γ coactivator 1α
PHB	Prohibitin
PKA	cAMP-protein kinase A
PPARγ	Peroxisome proliferator-activated receptor-γ
PTM	Post-translational modification
SC	Stem cell
SVZ	Subventricular zone
SWATH-MS	Sequential windowed acquisition of all theoretical fragment ion mass spectra
TAF1	TATA box binding protein (TBP)-associated factor 1
TBP	TATA box binding protein
TCA	Tricarboxylic acid
TGFβ	Transforming growth factor β
TMRM	tetramethylrhodamine, methyl ester
TRP2	Potential channel 2
UPRmt	mitochondrial unfolded protein response
WDR5	WD repeat-containing protein 5

Curriculum Vitae

Hongbo ZHANG

hbzhang.sjtu@gmail.com

Ave. Due Tir-Federal 92, Room 423, CH-1024 Ecublens VD, Switezerland. +41 78 790 03 03

Education

Ph.D. in Biochemistry and Molecular Biology, 2016
Swiss Federal Institute of Technology Lausanne (EPFL), Switzerland.
Thesis supervisor: Prof. Johan Auwerx, M.D., Ph.D.

M.Sc. in Biochemistry and Molecular Biology, 2010
Shanghai Jiao Tong University, P.R. China.
Thesis supervisor: Prof. Qin Wang, Ph.D.

B.Sc. in Biotechnology, 2006
Hunan Agricultural University, P.R. China.
Thesis supervisor: Prof. Da Luo, Ph.D.

Research Experience

Swiss Federal Institute of Technology Lausanne (EPFL), Switzerland. 2012.02-Present
Graduate Researcher with Prof. Johan Auwerx,
• Metabolic regulation of stem cell senescence by NAD+ levels and mitochondrial function.
• Molecular and functional characterization of GCN5 in skeletal muscle stem cell function.
• Role of GCN5 in skeletal muscle structural homeostasis.
• Molecular characterization of P/CAF in skeletal muscle energy metabolism.
• Functional characterization of PARP1 inhibitors on mitochondrial function in muscle.

University of Zurich, Switzerland. 2010.10-2012.01
Research Scientist with Prof. Carsten Wagner and PD. Andreas Serra.
• Characterization of calcium and phosphate regulation in polycystic kidney disease.
• Role of FGF23 and Klotho in calcium and phosphate homeostasis.
• Mechanical characterization of FGF23 resistance in polycystic kidney disease.

Shanghai Jiao Tong University, P.R. China. 2007.09-2010.03
Graduate Researcher with Prof. Qin Wang.
• Mechanisms of induced pancreatic beta cell apoptosis.
• Protective role of prolactin on pancreatic beta cell apoptosis.

Shanghai Institutes for Biological Sciences, Chinese Academy of Sciences, P.R. China.
200512-2007.08
Research assistant with Prof. Da Luo.
- The role of BIO in the flower development of Lotus Japonicus (Lj).
- Establishment of virus-induced gene silencing (VIGS) in soybeans.
- Screening of cross-species SNP molecular markers in legumes.

Awards and honors

Young Investigator Award, 1st prize, Swiss physiological society, 2016
The Lausanne Integrative Metabolism and Nutrition Alliance travel grant, LIMNA. 2016
CARIGEST Ph.D. fellowship for stem cell research, Carigest SA. 2014-2016
Ph.D. fellowship for study abroad, China Scholarship Council. 2010-2014
Excellent Student Scholarship, Shanghai Jiao Tong University. 2007-2008
Best Graduation Thesis, Hunan Agricultural University. 2006
Government Scholarship, Hunan province. 2005

Teaching and mentoring experiences

Supervisor of Master student thesis, 640 hours, 2016
Project Supervisor of graduate student Lab Immersion (Bio-501), 224 hours, 2015
Teaching assistant of graduate student course Scientific project design in Drug Discovery
(Bio-494) , 40 hours, 2015
Teaching assistant of undergraduate student course Biological Chemistry (Bio-212), 186
hours, 2012-2014

Invited talks

Swiss Physiology Meeting 2016, Fribourg, Switzerland. 2016
Keystone Symposia "Epigenetic and Metabolic Regulation of Aging and Aging-Related
Diseases", Santa Fe, USA. 2016
The 5th Lausanne Integrative Metabolism and Nutrition Alliance Symposia, lausanne,
Switzerland. 2016

Patents

1   **Zhang, H**., Menzies, K. J., Auwerx, J. Ryu, D. Agents and methods using thereof for
     the prevention and treatment of stem cells senescence. European Patent, filed on 8th
     September 2015

2   **Zhang, H**., Menzies, K. J., Auwerx, J. Ryu, D. Agents and methods using thereof for
     the prevention and treatment of stem cell muscle disorders. European Patent, filed on
     8th September 2015

Publications

1   **Zhang, H.**, Ryu, D., Wu, Y., Gariani, K., Wang, X., Luan, P., D'Amico, D., Ropelle, E. R., Lutolf, M. P., Aebersold, R., Schoonjans, K., Menzies, K. J. & Auwerx, J. NAD$^+$ repletion improves mitochondrial and stem cell function and enhances life span in mice. *Science*, doi:10.1126/science.aaf2693 (2016).

       Chosen for perspective in *Science*, 352, 1396 (2016), and highlighted in *Nature Reviews Molecular Cell Biology*, 17, 331 (2016).

2   Ryu, D.*, **Zhang, H.***, Ropelle, E. R.*, Mazala, D. G., Sorrentino, V., Mázala D. G., Mouchiroud, L., Marshall, P. L., Campbell, M. D., Ali, A. S., Knowels, G. M., Bellemin, S., Lyer, S., Wang, X., Gariani, K., Sauve, A. A., Canto, C., Conley, K. E., Walter, L., Lovering, R. M., Chin, E. R., Jasmin, B. J., Marcinek, D. J. Menzies, K. J., & Auwerx, J. NAD+ repletion improves muscular dystrophy by countering increased levels of PARylation. *Science Translational Medicine*, 8 (361): 361ra139. (2016) (***, equal contribution**).

3   Menzies, K. J.*, **Zhang, H.***, Katsyuba, E.* & Auwerx, J. Protein acetylation in metabolism - metabolites and cofactors. *Nature Reviews Endocrinology*, 12, 43-60, doi:10.1038/nrendo.2015.181 (2016). (*, **equal contribution**)

4   Gariani, K., Ryu, D., Menzies, K. J., Yi, H. S., Stein, S., **Zhang, H.**, Perino, A., Lemos, V., Katsyuba, E., Jha, P., Vijgen, S., Rubbia-Brandt, L., Kim, Y. K., Kim, J. T., Kim, K. S., Shong, M., Schoonjans, K., Auwerx, J. Inhibiting poly ADP-ribosylation increases fatty acid oxidation and protects against fatty liver disease. *Journal of Hepatology*, doi: 10.1016/j.jhep.2016.08.024 (2016).

5   Rabhi, N., Denechaud, P. D., Gromada, X., Hannou, S. A., **Zhang, H.**, Rashid, T., Salas, E., Durand, E., Sand, O., Bonnefond, A., Yengo, L., Chavey, C., Bonner, C., Kerr-Conte, J., Abderrahmani, A., Auwerx, J., Fajas, L., Froguel, P. & Annicotte, J. S. KAT2B Is Required for Pancreatic Beta Cell Adaptation to Metabolic Stress by Controlling the Unfolded Protein Response. *Cell Reports*, doi:10.1016/j.celrep.2016.03.079 (2016).

6   Gariani, K., Menzies, K. J., Ryu, D., Wegner, C. J., Wang, X., Ropelle, E. R., Moullan, N., **Zhang, H.**, Perino, A., Lemos, V., Kim, B., Park, Y. K., Piersigilli, A., Pham, T. X., Yang, Y., Siah Ku, C., Koo, S. I., Fomitchova, A., Canto, C., Schoonjans, K., Sauve, A. A., Lee, J. Y. & Auwerx, J. Eliciting the mitochondrial unfolded protein response via NAD repletion reverses fatty liver disease. *Hepatology*, doi:10.1002/hep.28245 (2015).

7   Spichtig, D.*, **Zhang, H.***, Mohebbi, N., Pavik, I., Petzold, K., Stange, G., Saleh, L., Edenhofer, I., Segerer, S., Biber, J., Jaeger, P., Serra, A. L. & Wagner, C. A. Renal expression of FGF23 and peripheral resistance to elevated FGF23 in rodent models of polycystic kidney disease. *Kidney International* 85, 1340-1350, doi:10.1038/ki.2013.526 (2014). (***, equal contribution**).

       Highlighted in *Kidney international* 85, 1260-1262.

8   Ryu, D., Jo, Y. S., Lo Sasso, G., Stein, S., **Zhang, H.**, Perino, A., Lee, J. U., Zeviani, M., Romand, R., Hottiger, M. O., Schoonjans, K. & Auwerx, J. A SIRT7-dependent

acetylation switch of GABPbeta1 controls mitochondrial function. *Cell Metabolism* 20, 856-869, doi:10.1016/j.cmet.2014.08.001 (2014).

9   Pirinen, E., Canto, C., Jo, Y. S., Morato, L., **Zhang, H**., Menzies, K. J., Williams, E. G., Mouchiroud, L., Moullan, N., Hagberg, C., Li, W., Timmers, S., Imhof, R., Verbeek, J., Pujol, A., van Loon, B., Viscomi, C., Zeviani, M., Schrauwen, P., Sauve, A. A., Schoonjans, K. & Auwerx, J. Pharmacological Inhibition of Poly(ADP-Ribose) Polymerases Improves Fitness and Mitochondrial Function in Skeletal Muscle. *Cell Metabolism*, doi:10.1016/j.cmet.2014.04.002 (2014).